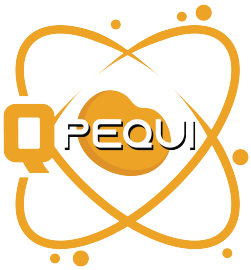

Federal University of Goiás

Institute of Physics

Quantum Pequi Group

Krylov Complexity and Dynamical Criticality in the quenched Lipkin-Meshkov-Glick model

---

PhD in Physics

Pedro Henrique Santos Bento

Goiânia, 2026

Brazil

Acknowledgements

Me reservo aqui o direito de agradecer em português às pessoas importantes que ajudaram a tornar esta tese possível. Esta tese é fruto de quase cinco anos de luta, aprendizado e persistência e por isso, eu agradeço:

Imensamente ao Lucas Chibebe Céleri, meu orientador de doutorado, por todos os ensinamentos, conselhos e a paciência que teve comigo ao longo desses quase cinco anos. A sua dedicação à ciência é inspiradora. Espero chegar um dia a ser pelo menos 10% do que você é.

Aos meus pais, Iran e Raquel, que sempre me apoiaram em tudo o que fiz até aqui. Você são os melhores.

À minha psicanalista, Tati, pelos 4 anos de análise. Sua escuta é transformadora! Não sei explicar o quanto você é importante para mim. Eu te desejo todo o amor e sucesso deste mundo.

Aos meus amigos de pós-graduação Rodrigo, Igor, Aryadine, Alexandre Augusto, João Vitor, Ítalo, Thiago, Gustavo Oliveira, Midana, Rhayson, Maurilho, Gabriela, Murilo e Éder, pelas longas noites de cerveja, conversa e risadas

Em especial ao Andesson, Tássia, Débora, Gabriel, Ronaldo e Marcelo. Vocês sempre terão um lugar especial na minha história e na minha vida. Vocês tornaram tudo mais leve. O que teria sido de mim sem vocês? Não consigo imaginar! Amo vocês!

Aos meus amigos da UFU, Rafael, Marcelo, Osvaldo e Pedro Palheta pelas conversas empolgantes sobre física, carreira e a vida. Um dia conseguiremos estar juntos de novo e eu espero que no mesmo departamento como docentes.

Por fim, à CAPES pela bolsa de doutorado e ao PPGF da UFG por todo o trabalho prestado e pela prorrogação da bolsa em 6 meses.

List of Abbreviations

FCTFIM	Fully-connected transverse field Ising model
LMG	Lipkin, Meshkov, Glick.
TFIM	Transverse field Ising model
TL	Thermodynamic limit.
QPT	[Equilibrium] Quantum phase transition.
DPT-I	Dynamical phase transition of type I (based on order parameter).
DPT-II	Dynamical phase transition of type II (based on Loschmidt functions).
DCP	Dynamical critical point
ESQPT	Excited-state quantum phase transition
GME	Generalized microcanonical ensemble

List of Symbols

j	Total spin angular momentum.
N	Number of spins.
J	Coupling strength between spins.
$\hat{H}$	Fully connected transverse field Ising or Lipkin-Meshkov-Glick hamiltonian.
$\hat{H}_{\text{LMG}}$	Original Lipkin-Meshkov-Glick hamiltonian of N fermions distributed in two levels.
$H_{\text{cl}} \equiv H_{\text{cl}}(q,p)$	Classical LMG hamiltonian valid as $N \to \infty$.
$\mathcal{H}_N$	Hilbert space of N spin-$1/2$ system
$\mathcal{D}_N$	Dicke subspace
$\mathbb{S}^2$	Usual 2-dimensional sphere - Classical manifold of the LMG model.
$\hat{\mathbf{S}} = \frac{1}{2}\sum_{i=1}^{N}(\hat{\sigma}_i^x, \hat{\sigma}_i^y, \hat{\sigma}_i^z)$	Collective spin operators.
$\hat{\mathbf{s}} = \lim_{N\to\infty} \frac{1}{N}\hat{\mathbf{S}}$	Vector of the N-normalized collective spin operators as $N \to \infty$.
$\mathbf{M} = \lim_{j\to\infty} \frac{1}{j}\langle\hat{\mathbf{S}}\rangle$	Vector of the j-normalized average magnetizations as $j \to \infty$.
h_c^{eq}	Critical point of the equilibrium phase transition.
h_c^{d}	Critical point of the dynamical phase transition.
$C_{\mathcal{K}}(t) \equiv C(t)$	Time-dependent Krylov complexity
$\overline{C}$	Infinite time averaged Krylov complexity.
$\mathcal{K} = \{\lvert K_1\rangle, \lvert K_2\rangle, \cdots\}$	Krylov basis.
$K = \lvert\mathcal{K}\rvert$	Dimension of the Krylov basis.
$\hat{K} = \sum_n n\lvert K_n\rangle\langle K_n\rvert$	Krylov operator.

Abstract

The recent finding that among all the bases in the Hilbert space of quantum systems, the Krylov basis is the one which minimizes the spread of the system's state, has prompted intense research in the recent years on the spread of evolving quantum states, mainly in quantum chaotic many-body systems in the Heisenberg picture. One of the fruits produced by these investigations is a new quantity which has expanded the understanding about the complexity behind quantum evolutions called Krylov complexity. This new measure of complexity, which upper bounds other related measures such as out-of-time order correlators and operator size, has already reached quantum field theories, open or isolated, integrable or chaotic quantum systems. A particularly striking manifestation of critical behavior in nonequilibrium quantum systems is the dynamical quantum phase transition (DQPT), which extends the notion of phase transitions to real-time evolution. At the same time, excited-state quantum phase transitions (ESQPTs) encode criticality directly in the spectral properties of the system. Motivated by the question of how complexity responds to both dynamical and spectral critical phenomena, we investigate the time evolution of Krylov complexity in the Schrödinger picture in scenarios exhibiting DQPTs and ESQPTs. Focusing on an infinite-range ferromagnetic model, we show that Krylov complexity behaves as an effective probe of both dynamical and spectral phase transitions. In particular, we demonstrate that Krylov complexity acts as an order parameter for DQPTs and, in a specific regime, we establish a simple and explicit relation between Krylov complexity and magnetization.

Keywords: Krylov complexity; Dynamical phase transition; Excited-state quantum phase transition; order parameter.

Contents

List of Figures

List of Tables

Chapter 1

Introduction

Understanding the nonequilibrium dynamics of quantum many-body systems has emerged over the past decades as one of the central challenges in contemporary physics [1]. Experimental advances in platforms such as ultracold atoms, trapped ions, and superconducting circuits have enabled unprecedented control over strongly correlated quantum systems, allowing direct exploration of dynamical regimes that lie beyond the traditional framework of equilibrium physics. In this setting, fundamental questions concerning the emergence of collective behavior, the spreading of quantum information, quantum chaos, and the limits of dynamical predictability have gained renewed relevance, both from a conceptual standpoint and in connection with applications in quantum computation and quantum simulation [2].

A recurring theme in the study of complex many-body systems is the emergence of qualitative changes in their macroscopic behavior as external parameters are varied. In equilibrium statistical physics, such changes are naturally captured by the concept of phase transitions, which provide a unifying framework to classify collective phenomena in terms of symmetry breaking, order parameters, and universal critical behavior. Remarkably, the notion of phase transitions has proven to be robust far beyond its original thermodynamic setting, offering a powerful language to describe the reorganization of quantum states and correlations in interacting many-body systems.

1.1 Quantum Phase Transitions at Equilibrium

Quantum phase transitions (QPTs) occur at zero temperature and are driven by quantum fluctuations induced by variations of external control parameters in the system Hamiltonian [3]. In contrast to classical phase transitions, which are governed by thermal fluctuations, QPTs reflect profound reorganizations of the ground state of a quantum many-body system as a critical point is crossed. These transitions are typically associated with nonanalytic behavior of ground-state properties, the closing of excitation gaps, and the emergence of universal scaling laws that are largely independent of microscopic details.

Within the equilibrium framework, quantum phase transitions are commonly understood in terms of symmetry principles and order parameters, which capture the emergence or disappearance of long-range order across a critical point. The low-energy physics near criticality is dominated by diverging correlation lengths and times, giving rise to universal behavior that can be classified into universality classes. As a result, systems with distinct microscopic realizations may exhibit identical critical exponents and scaling functions, emphasizing the collective and model-independent nature of quantum critical phenomena [4].

Despite their success in characterizing equilibrium properties, the traditional theory of quantum phase transitions is intrinsically rooted in ground-state physics and static observables. However, in many experimentally relevant situations, quantum systems are prepared far from equilibrium and subsequently evolve unitarily in time, for instance following a sudden or slow quench of a control parameter. This raises a fundamental question: to what extent can concepts originally developed for equilibrium critical phenomena be generalized to describe genuine dynamical processes in isolated quantum many-body systems [1, 2]?

Within this broader nonequilibrium perspective, dynamical quantum phase transitions (DQPTs) have emerged as a powerful conceptual framework to characterize qualitative changes in the real-time evolution of isolated quantum systems. Rather than being defined through static order parameters, DQPTs are associated with nonanalytic behavior in dynamical quantities as a function of time, reflecting abrupt reorganizations of the evolving quantum state. Originally introduced through analogies with equilibrium phase transitions, this notion has proven fruitful in revealing universal features of nonequilibrium dynamics across a wide variety of quantum many-body models [5–7].

Beyond ground-state criticality, interacting quantum many-body systems may also exhibit singular behavior at finite energies in their excitation spectrum, known as excited-state quantum phase transitions (ESQPTs). These transitions are associated with nonanalyticities in the density of states and with qualitative changes in the structure of excited eigenstates, reflecting a reorganization of the underlying classical phase space in the semiclassical limit. Unlike conventional quantum phase transitions, ESQPTs do not require tuning an external control parameter across a critical point, but instead emerge as a function of energy, providing a natural bridge between spectral properties and nonequilibrium quantum dynamics [8].

Taken together, equilibrium quantum phase transitions, DQPTs, and ESQPTs highlight complementary facets of critical behavior in quantum many-body systems. While QPTs organize qualitative changes of the ground state, DQPTs reveal sharp signatures of criticality in real-time evolution, and ESQPTs expose singular structures in the excited-state spectrum that can underlie such dynamical phenomena. This interplay suggests that spectral singularities and nonequilibrium dynamics are deeply intertwined, calling for diagnostic tools capable of capturing how quantum information and operator complexity spread across the many-body Hilbert space. Identifying such tools is essential for developing a unified understanding of criticality that transcends

the equilibrium paradigm and naturally incorporates dynamical and spectral aspects on equal footing [8, 9].

1.2 Quantum Complexity

In recent years, the notion of complexity has gained renewed prominence in quantum physics, driven largely by developments at the interface between quantum information, quantum chaos, and high-energy theory [10]. In particular, studies of black hole dynamics and holography have revealed that conventional observables, such as correlation functions or entanglement entropies, may be insufficient to fully characterize the long-time evolution of strongly interacting quantum systems. This has led to the proposal that quantum complexity, loosely defined as a measure of how difficult it is to prepare or describe a quantum state starting from a simple reference, plays a fundamental role in understanding information scrambling, thermalization, and the emergence of semiclassical spacetime in holographic settings.

Motivated by these developments, the notion of complexity has gradually permeated the study of quantum many-body systems, where it has become closely intertwined with ideas of quantum chaos, thermalization, and information scrambling [11]. In this context, particular attention has been devoted to diagnostics capable of capturing the sensitivity of quantum dynamics to perturbations and the rapid spreading of initially localized information across many degrees of freedom. Prominent examples include out-of-time-ordered correlators, which provide a quantitative probe of operator growth and chaos, as well as bounds on information scrambling inspired by black hole physics [12].

Despite their success in characterizing information scrambling and quantum chaos, many of the existing diagnostics focus on specific aspects of the dynamics and do not provide a direct measure of how complex a quantum state becomes under time evolution. Quantities such as out-of-time-ordered correlators probe the growth of operators, while entanglement measures quantify the buildup of nonlocal correlations, but neither directly tracks the progressive exploration of Hilbert space by the evolving quantum state itself. This limitation has motivated the search for alternative frameworks capable of capturing the dynamical buildup of complexity in a more global and physically transparent manner [11].

Among the various proposals put forward to quantify dynamical complexity, Krylov complexity has recently emerged as a particularly insightful framework [13]. Originally formulated in the context of operator dynamics, this approach is based on tracking how an initially simple operator spreads under Heisenberg time evolution when expanded in an orthogonal basis generated iteratively by repeated commutation with the Hamiltonian. The resulting Krylov basis provides a natural notion of distance in operator space, allowing one to quantify the growth of complexity as a dynamical process. More recently, analogous constructions have been extended to the Schrödinger picture, where Krylov complexity characterizes the spreading of quantum

states under unitary time evolution [14]. In this thesis, we focus on this state-based formulation, which offers a natural perspective for investigating nonequilibrium dynamics and its relation to spectral critical phenomena.

Applications of Krylov complexity have already yielded significant insights into the dynamical behavior of quantum many-body systems. In particular, its growth has been shown to display distinct regimes depending on whether the underlying dynamics is chaotic or integrable, and to encode information about operator spreading, spectral properties, and the onset of thermalization. Moreover, recent studies have suggested that Krylov complexity can serve as a sensitive probe of dynamical crossovers and critical behavior, highlighting its potential as a unifying diagnostic across different physical settings. For a comprehensive overview of the current state of the art in Krylov complexity, we refer the reader to two recent reviews [10, 11].

1.3 Scope and Organization of the Thesis

The central goal of this thesis is to investigate how nonequilibrium quantum critical phenomena are reflected in the dynamical growth of complexity in quantum many-body systems. Building on the concepts of equilibrium and dynamical quantum phase transitions, as well as excited-state quantum phase transitions, we explore Krylov complexity as a unifying diagnostic capable of linking spectral properties, real-time dynamics, and qualitative changes in state evolution. By focusing on the Schrödinger-picture formulation of Krylov complexity, this work aims to elucidate how dynamical signatures of criticality emerge from the underlying structure of the many-body spectrum.

This thesis is organized as follows:

- In Chapter 2, we introduce the quantum many-body model used as a testbed to show the results. We discuss their equilibrium properties and spectral structure, with particular emphasis on excited-state quantum phase transitions and the role of critical energies.
- Chapter 3 is devoted to nonequilibrium quantum dynamics. We analyze quantum quench protocols that give rise to dynamical quantum phase transitions, highlighting the emergence of nonanalytic behavior in time-evolved quantities and its relation with excited-state quantum phase transition.
- In Chapter 4, we present the formalism of Krylov complexity. We introduce the Lanczos construction for both quantum operators and states and discuss how the resulting complexity encodes information about dynamical regimes and spectral properties.

- The main results of the thesis are presented in Chapter 5, where Krylov complexity is employed as a diagnostic tool for dynamical and excited-state quantum criticality. Connections between dynamical quantum phase transitions and excited-state critical phenomena are explored.
- Finally, Chapter 6 summarizes the main findings of this thesis and outlines possible directions for future research.

Chapter 2

The Lipkin-Meshkov-Glick model

In this chapter, we explore important characteristics of the Lipkin-Meshkov-Glick (LMG) model [15–17] that will be used to show our results in the last chapter. After presenting the hamiltonian, we firstly discuss general facts regarding spin systems with permutational symmetry. After we particularize the discussion deriving the classical LMG hamiltonian and discussing important features as the classical phase space, ground-state and excited state quantum phase transitions.

2.1 The fully connected transverse field Ising model

Consider the so-called fully connected transverse field Ising model (FCTFIM) described by the following hamiltonian

$$\hat{H} = -\frac{J}{4N}\sum_{i,j=1}^{N}\hat{\sigma}_i^z\hat{\sigma}_j^z + \frac{h}{2}\sum_{i=1}^{N}\hat{\sigma_i^x}. \tag{2.1}$$

where $\hat{\sigma}_i^{x,y,z}$ are the Pauli local operators of the i-th spin. This model describes a set of N spins-1/2 with all-to-all ferromagnetic interaction of strength $J > 0$ in the $\hat{z}$ direction and a transverse magnetic field with strength h along the $\hat{x}$ direction. Because all the spins are connected to each other with equal strength, this hamiltonian describes a system with infinite-range interaction, also referred in the literature as collective systems. Experimental realizations will be listed in the section 2.7. Throughout this thesis, we will always consider N even and positive h and J.

As it will become clearer along this chapter, it is convenient to express the hamiltonian (2.1) in terms of collective spin variables $\hat{S}_{x,y,z} = \sum_{i=1}^{N}\hat{\sigma}_i^{x,y,z}/2$, taking it to the form[1]

$$\hat{H} = -\frac{J}{N}\hat{S}_z^2 + h\hat{S}_x. \tag{2.2}$$

This hamiltonian expressed in terms of collective spin variables corresponds to a particular case of the well known Lipkin-Meshkov-Glick (LMG) model [15–17]. The LMG model was proposed

[1]Note that this substitution also produces a constant term stemming from the diagonal terms of $\hat{S}_z^2$, however we choose to neglect it for now.

in the 1960's in the context of nuclear physics as being a toy model of N fermions distributed in two levels separated by energy ϵ with each level being N-fold degenerate and described by the hamiltonian

$$\hat{H}_{\text{LMG}} = \frac{1}{2}\epsilon \sum_{p,\sigma} \sigma \hat{a}^\dagger_{p\sigma}\hat{a}_{p\sigma} + \frac{1}{2}V \sum_{p,p',\sigma} \hat{a}^\dagger_{p\sigma}\hat{a}^\dagger_{p'\sigma}\hat{a}_{p'-\sigma}\hat{a}_{p-\sigma} + \frac{1}{2}W \sum_{p,p',\sigma} \hat{a}^\dagger_{p\sigma}\hat{a}^\dagger_{p'-\sigma}\hat{a}_{p'\sigma}\hat{a}_{p-\sigma} \tag{2.3}$$

where $\hat{a}^\dagger_{p\sigma}$ ($\hat{a}_{p\sigma}$) denotes the creation (annihilation) operator for a particle in the state p of the σ level and V and W denote the strength of the interactions. The term proportional to V scatters a pair of particles in the same level to the other one and the term proportional to W scatters a particle up while scatters another particle down. As each particle has only two available levels, it is convenient to map the hamiltonian into another using Pauli matrices by the following prescription

$$\hat{S}_+ = \sum_p \hat{a}^\dagger_{p+1}\hat{a}_{p-1} \tag{2.4a}$$

$$\hat{S}_- = \sum_p \hat{a}^\dagger_{p-1}\hat{a}_{p+1} \tag{2.4b}$$

$$\hat{S}_z = \frac{1}{2}\sum_{p,\sigma} \sigma \hat{a}^\dagger_{p\sigma}\hat{a}_{p\sigma} \tag{2.4c}$$

which allows to rewrite the hamiltonian in the form

$$\hat{H}_{\text{LMG}} = \epsilon\hat{S}_z + \frac{1}{2}V(\hat{S}^2_+ + \hat{S}^2_-) + \frac{1}{2}W(\hat{S}_+\hat{S}_- + \hat{S}_-\hat{S}_+). \tag{2.5}$$

In the particular case $V = W$, it reduces to

$$\hat{H}_{\text{LMG}} = \epsilon\hat{S}_z + 2V\hat{S}^2_x \tag{2.6}$$

that corresponds to the hamiltonian (2.2).

It is evident that the hamiltonian (2.1) has permutation invariance of the N spin-$1/2$ particles and in what follows we explore this property to characterize its subspaces. We refer the appendix A for a short introduction to the permutation group and some concepts which shall appear in the next subsection.

2.1.1 Permutation invariance in a hamiltonian of N particles

[2]If a quantum system is invariant under all permutations of its particles, then given its hamiltonian $\hat{H}$, one verifies that $P\hat{H}P^{-1} = H$ for all $P \in \mathcal{S}_N$. It implies that P is a constant of motion,

[2]This subsection is strongly based on the reference [18].

since

$$\frac{d}{dt}P = -i[P, H] + \frac{\partial P}{\partial t} = 0, \quad \forall P \in \mathcal{S}_N. \tag{2.7}$$

and therefore there are $N!$ conserved quantities. However, as two permutations in general do not commute, we cannot simultaneously assign numerical values for the action of all P's on any state. The existence of constants of motion which do not commute can be then a sign that the system is degenerate. Thus, in order to differentiate the degenerate states, we must seek another function χ of the P's such that $P\chi P^{-1} = \chi,\ \forall P$.

One possibility is $\chi_{\mathcal{C}} = \sum_{P' \in \mathcal{C}} P'$, the sum of all permutations in a given conjugacy class $\mathcal{C}$, since $P\chi_{\mathcal{C}}P^{-1} = \sum_{P' \in \mathcal{C}} PP'P^{-1}$ yields exactly the same terms only summed in a different order. Hence, upon this choice, there will be one χ for each conjugacy class and no independent χ else, since any function of the P's is reducible to a linear combination of the P's and thus will not commute with every P unless the coefficients of conjugate P's are all the same. An alternative expression for χ is $\chi(P_{\mathcal{C}}) = (N!)^{-1} \sum_P PP_{\mathcal{C}}P^{-1}$ now with the sum over the entire group $\mathcal{S}_N$. Since the similarity transformation only rearranges the numbers, keeping the cycle-type of $P_{\mathcal{C}}$ the same, then $\chi(P_{\mathcal{C}})$ still involves only the permutations in the same conjugacy class. In other words, if P and Q are conjugate permutations, then $\chi(P) = \chi(Q)$.

Now we have a novel set of operators $\{\chi_1, \chi_2, \cdots, \chi_{p(N)}\}$ such that $[\chi_i, P] = 0$ for all P and χ_i by construction. Since there is one χ for each conjugacy class of $\mathcal{S}_N$, thus the number of χ's is the number of integer partitions of N, $p(N)$. One way to know how the eigenstates of H transform under the action of the χ's is the following: the product of any two χ's, $\chi_p\chi_q$, is expressible as a linear function of the P's and since every χ commutes with every P, then it must be expressible as a linear function of the χ's, i.e.,

$$\chi_p\chi_q = a_1\chi_1 + a_2\chi_2 + \cdots + a_{p(N)}\chi_{p(N)} \tag{2.8}$$

with a_i being numbers. For each solution of the equation above, we have a representation of $\mathcal{S}_N$ and an exclusive set of states. First, every group has the trivial representation in which $\chi_i = \mathbb{1},\ \forall i$ and that corresponds to permutation invariant states. It means that given the common eigenstates of H and $\{\chi_i\}_i$, $|E, \chi\rangle$, then these states obey the equation $P|E, \chi_i = \mathbb{1}\rangle = 1|E, \chi_i = \mathbb{1}\rangle$. Second, another natural representation of $\mathcal{S}_N$ is the sign representation that corresponds to the states satisfying the relation $P|E, \chi_i = \pm\mathbb{1}\rangle = (-1)^{R(P)}|E, \chi_i = \pm\mathbb{1}\rangle$ in which the sign depends if P is even or odd. Finally, the group $\mathcal{S}_N$ always has a representation that is reducible and given by the direct sum of the trivial representation and another representation of dimension $N - 1$, with this latter one given by matrices whose columns has exactly one element being 1 and all the others elements being 0. Just to mention, the antisymmetric and symmetric subspaces of the sign representation constitute the two most important representations as they describe fermionic and bosonic systems respectively. In what follows, we particularize the discussion to spin-1/2

hamiltonians.

2.1.2 N spin-$1/2$ hamiltonians and the Dicke subspace

Let us start by recalling that the Hilbert space of a N spin-1/2 system, which we denote by $\mathcal{H}_N$, can be constructed starting with one spin and successively adding spins one by one until the N-th is added. For example, for two spins, in the usual $(\mathbf{S}^2, S_z)$ common basis, we have one antisymmetric singlet state (total spin $j = 0$ representation) and three symmetric triplet states (total spin $j = 1$ representation) [19]. The process of successively adding more spins is schematically sketched in Fig. 2.1 below. From top to bottom, one spin is added at once as indicated in the right most column by the number N. The numbers in each cell denotes the spin-j representation and the number in brackets is the dimension $(2j+1)$ of the representation. It is clear that the sum of all dimensions in the same row yields the dimension of the Hilbert space, which is 2^N. The arrows indicate how the irreducible spin-s representations split into two irreducible spin $|j - 1/2|$ and $(j + 1/2)$ representations upon adding a new spin. Notice that the dimension of one representation, when splitted upon the addition of a new spin-1/2, doubles from $2j + 1$ to $[2(j - 1/2) + 1] + [2(j + 1/2)] = 2(2j + 1)$.

As argued in the previous subsection, since we always have a representation in which all the eigenstates of H are symmetric under permutations, then these states naturally lie in the same subspace. The representation with the largest total spin in each row of Fig.2.1 (marked with a box) is the totally symmetric one, i.e. states lying in this representation are eigenstates of $\{\chi_1, \cdots, \chi_{p(N)}\}$ with eigenvalue equal to one. This totally symmetric subspace is called *Dicke subspace*, whose dimension is $N + 1$ and corresponds to the total spin-$N/2$ irreducible representation. In general, the representations of the remaining cells are not spanned by the eigenstates of $\{\hat{\chi}_i\}_i$. In this thesis, we do not proceed with the discussion of these other nonsymmetric spaces, however it is important to mention that they must be taken into account when one deals with thermal density matrices.

One can prove that symmetric states under permutation are eigenstates of $\mathbf{S}^2$ with eigenvalues $\frac{N}{2}\left(\frac{N}{2}+1\right)$ and for this we follow the demonstration in [20]. Let

$$|N_+\rangle = \binom{N}{N_+}^{1/2} P|\uparrow\cdots\uparrow\downarrow\cdots\downarrow\rangle \tag{2.9}$$

be the normalized permutation invariant state of N elementary spins with N_+ up spins called Dicke state, where $P = \frac{1}{N!}\sum_{p\in\mathcal{S}_N} p$ acts as a projection operator into the Dicke subspace. Since we have $N_+ \in \{0, \cdots, N\}$, thus there are $N + 1$ independent states parametrized by N_+ with this symmetry. Now, given the operator $\mathbf{S}^2 = \sum_{i,j=1}^{N} \mathbf{S}_i \cdot \mathbf{S}_j$, its off-diagonal terms act on direct

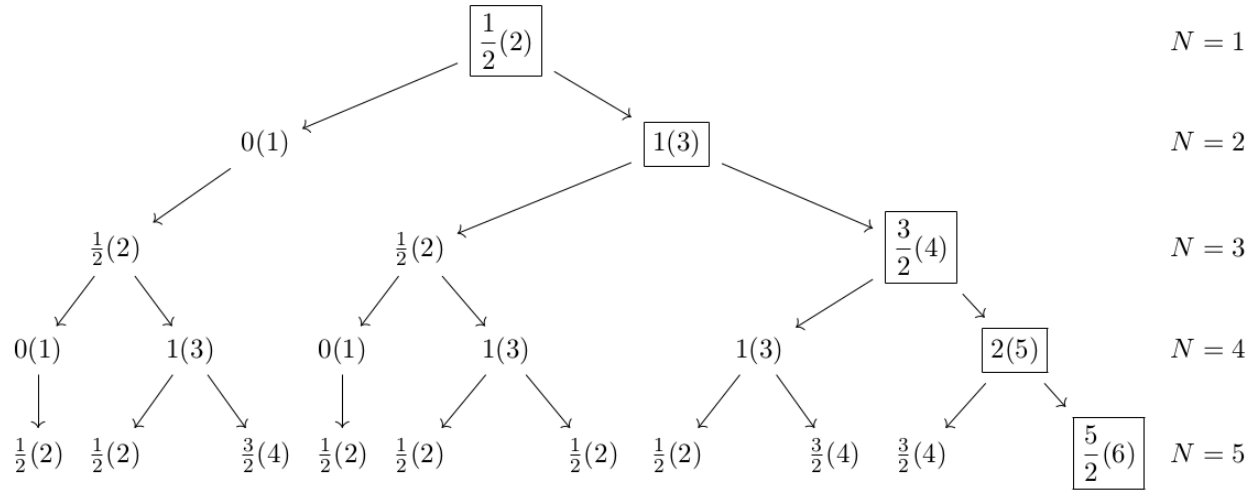

FIGURE 2.1: Hilbert space sectorization of a N spin-$1/2$ system starting with one spin (top row) and adding one additional spin at each row. Each cell represents one subspace of the Hilbert space with fixed number of particles (indicated in the left most column), and total spin j given by the first number in each cell. The number in brackets is $(2j+1)$, the dimension of the subspace. All of these subspaces are mutually orthogonal. The sum of dimensions of each subspace in the same row amounts 2^N, the dimension of the Hilbert space of N spin-1/2 particles. The last cell in each row (boxed) denotes the totally symmetric, permutation invariant, Dicke subspace of N spins. Figure taken from Ref.[20].

product states of two spins $|s_i, s_j\rangle$, with $s_i, s_j \in \{\uparrow, \downarrow\}$ as

$$\mathbf{S}_i \cdot \mathbf{S}_j |s_i, s_j\rangle = \frac{1}{4} \begin{cases} 2|\overline{s}_i, \overline{s}_j\rangle - |s_i, s_j\rangle, & s_i \neq s_j \\ |s_i, s_j\rangle, & s_i = s_j \end{cases} \tag{2.10}$$

where $\overline{s}$ is obtained by flipping s, that is, $\overline{\uparrow} = \downarrow$ and $\overline{\downarrow} = \uparrow$. Note that the number of up and down spins is not changed under the action of $\mathbf{S}_i \cdot \mathbf{S}_j$, either for a pair of parallel or antiparallel spins. For the diagonal terms of $\mathbf{S}^2$, we use the fact that $|s_i\rangle$ is an eigenstate of $\mathbf{S}_i^2$ with eigenvalue $\frac{1}{2}\left(\frac{1}{2}+1\right)$. Thus, we have

$$\begin{aligned} \mathbf{S}^2|N_+\rangle &= \mathbf{S}^2 \binom{N}{N_+}^{1/2} P|\uparrow\cdots\uparrow\downarrow\cdots\downarrow\rangle \\ &= \binom{N}{N_+}^{1/2} P\left[N\frac{1}{2}\left(\frac{1}{2}+1\right) + \sum_{i\neq j} \mathbf{S}_i \cdot \mathbf{S}_j\right] |\uparrow\cdots\uparrow\downarrow\cdots\downarrow\rangle \\ &= \left[N\frac{1}{2}\left(\frac{1}{2}+1\right) + N(N-1)\frac{1}{4}\right] \binom{N}{N_+}^{1/2} P|\uparrow\cdots\uparrow\downarrow\cdots\downarrow\rangle \\ &= \frac{N}{2}\left(\frac{N}{2}+1\right)|N_+\rangle, \end{aligned} \tag{2.11}$$

then proving that Dicke states in Eq.(2.9) belong to the spin-$N/2$ representation. As we consider $j = N/2$ in the LMG model (2.2) for the derivation of our results in the last chapter of this thesis, then we can say the LMG model is equivalent to the Dicke subspace of the FCTFIM (2.1).

2.2 The classical LMG hamiltonian

Until this point, we handled with two sets of quantum states, namely, we started with the 2^N-dimensional Hilbert space $\mathcal{H}_N = \otimes^N \mathbb{C}^2$ of the FCTFIM described by the hamiltonian (2.1). Then we introduced the $(N+1)$-dimensional Dicke subspace $\mathcal{D}_N \cong \ell^2(\mathbb{Z}_{N+1})$, whose relation with the previous one is

$$\mathcal{H}_N \supset \mathcal{D}_N, \tag{2.12}$$

where the subscript N indicates the number of spins. This reduction in dimensionality from 2^N to $N+1$ is one of the key features that makes this system particularly appealing, as it significantly simplifies its computational simulation. For example, in many situations one is interested in the time evolution of the ground state, which is symmetric under particle exchange and thus lies entirely within the Dicke subspace. Moreover, since the LMG Hamiltonian commutes with the spin operator $\hat{\mathbf{S}}^2$ for all values of J and h, then $\hat{H}$ does not mix subspaces with different total spin momentum j, thus the time evolution of any state initially in the Dicke subspace remains confined to it. Therefore, simulations can be restricted to this subspace without loss of generality in such cases.

Now we show that there is an approximate mapping of the hamiltonian (2.1) on $\mathcal{D}_N$ to a system of a fictitious particle described by the effective hamiltonian

$$H_{\text{cl}}(q,p) = -h + h\frac{q^2+p^2}{2} - J\frac{q^2}{8}(4-q^2-p^2), \tag{2.13}$$

where $(q,p) \in [-2,2]$ are position and momentum variables respectively. Furthermore, the variables (q,p) satisfy the relation $q^2+p^2 \leq 4$, thus defining a spherical phase space

$$\mathcal{M} = \mathbb{S}^2 = \{(q,p) \in \mathbb{R}^2 \mid q^2+p^2 \leq 4\}. \tag{2.14}$$

In the TL, this effective mapping becomes exact, i.e., it is possible to show that the expectation value of operators $\langle \hat{O} \rangle$ is given by [20, 21]

$$\langle \hat{O} \rangle = O_{\text{cl}} + \mathcal{O}(1/N) \tag{2.15}$$

where O_{cl} follows from the classical equations of motion of H_{cl}. Thus, we have the final pictoric relation between the three sets of states

$$\mathcal{H}_N \supset \mathcal{D}_N \xrightarrow{N\to\infty} \mathbb{S}^2. \tag{2.16}$$

To derive the classical LMG hamiltonian, we start with the hamiltonian (2.1)

$$\hat{H} = -\frac{J}{4N}\sum_{i,j=1}^{N}\hat{\sigma}_i^z\hat{\sigma}_j^z + \frac{h}{2}\sum_{i=1}^{N}\hat{\sigma_i^x}. \tag{2.17}$$

We then introduce the rescaled collective spin operators $\hat{s}_{x,y,z} = \hat{S}^{x,y,z}/N$, which are intensive quantities whose expectation values remain of order $\mathcal{O}(1)$ in the large-N limit. In terms of these rescaled operators, the Hamiltonian becomes

$$\hat{H} = -NJ\hat{s}_z^2 + Nh\hat{s}_x. \tag{2.18}$$

The rescaled spin operators $\hat{s}_\alpha$ obey the commutation relations

$$[\hat{s}_x, \hat{s}_y] = \frac{i}{N}\hat{s}_z \tag{2.19}$$

indicating that $1/N$ plays the role of an effective Planck constant, $\hbar_{\text{eff}} = 1/N$. Hence, the thermodynamic limit $N \to \infty$ coincides with the usual semiclassical limit $\hbar_{\text{eff}} \to 0$ [20, 22]. This correspondence justifies the use of semiclassical methods throughout this thesis in the TL. More significantly, it underpins the exactness of the mean-field factorization in the LMG model: as the system size grows, quantum correlations and fluctuations diminish, and the dynamics become increasingly classical. Consequently, the mean-field approximation becomes exact in the large-N limit.

Consider the intensive collective spin variables $\hat{\mathbf{s}} = (\hat{s}_x, \hat{s}_y, \hat{s}_z)$ now defined in the TL,

$$\hat{\mathbf{s}} = \lim_{N\to\infty}\frac{1}{N}(\hat{S}_x, \hat{S}_y, \hat{S}_z). \tag{2.20}$$

Let us also define the average magnetization vector in the TL as

$$\mathbf{M} = (X, Y, Z) = \lim_{j\to\infty}\frac{1}{j}(\langle\hat{S}_x\rangle, \langle\hat{S}_y\rangle, \langle\hat{S}_z\rangle). \tag{2.21}$$

It is straightforward to show that this vector lies on the unit sphere, since

$$\begin{aligned}\mathbf{M}^2 &= \lim_{j\to\infty}\frac{1}{j^2}\left(\langle\hat{S}_x\rangle^2 + \langle\hat{S}_y\rangle^2 + \langle\hat{S}_z\rangle^2\right)\\ &= \lim_{j\to\infty}\frac{1}{j^2}j(j+1) = 1.\end{aligned} \tag{2.22}$$

This implies

$$\frac{\mathrm{d}}{\mathrm{d}t}\mathbf{M}^2 = 0, \tag{2.23}$$

i.e., $\mathbf{M}^2$ is a conserved quantity. Naturally, this conservation follows directly from the fact that the total spin operator $\hat{\mathbf{S}}^2$ commutes with the LMG Hamiltonian. Due to the quantities $\langle \hat{s}_{x,y,z} \rangle$ are also restricted to a sphere, we can parametrize its expected values using spherical coordinates in the form

$$\langle \hat{s}_x \rangle = \frac{1}{2} \sin\theta \cos\phi \tag{2.24a}$$

$$\langle \hat{s}_y \rangle = \frac{1}{2} \sin\theta \sin\phi \tag{2.24b}$$

$$\langle \hat{s}_z \rangle = \frac{1}{2} \cos\theta. \tag{2.24c}$$

Thus, the energy per spin in the TL, according to equation (2.18), is given by

$$H_{\mathrm{cl}}(\theta,\phi) = \frac{\langle H \rangle}{N} = -J\langle \hat{s}_z \rangle^2 + h\langle \hat{s}_x \rangle = -\frac{J}{4}\cos^2\theta + \frac{h}{2}\sin\theta\cos\phi \tag{2.25}$$

where we have used Eq. (2.15) to justify the first equality and the mean-field factorization $\langle \hat{A}\hat{B} \rangle = \langle \hat{A} \rangle \langle \hat{B} \rangle$. Given a certain energy ϵ, then $H_{\mathrm{cl}}(\theta,\phi) = \epsilon$ defines the classical energy shell of the phase space. Note that $H_{\mathrm{cl}}(\theta,\phi)$ is the same hamiltonian of a classical top [23, 24], thus interestingly when we sum the magnetization of each spin of LMG model, in each direction, and takes the average per spin in the TL, this vector behaves exactly like a classical top, in other words, a vector on a sphere.

Finally we can also introduce position and momentum generalized coordinates (q,p) using the canonical prescription [25]

$$\frac{\langle \hat{S}_x \rangle}{j} = \frac{q^2+p^2}{2} - 1 \tag{2.26a}$$

$$\frac{\langle \hat{S}_z \rangle}{j} = \frac{q}{2}\sqrt{4-q^2-p^2} \tag{2.26b}$$

with q and p restricted to the interval $[-2,2]$ and rewrite the hamiltonian (2.18) in the form

$$H_{\mathrm{cl}}(q,p) = -h + h\frac{q^2+p^2}{2} - J\frac{q^2}{8}(4-q^2-p^2). \tag{2.27}$$

It is a well-known fact that classical Hamiltonians can capture quantum properties, but never all of them. However, the LMG model is quite a favorable case because:

- The Hilbert space collapses into a single collective spin.

- The semiclassical limit is controlled, since two parameters of the system (N and the local total spin $s = 1/2$) defines the TL and are connected to $\hbar$.
- As we will see in this chapter, the critical phenomena of our interest have a clear interpretation in terms of classical orbits and separatrix.

Once we have the classical Hamiltonian in terms of q and p, we can study equilibrium and non-equilibrium properties.

2.3 Equations of motion and Bloch sphere

Time evolution in the LMG model implies to study the trajectory described by the collective spin in the sphere $\mathbb{S}^2$. Equations for the time evolution of the collective spin $\mathbf{M}$ can be obtained by means of the Ehrenfest theorem. Given the expected value of any quantum operator, $\langle \hat{A} \rangle$, the Ehrenfest theorem states that

$$\frac{\mathrm{d}\langle \hat{A} \rangle}{\mathrm{d}t} = -i\langle [\hat{A}, \hat{H}] \rangle. \tag{2.28}$$

For instance, in the case of the LMG model, if $\langle \hat{A} \rangle = X$ defined on Eq. (2.21), we have

$$\begin{aligned}
\frac{\mathrm{d}X}{\mathrm{d}t} &= \frac{\mathrm{d}}{\mathrm{d}t} \lim_{j\to\infty} \frac{1}{j} \langle \hat{S}_x \rangle \qquad (2.29)\\
&= \lim_{j\to\infty} \frac{1}{j} \frac{\mathrm{d}}{\mathrm{d}t} \langle \hat{S}_x \rangle \\
&= \lim_{j\to\infty} \frac{1}{j} - i\langle [\hat{S}_x, \hat{H}] \rangle \\
&= \lim_{j\to\infty} \frac{1}{j} - i \left\langle \left[\hat{S}_x, -\frac{J}{N} \hat{S}_z^2 + h\hat{S}_x \right] \right\rangle \\
&= \lim_{j\to\infty} \frac{J}{2j^2} i \left\langle \left[\hat{S}_x, \hat{S}_z^2 \right] \right\rangle \\
&= \lim_{j\to\infty} \frac{J}{2j^2} i \left\langle \left[\hat{S}_x, \hat{S}_z \right] \hat{S}_z + \hat{S}_z \left[\hat{S}_x, \hat{S}_z \right] \right\rangle \\
&= \lim_{j\to\infty} \frac{J}{2j^2} \left(\left\langle \hat{S}_y \hat{S}_z \right\rangle + \left\langle \hat{S}_z \hat{S}_y \right\rangle \right) = \lim_{j\to\infty} \frac{J}{2j^2} 2 \left\langle \hat{S}_y \right\rangle \left\langle \hat{S}_z \right\rangle \\
&= JYZ \qquad (2.30)
\end{aligned}$$

where we have used the mean-field fatorization. Analogously, the equations of motion for the collective spin variables in the TL are:

$$\frac{\mathrm{d}X}{\mathrm{d}t} = JYZ \tag{2.31a}$$

$$\frac{\mathrm{d}Y}{\mathrm{d}t} = -(h + JX)Z \tag{2.31b}$$

$$\frac{\mathrm{d}Z}{\mathrm{d}t} = hY. \tag{2.31c}$$

Because the mean-field factorization is employed, the equations above are often called mean-field equations.

These equations can be solved numerically by choosing initial conditions, corresponding to the initial quantum state of the dynamics $|\psi_0\rangle = |\psi(t=0)\rangle$, giving as output the corresponding trajectory of the averaged magnetization vector. The equation (2.22) reveals that for any initial condition, the trajectory of $\mathbf{M}$ is restricted to the surface of the sphere $X^2 + Y^2 + Z^2 = 1$, the so-called Bloch sphere [26]. In the TL, the quantum states living on this sphere can be written in terms of the notorious Bloch coherent states. Although, by definition, a phase space involves only the generalized coordinates (q, p), this classical manifold $\mathbb{S}^2$ parametrized by the average magnetizations (X, Y, Z) is also referred as phase space in the literature due to the direct relation between $\mathbf{M}$ and the expectation value of $\hat{\mathbf{s}}$, namely, $\langle\hat{\mathbf{s}}\rangle = \mathbf{M}/2$.

Equations (2.31) allow for a qualitative analysis of the system through trajectories on the Bloch sphere, making it possible to distinguish between oscillatory behavior, stationary regimes, and precessional trajectories associated with different values of the magnetic field h. Just by numerically solving the mean-field equations, we can note some aspects from the dynamics of the collective spin $\mathbf{M}$. Given some initial state, we note that the higher is the h value, the longer is the trajectory of the collective spin through the Bloch sphere. This evolution is illustrated graphically (see Fig. 2.2) and anticipates the behavior that will later be reflected by the Krylov complexity. As we will see in Chapter 5, Krylov complexity faithfully captures these dynamical differences.

2.4 Phase space and quantum phase transition

One way to probe the structure of the phase space of the classical LMG model is by looking for its stationary points. We begin by writing the Hamilton equations, namely

$$\frac{\mathrm{d}q}{\mathrm{d}t} = \frac{\partial H_{\mathrm{cl}}(q,p)}{\partial p} = p\left(\frac{J}{4}q^2 + h\right) \tag{2.32}$$

$$\frac{\mathrm{d}p}{\mathrm{d}t} = -\frac{\partial H_{\mathrm{cl}}(q,p)}{\partial q} = q\left[\frac{J}{4}(4 - 2q^2 - p^2) - h\right]. \tag{2.33}$$

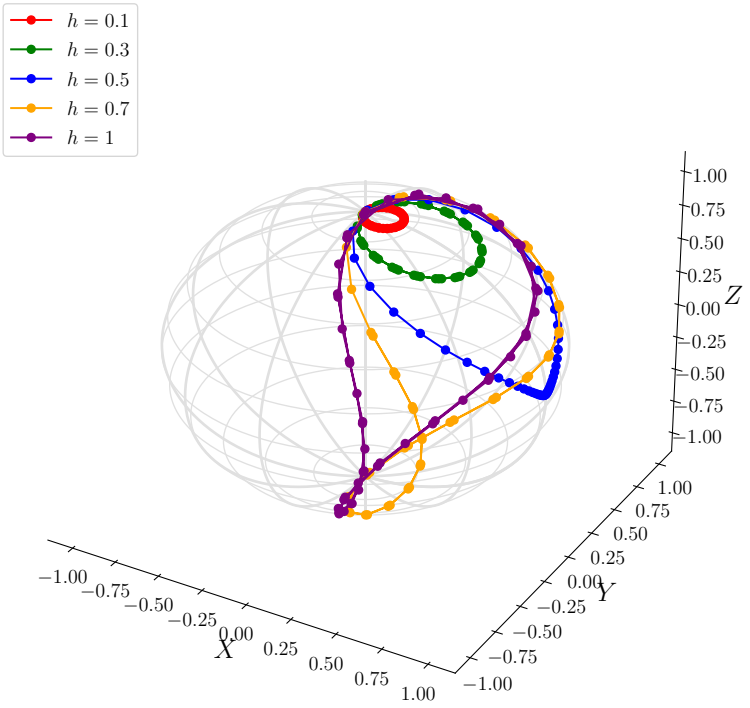

FIGURE 2.2: Trajectories in the Bloch sphere of the collective spin in the TL for different values of magnetic field h, $J = 1$ and the same initial state $|\psi_0\rangle = |\uparrow\rangle_z$. For increasingly higher values of h, the trajectory of the collective spin becomes longer in the Bloch sphere.

Imposing that $\dot{q} = 0$ and $\dot{p} = 0$, we get three solutions for $J > 0$

$$(q, p) = (0, 0) \tag{2.34a}$$

$$(q, p) = (\pm\sqrt{2(J - h)/J}\ ,\ 0). \tag{2.34b}$$

At this point, it is worth emphasizing that all stationary solutions are of the form $(q, p) = (Q, 0)$ giving rise to two qualitatively distinct regimes: $J \leq h$ and $J > h$.

For $J \leq h$, there is only the stationary point $(q, p) = (0, 0)$ whose energy is $\epsilon \equiv H_{\text{cl}}(0, 0) = -h$. A simple analysis of the second derivatives reveals that it corresponds to a minimum point, precisely the ground-state when $J \leq h$. Looking at equations (2.26a) and (2.26b), one can see that this ground-state has maximal projection in the $-\hat{x}$ direction. In other words, when $J \leq h$, the term in the hamiltonian proportional h dominates and fixes the collective spin antiparallel to the magnetic field in the ground-state, defining a paramagnetic phase.

By contrast, when $J > h$, firstly there are two stationary points with $q = \pm\sqrt{2(J - h)/J}$ respectively. Clearly, since $H_{\text{cl}}(q, p) = H_{\text{cl}}(-q, p)$, these two points are degenerate with the energy $\epsilon = -(h^2 + J^2)/2J$ and they correspond to the ground-state for $J > h$ after an analysis of second derivatives. Furthermore, unlike the unique ground-state in the paramagnetic phase, these two degenerate ground-states display finite average magnetization in both $\hat{x}$ and $\hat{z}$ directions,

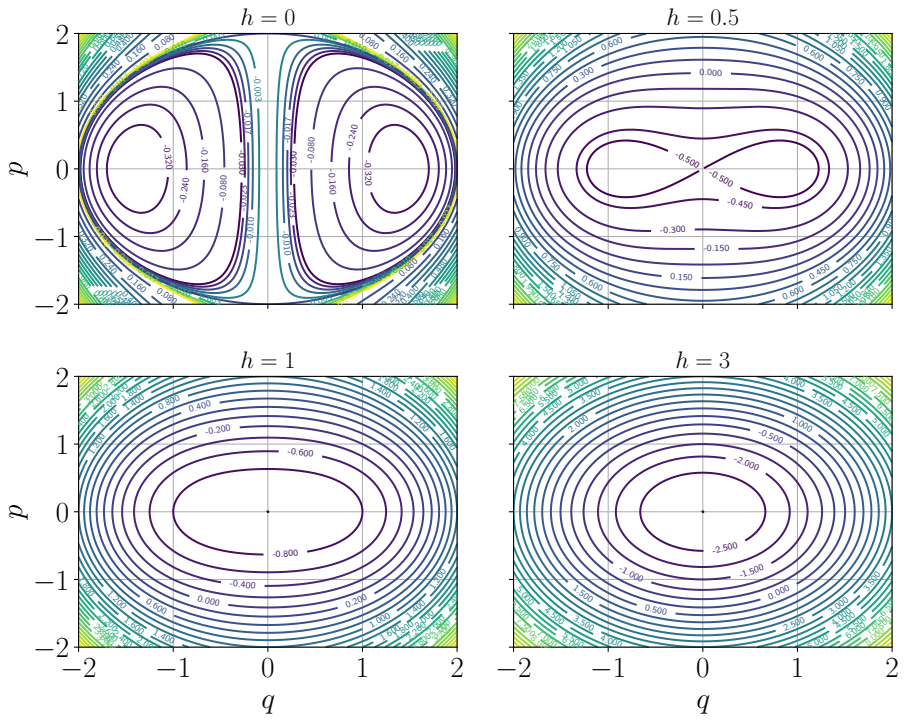

FIGURE 2.3: Orbits in the phase space of the classical LMG model for $J = 1$ and different values of h. The small numbers appearing over the lines in each panel correspond to the energy of the orbit. When $J > h$ (upper panels), two ground-states appear along with a trajectory that seems to cross itself. When $J \leq h$ (lower panels), there is only one ground-state and the phase space resembles the phase space of a harmonic oscillator.

thus defining a ferromagnetic phase in the system. Additionally, one third stationary point is found at $(q, p) = (0, 0)$, however the second derivatives reveal that it is a local maximum with energy $\epsilon = -h$.

Figure 2.3 shows a portrait of the classical phase space for different values of h, with $J = 1$. Each line represents a contour for a given energy $H_{\text{cl}}(q, p) = \epsilon$, with the corresponding energy indicated along the curve within the figure. For $J \ll h$, the term proportional to h from the Hamiltonian dominates, yielding $H_{\text{cl}} \approx -h + h(q^2 + p^2)/2$, and the phase space resembles that of a harmonic oscillator as h increases, featuring a unique ground state at $(q, p) = (0, 0)$. This behavior is illustrated in the bottom panels of Figure 2.3. On the other hand, the term proportional to J in the Hamiltonian introduces distortions in the phase space relative to the harmonic oscillator behavior. For $0 < h \leq J$, the ground state becomes doubly degenerate, located at $(q, p) = (\pm\sqrt{2(J - h)/J},\ 0)$, and an unstable fixed point (local maximum) appears at $(q, p) = (0, 0)$, giving rise to a heteroclinic orbit that seems to cross itself (see the upper right panel of Figure 2.3) [27, 28]. This heteroclinic orbit, whose energy is $\epsilon_c = -h$, functions as a separatrix in phase space: for $\epsilon < \epsilon_c$, trajectories are trapped within either the left ($q < 0$) or right

sides ($q > 0$), depending on the initial condition. If there is no such constraint ($\epsilon > \epsilon_c$), the trajectories can explore the entire available phase space. The origin of this separatrix is attributed to the so-called excited-state quantum phase transition (ESQPT) [8], a particularly intriguing phenomenon that makes the LMG model one of the richest toy models — a topic we explore in the next section. See the appendix B for an analysis of trajectories behavior near the unstable point.

The two regions of the parameter space, $J < h$ and $J \geq h$, define two different magnetic phases of the system as mentioned above: in the former, the ground-state is unique and has maximal projection in the $\hat{x}$ direction and in the last phase the ground-state is two-fold degenerate and has finite projection along the interaction direction $\hat{z}$. The transition point $h = J$ marks a second-order ground-state phase transition (QPT) described by the order parameter $\langle\psi_0|\hat{S}_z|\psi_0\rangle$ [27, 29], which we discuss below.

2.4.1 The $\mathbb{Z}_2$ symmetry: spin flipping invariance

The symmetry responsible for the QPT in the LMG model is a discrete symmetry, referred in different ways in the literature: $\mathbb{Z}_2$ symmetry, spin-flip symmetry or parity symmetry [7, 27]. Let us clarify each of these names. Looking at the FCTFIM hamiltonian (2.1), one can see that its expression remains unchanged if we flip the direction of each spin along $\hat{z}$ direction, i.e., if we make the transformation $\hat{\sigma}_i^z \to -\hat{\sigma}_i^z$ for each i. This change is equivalent to make $\hat{S}_z \to -\hat{S}_z$ in the collective version (2.2) of the hamiltonian. This invariance under flipping of spins along $\hat{z}$ is naturally called spin-flip symmetry. On the other hand, the name $\mathbb{Z}_2$ symmetry refers to the fact that the operations of identity and inversion in the context of group theory form the group $\mathbb{Z}_2$ and the LMG hamiltonian is invariant under its action along $\hat{z}$ direction. Finally, the name parity symmetry is quite common in particle physics contexts and it is usually related to spatial inversion $\hat{z} \to -\hat{z}$, producing the same effect as the spin-flip symmetry in this case.

The transformation $\hat{S}_z \to -\hat{S}_z$ can be realized by a rotation around the x axis of π. Thus, the symmetry operator which represents this transformation is

$$\hat{\Pi} = e^{-i\pi\hat{S}_x} = \prod_{i=1}^{N} e^{-i\frac{\pi}{2}\hat{\sigma}_x^i}. \tag{2.35}$$

and acts on each collective spin according to

$$\hat{\Pi}\hat{S}_z\hat{\Pi}^{-1} = -\hat{S}_z, \qquad \hat{\Pi}\hat{S}_y\hat{\Pi}^{-1} = -\hat{S}_y, \qquad \hat{\Pi}\hat{S}_x\hat{\Pi}^{-1} = \hat{S}_x. \tag{2.36}$$

After expanding the exponential,

$$
\begin{aligned}
e^{-i\frac{\pi}{2}\hat{\sigma}_x^i} &= \sum_{n=0}^{]\infty} \left(-i\frac{\pi}{2}\sigma_x^i\right)^n \frac{1}{n!} \\
&= I - i\frac{\pi}{2}\sigma_x^i + \left(-i\frac{\pi}{2}\right)^2 \frac{1}{2}\left(\sigma_x^i\right)^2 + \left(-i\frac{\pi}{2}\right)^3 \frac{1}{3!}\left(\sigma_x^i\right)^3 + \cdots \\
&= I + \sigma_x^i\left[-i\frac{\pi}{2} + \left(-i\frac{\pi}{2}\right)^3 \frac{1}{3!} + \left(-i\frac{\pi}{2}\right)^5 \frac{1}{5!} + \cdots\right] + \left[\left(-i\frac{\pi}{2}\right)^2 \frac{1}{2!} + \left(-i\frac{\pi}{2}\right)^4 \frac{1}{4!} + \cdots\right] \\
&= I - i\sin\left(\frac{\pi}{2}\right)\sigma_x^i + \cos\left(\frac{\pi}{2}\right) \\
&= I - i\sigma_x^i.
\end{aligned}
\tag{2.37}
$$

and neglecting the identity I, since it commutes with every operator, we can represent this operation in the reduced form:

$$
\hat{\Pi} = \prod_{i=1}^{N} \hat{\sigma}_x^i. \tag{2.38}
$$

Note that the factor $-i$ multiplying σ_x^i in the last line of Eq. (2.37) can be seen as a global phase factor, which does not change observables and can be omitted as well. By construction, it is evident that $[\hat{\Pi}, \hat{H}] = 0$ for all J and h values, implying that these operators can be simultaneously diagonalized by the same eigenvectors.

As mentioned above, for $J \leq h$ the ground-state is unique $|\psi_0\rangle = |\leftarrow\rangle$ and has maximal projection along $-\hat{x}$ direction, that is, $\langle\psi_0|\hat{S}_x|\psi_0\rangle = -j$, hence

$$
\langle\hat{S}_z\rangle = 0, \qquad \text{for } J \leq h. \tag{2.39}
$$

In this case, the ground-state is symmetric as it satisfies $\hat{\Pi}|\psi_0\rangle = |\psi_0\rangle$. Conversely, in the ferromagnetic phase ($J > h$) and TL, there are two ground states, $|\psi_0^+\rangle$ and $|\psi_0^-\rangle$. For instance, for $h = 0$, we have $|\psi_0^+\rangle = |\uparrow\rangle_z$ and $|\psi_0^-\rangle = |\downarrow\rangle_z$, which are the states in the Bloch sphere such that $\langle\hat{S}_z\rangle = \pm j$ respectively. Interestingly, although the hamiltonian in this phase remains symmetric under $\hat{\Pi}$, the ground-states spontaneously break the symmetry, since

$$
\hat{\Pi}|\psi_0^{\pm}\rangle = \pm|\psi_0^{\mp}\rangle \tag{2.40}
$$

and, as mentioned previously, since in the ferromagnetic phase the ground-states display finite magnetization along $\hat{z}$, then

$$
\langle\hat{S}_z\rangle \neq 0, \qquad \text{for } J > h. \tag{2.41}
$$

It turns out that the quantity $\langle\psi_0|\hat{S}_z|\psi_0\rangle$ works as an order parameter for the QPT in the LMG

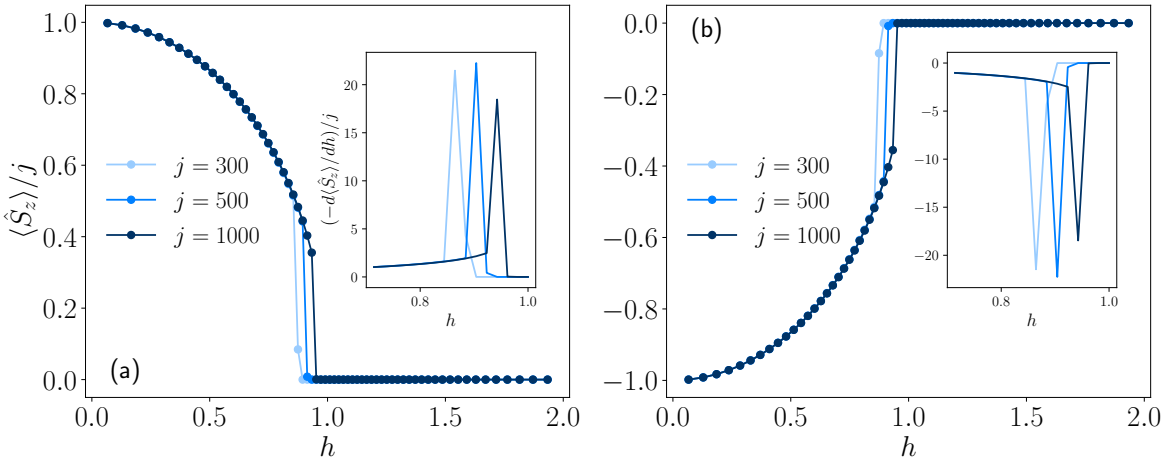

FIGURE 2.4: Total magnetization S_z of the ground-state as a function of the magnetic field strength h for $J = 1$. This quantity is the order parameter of the QPT in the LMG model: in the ferromagnetic phase ($h < J$), the ground-state breaks the $\mathbb{Z}_2$ symmetry and displays (a) positive finite magnetization or (b) negative finite magnetization, since the ground-state if two-fold degenerate in this phase. On the other hand, in the paramagnetic phase ($h \geq J$) the ground-state preserves the symmetry and displays null total magnetization. As $N = 2j$ increases, the non-analytic point approaches the critical point $h = J$. Inset: the numerical derivative of the magnetization w.r.t. h, showing a divergent behavior and an approaching to the actual critical point as N increases.

model, revealing itself finite for $J > h$ and null for $J \leq h$ (see the figure 2.4). The transition between these behaviors is such that the derivative of $\langle \psi_0 | \hat{S}_z | \psi_0 \rangle$ w.r.t. h for fixed J diverges at the critical point $h = J$ in the TL, as illustrated in the inset of the same figure. This divergence is the hallmark of any QPT.

It is important to highlight that these mentioned facts hold only in the TL. For finite N and $J > h$, the ground-state is no longer degenerate, even for $h = 0$ [30]. Because the system has finite size, the quantum fluctuations couple the ground-states by allowing tunneling between them. Hence, the actual ground-state becomes the symmetric linear combination

$$|\psi_0^S\rangle = \frac{1}{\sqrt{2}} \left(|\uparrow\rangle + |\downarrow\rangle \right), \tag{2.42}$$

and the first excited state the antisymmetric linear combination

$$|\psi_1^A\rangle = \frac{1}{\sqrt{2}} \left(|\uparrow\rangle - |\downarrow\rangle \right) \tag{2.43}$$

for $h = 0$ as an example. The gap between the energy of these two states decays exponentially with the system size [30, 31]

$$\Delta \sim e^{-aN}. \tag{2.44}$$

Note that both of these two linear combinations are eigenstates of $\hat{\Pi}$ and therefore for finite N, the ground-state preserves the $\mathbb{Z}_2$ symmetry. Moreover, in the TL the quantum fluctuations are suppressed, the gap between the ground-state and the first excited-state goes to zero and the system is forced to choose between one of the states $\{|\psi_0^+\rangle, |\psi_0^-\rangle\}$, consequently breaking the symmetry.

The $\mathbb{Z}_2$ character of the parity operator $\hat{\Pi}$ is reflected in its eigenvalues, which takes only the values $\{\pm 1\}$. Accordingly, the eigenstates of the Hamiltonian can be labeled as $\{|E_n, \alpha\rangle\}$, with associated eigenvalues $\{E_{n,\alpha}\}$, satisfying[3]

$$\hat{H}|E_n, \alpha\rangle = E_{n,\alpha}|E_n, \alpha\rangle, \tag{2.45a}$$

$$\hat{\Pi}|E_n, \alpha\rangle = \alpha|E_n, \alpha\rangle, \tag{2.45b}$$

where $\alpha = \pm 1$ denotes the parity and n indexes the energy levels possessing well-defined $\hat{\Pi}$ symmetry. The effect of the commutation relation between $\hat{H}$ and $\hat{\Pi}$ on the Hilbert space is separating each j-sector into two orthogonal subspaces. For example, the LMG Hamiltonian takes the form

$$\hat{H} = \begin{pmatrix} H_+ & 0 \\ 0 & H_- \end{pmatrix}. \tag{2.46}$$

where H_+ is the subspace of states with positive parity ($\alpha = 1$) and dimension $N/2 + 1$ and H_- is the subspace of states with negative parity ($\alpha = -1$) and dimension $N/2$. In each two-dimensional parity subspace spanned by $\{|E_n, +\rangle, |E_n, -\rangle\}$, the matrix representation of $\hat{\Pi}$ takes the simple form

$$\hat{\Pi} = \begin{pmatrix} 1 & 0 \\ 0 & -1 \end{pmatrix}, \tag{2.47}$$

2.5 Energy spectrum, density of states and excited state quantum phase transition

The LMG model reveals itself even more interesting when we look at the higher energy levels. In this section, we review features regarding excited states in order to show the LMG model exhibits one additional critical phenomenon called excited state quantum phase transition (ESQPT)

[3] Except for the ground-state in the TL of the ferromagnetic phase.

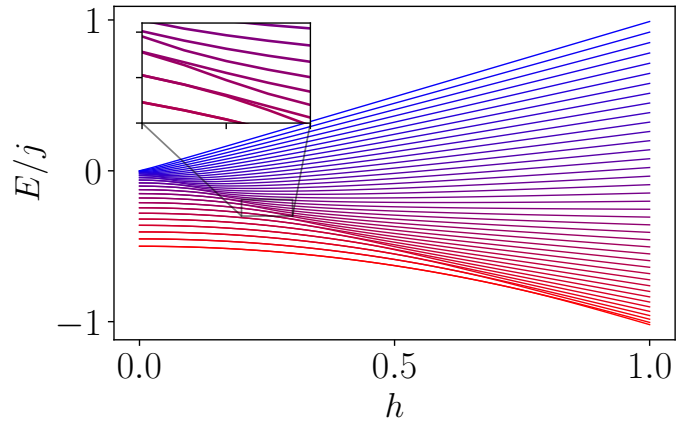

FIGURE 2.5: j-normalized energy levels of the LMG hamiltonian, Eq. (2.2), as a function of h for $J = 1$ and $N = 2j = 40$. From bottom to top, each line corresponds to the increasingly ordered energies $\{E_0(h), E_1(h), \cdots, E_{N+1}(h)\}$ respectively. One can see that in the ferromagnetic phase $(h < J)$ all the eigenstates of the hamiltonian with energy $E < E_c(h)$ are doubly degenerate, where $E_c(h)$ is a certain energy value depending on h. The inset makes easier the visualization by zooming in a region of splitting of energy levels. In the TL, $E_c(h) = -h$, precisely the energy of the separatrix orbit.

[8].

2.5.1 Effective double-well potential and sign symmetry

The figure 2.5 shows the j-normalized energy spectrum of the hamiltonian (2.2) as a function of h for $J = 1$ and $N = 2j = 40$. The lines from bottom to top correspond to the ground-states and excited states energies in increasing order respectively. The inset in the same figure zooms in a small region of the spectrum and highlights an interesting feature of the LMG hamiltonian: in the whole ferromagnetic phase ($h < J$), we see splitting of doubly degenerate eigenstates of the hamiltonian at a certain value of energy as a function of h. In other words, one can verify that not just the ground-state but all the eigenstates of the hamiltonian with energy $E < E_c(h)$ are doubly degenerate, where $E_c(h)$ is a certain energy value depending on h.

In the large-N regime, a numerical analysis of the energy spectrum reveals that the dependence with h of this transition energy between doubly and uniquely degenerate eigenstates is $E_c(h) = -h$, which is precisely the energy $\epsilon_c = -h$ in the TL of the separatrix orbit mentioned above in the section 2.4 [9, 32]. In fact, the change of degeneracy is related to the unstable point in the phase space. Let us prove this fact.

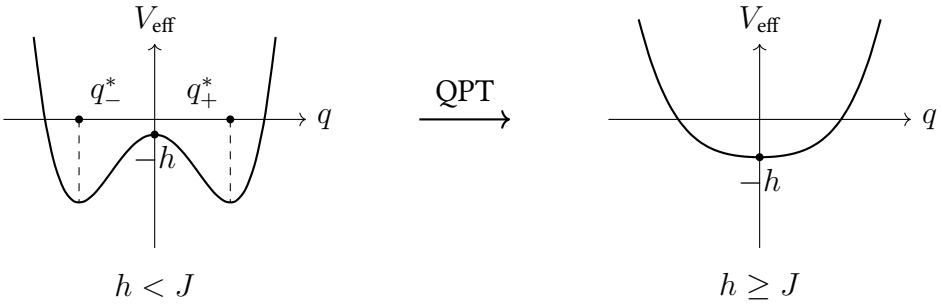

FIGURE 2.6: Shape transition in the effective potential from a double-well (left panel) in the ferromagnetic phase ($h < J$) to single-well shape (right panel) in the paramagnetic phase ($h \geq J$). The ground-state degeneracy changes from double to unique by crossing the QPT critical point $h = J$. Also, eigenstates with energy E less than the potential barrier's hight located at $q = 0$ in the ferromagnetic phase gets trapped either in one of the wells, thus having its magnetization sign conserved (see Eq.(2.26b)).

By separating quadratic and quartic terms in the classical hamiltonian, Eq. (2.27), one can rewrite it in the form

$$H_{\text{cl}}(q,p) = \frac{p^2}{2M(q)} + V_{\text{eff}}(q) \tag{2.48}$$

where

$$M(q) = \left(h - \frac{J}{4}q^2\right)^{-1} \tag{2.49}$$

$$V_{\text{eff}}(q) = \left(\frac{h-J}{2}\right)q^2 + \frac{J}{8}q^4 - h, \tag{2.50}$$

this hamiltonian can be seen as that one of a classical particle with position-dependent mass $M(q) = \left(h - \frac{J}{4}q^2\right)^{-1}$ in the effective double-well potential $V_{\text{eff}}(q) = \left(\frac{h-J}{2}\right)q^2 + \frac{J}{8}q^4 - h$. For $J > 0$, the analysis of its minima was done in the section 2.4: for $h < J$, the effective potential has two minima at $p = 0$ in the positions $q_\pm^* = \pm\sqrt{2(J-h)/J}$, which can be found by solving the equation $\frac{\mathrm{d}V_{\text{eff}}}{\mathrm{d}q} = 0$ and proceeding with the analysis of the second derivative sign. Besides these two minima, there is a third singular point at $q^* = 0$, which, however, is a local maximum point (unstable point) in the ferromagnetic phase, revealing the double-well shape of V_{eff}. On the other hand, for $h \geq J$, there is only one real solution of the equation $\frac{\mathrm{d}V_{\text{eff}}}{\mathrm{d}q} = 0$ as described previously at $(q,p) = (0,0)$, but now this point is a global minimum of V_{eff}. Thus, as mentioned before, the critical point $h = h_c = J$ marks a pitchfork bifurcation in the ground-state phase diagram $\langle \hat{S}_z \rangle \times h$ for fixed J (see figure 2.4 containing only one branch of the bifurcation) and a shape transition of the classical landscape from double to single-well as illustrated in Fig. 2.6.

Thus, when the system energy is $\epsilon < \epsilon_c$, the classical particle does not have enough energy to cross the central barrier of the double-well potential. It therefore remains trapped in one of

the wells and the phase space becomes topologically disconnected, that is, initial conditions in each side cannot access the other one. In contrast, for $\epsilon > \epsilon_c$, the particle can overcome the barrier and explore the whole available phase space. Since the average magnetization $\langle \hat{S}_z \rangle$ is proportional to q [Eq. (2.26b)], the sign of $\langle \hat{S}_z \rangle$ remains fixed along classical trajectories whenever $\epsilon < \epsilon_c$, being always positive or negative depending on the initial conditions. In other words, $\mathrm{sign}(Q(t)) = \mathrm{sign}(Z(t))$ is conserved during the dynamics. In terms of the Bloch sphere, the Bloch vector $\mathbf{M}$ has its precession restricted to one of the hemispheres depending on the initial conditions when $\epsilon < \epsilon_c$. For $\epsilon = \epsilon_c$, the Bloch vector touches the Equator line and for $\epsilon > \epsilon_c$, it is allowed to explore both hemispheres.

From the quantum perspective, this classical separation of phase space corresponds to the existence of states that are localized in each well. These localized states are the building blocks of the symmetric and antisymmetric combinations discussed in the previous section. Recovering the notation of the last section, a priori the states $\{|E_n, +\rangle, |E_n, -\rangle\}$ are, then, delocalized states, that is, states spreaded through both wells without definite $\mathrm{sign}(Z)$, which means that each $|E_n, \alpha\rangle$ must be a linear combination of states localized in one of the wells. The ground-state in the TL, however, is a special state, since the suppression of the quantum fluctuations makes the system choose one of these localized states, thus breaking the symmetry $\hat{\Pi}$.

Motivated by the conservation of $\mathrm{sign}(Z)$, the authors in [9, 32] introduced the heuristic operator

$$\hat{\mathcal{C}} = \mathrm{sign}(\hat{S}_z), \tag{2.51}$$

which commutes only with the Hamiltonian projected onto its subspaces where $E < E_c$,

$$[\hat{H}, \hat{\mathcal{C}}] \xrightarrow{N\to\infty,\ E<E_c} 0. \tag{2.52}$$

This means that $\hat{\mathcal{C}}$ is a partial symmetry of the LMG model and it is the one responsible for making all the eigenstates with $E < E_c$ doubly degenerate, thus proving the initial assertion. In this sense, if the operator $\hat{\mathcal{C}}$ is responsible for identifying in which well the state is localized, then given generic localized states $|L_n\rangle$ and $|R_n\rangle$, as mentioned above

$$|E_n, \pm\rangle = \frac{|R_n\rangle \pm |L_n\rangle}{\sqrt{2}} \tag{2.53}$$

and thus

$$|L_n\rangle = \frac{|E_n, +\rangle\ - |E_n, -\rangle}{\sqrt{2}}, \qquad |R_n\rangle = \frac{|E_n, +\rangle\ + |E_n, -\rangle}{\sqrt{2}}. \tag{2.54}$$

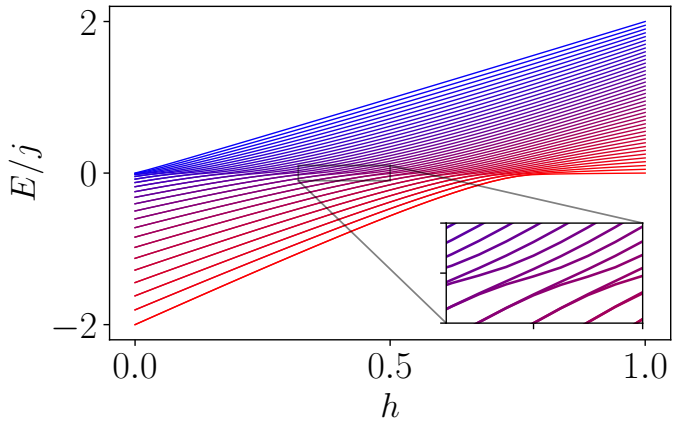

FIGURE 2.7: j-normalized energy levels of the parametrized LMG hamiltonian, Eq. (2.57), as a function of h for $N = 2j = 40$. The parametrization fixes the critical energy at $E_c = 0$. The inset helps the visualization of the splitting of levels in the region $E = 0$.

Now, because the operator $\hat{\mathcal{C}}$ must satisfy $\hat{\mathcal{C}}|L_n\rangle = -|L_n\rangle$ and $\hat{\mathcal{C}}|R_n\rangle = +|R_n\rangle$, then

$$\langle E_n, \pm|\hat{\mathcal{C}}|E_n, \mp\rangle = 1 \tag{2.55}$$

and therefore, in the parity-$\hat{\Pi}$ basis, the operator $\hat{\mathcal{C}}$ has the matrix form

$$\hat{\mathcal{C}} = \begin{pmatrix} 0 & 1 \\ 1 & 0 \end{pmatrix}. \tag{2.56}$$

The eigenvalues of $\hat{\mathcal{C}}$ in the localized basis $\{|L_n\rangle, |R_n\rangle\}$ must be identified using a different quantum number, let us choose β, since this symmetry is independent of $\hat{\Pi}$. Due to the matrix form of $\hat{\mathcal{C}}$, we have again $\beta \in \{\pm 1\}$, making $\hat{\mathcal{C}}$ be another $\mathbb{Z}_2$-type symmetry operator. For all values of J and h such that $J > h$, while the symmetry $\hat{\Pi}$ is broken only by the ground-state in the TL, the symmetry $\hat{\mathcal{C}}$ is broken by those eigenstates of $\hat{H}$ in the TL only in the range $E_n > E_c$, $\forall n$.

The character of genuine symmetry of $\hat{\mathcal{C}}$ is questionable for two reasons: (i) the operator $\hat{\mathcal{C}}$ commutes with $\hat{H}$ only in a certain region of the spectrum and (ii) taking the sign of an operator is a highly nonlinear and non-smooth operation, thus not allowing a representation of $\hat{\mathcal{C}}$ in terms of unitary or anti-unitary operators as expected from a symmetry operator. Thereby, $\hat{\mathcal{C}}$ is more like an emergent symmetry of the semiclassical problem and not a fundamental symmetry of the quantum LMG hamiltonian, Eq.(2.2). Finally, it is interesting to note that one can eliminate the dependence of E_c with h by parametrizing the LMG hamiltonian only in terms of h in the form

$$\hat{H}_h = -4\frac{1-h}{N}\hat{S}_z^2 + h\left(\hat{S}_x + \frac{N}{2}\right). \tag{2.57}$$

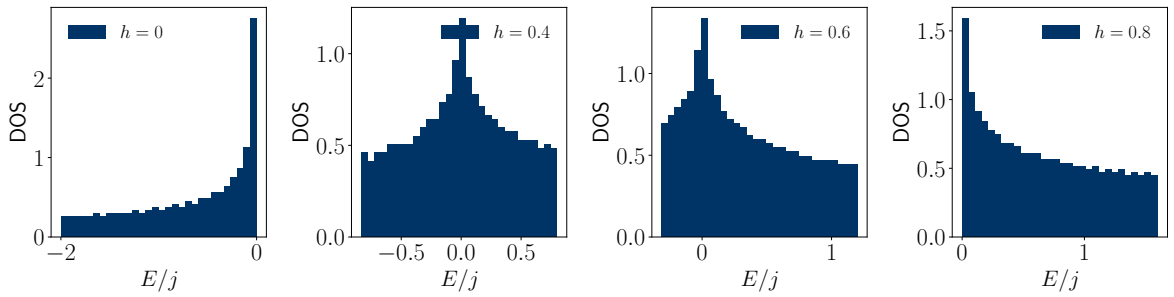

FIGURE 2.8: Histogram of the energy eigenvalues as a function of the j-normalized energy for $N = 800$ and different values of h. Using the parametrized version of the LMG model [Eq. (2.57)], a sharp peak appears at $E/j = 0$ corresponding to the critical energy of the ESQPT. In the TL, this peak becomes a logarithmic divergence in the DOS.

Upon this parametrization, which replaces J for $1-h$, the critical energy remains fixed at $E_c = 0$ and the energy spectrum has the form of the Fig. 2.7. This version of the LMG model appeared several times in the literature, e.g. in [25, 33, 34], and will be used later in this thesis.

2.5.2 Density of states and period of the separatrix orbit

The instability point in the ferromagnetic phase has important consequences for the density of states (DOS) and other properties of the model. One way to probe the DOS is by constructing a histogram of the eigenvalues of the LMG Hamiltonian. As shown in Fig. (2.8), a pronounced peak emerges at an energy that coincides with the unstable point of the classical phase space. In the TL, this peak turns into a logarithmic divergence, which constitutes the hallmark of the excited-state quantum phase transition (ESQPT) in the model [27]. An elegant theoretical framework for ESQPTs in systems with an arbitrary number f of degrees of freedom and unrestricted Hamiltonian functions $H(\mathbf{q}, \mathbf{p})$ was developed in Ref. [35] (see also Ref. [8]), and forms the basis of the discussion presented here.

The quantum level density for a system with discrete energy spectrum is defined by

$$\nu(E) = \sum_i \delta(E - E_i) \tag{2.58}$$

where δ is the Dirac distribution and $E_0 \leq E_1 \leq \cdots$ are the energy eigenvalues. The density of levels can always be written as the sum [36]

$$\nu(E) = \overline{\nu}(E) + \nu_{\text{osc}}(E) \tag{2.59}$$

with $\overline{\nu}(E)$ being the component which captures the mean energy dependence of $\nu(E)$ and $\nu_{\text{osc}}(E)$

being oscillatory component with mean zero which includes the effects of the quantum fluctuations. In the semiclassical limit, the oscillatory component becomes infinitely rapid and is washed out under arbitrarily weak energy smoothing. Consequently, we focus exclusively on the smooth part of the level density, that can be determined by the Weyl approximation calculating the size of the accessible phase space at a given energy [36]

$$\overline{\nu}(E) = \left(\frac{1}{2\pi\hbar}\right)^f \int \mathrm{d}^{2f}\mathbf{z}\, \delta(E - H(\mathbf{z})) = \frac{\partial}{\partial E}\Omega(E) \tag{2.60}$$

where $\mathbf{z} = (\mathbf{x}, \mathbf{p})$ is a $2f$-dimensional vector containing f-dimensional vectors of coordinates $\mathbf{q}$ and momenta $\mathbf{p}$ and $H(\mathbf{z})$ is the classical Hamiltonian of the system. Since the Dirac distribution can be written as the derivative of the Heaviside step function, then $\overline{\nu}(E)$ is the derivative of the volume function $\Omega(E) = \int_{H(\mathbf{z})\leq E} \mathrm{d}^{2f}\mathbf{z}$, which measures the volume of the phase space region satisfying $H(\mathbf{z}) \leq E$.

The component $\overline{\nu}(E)$ can develop non-analytic points even for analytical classical Hamiltonian forms at the points where the constant energy hypersurface crosses a stationary point of H. Indeed, one sees often in the literature the argument that $\overline{\nu}(E)$ shall develops non-analyticities since the Dirac delta can be rewritten using the identity

$$\delta(\chi(\mathbf{z})) = \sum_i \frac{\delta(\mathbf{z} - \mathbf{z}_{0i})}{|\nabla_n \chi(\mathbf{z}_{0i})|} \tag{2.61}$$

where $\chi(\mathbf{z})$ is any function satisfying $\chi(\mathbf{z}_{0i}) = 0$, that is, $\{\mathbf{z}_{0i}\}_i$ are the roots of χ and ∇_n stands for the n-dimensional gradient[4]. Thereby, it would appear in the integration of Eq. (2.60) the inverse gradient $1/|\nabla_{2f} H|$, which produces non-analyticities in the stationary points $\mathbf{z}^* = (\mathbf{q}^*, \mathbf{p}^*)$ where $\nabla_{2f} H(\mathbf{z}^*) = 0$. Although the vanishing of the gradient at stationary points is invoked heuristically, the true origin of the non-analytic behavior lies in the change of topology of the classical energy surface, which we clarify below.

Once again we can split the component $\overline{\nu}(E)$ isolating the local behavior of H near a certain stationary point $\mathbf{z}^*$ from the rest of the available phase space by writing

$$\overline{\nu}(E) = \overline{\nu}_{\mathrm{reg}}(E) + \overline{\nu}_{\mathbf{z}^*}(E). \tag{2.62}$$

The irregular part $\overline{\nu}_{\mathbf{z}^*}$ contains integration over a small phase space neighborhood of the stationary point and captures all non-analytic behavior of $\overline{\nu}(E)$ due to the stationary point. The regular part $\overline{\nu}_{\mathrm{reg}}(E)$ contains the integration over the rest of the accessible phase space and yields an analytic contribution to $\overline{\nu}(E)$. Thus, it is sufficient to analyze the properties of the irregular to study the singularities in the level density.

[4] This notation can be tricky. For example, note that ∇_2 is not the laplacian ∇^2.

A stationary point $\mathbf{z}^*$ is non-degenerate if the Hessian matrix of the second derivatives, with elements $\mathcal{H}_{ij}(\mathbf{z}^*) = \frac{\partial^2 H}{\partial \mathbf{z}_i \partial \mathbf{z}_j}\Big|_{\mathbf{z}^*}$, has no zero eigenvalues. In this case, the Morse lemma [37] guarantees that close to $\mathbf{z}^*$, one can choose coordinates $\mathbf{y}$ such that

$$H(\mathbf{y}) = H(\mathbf{z}^*) - \mathbf{y}_1^2 - \cdots - \mathbf{y}_r^2 + \mathbf{y}_{r+1}^2 + \cdots + \mathbf{y}_{2f}^2. \tag{2.63}$$

The equation above is simply an expansion of the Hamiltonian function near the point $\mathbf{z}^*$ truncated in the second order term. The term r is called index of the stationary point and corresponds to the dimension of the subspace of positive eigenvalues of the Hessian matrix, while $s = 2f - r$ corresponds to the dimension of the subspace of negative eigenvalues. Note that the negative terms correspond to directions in the phase space contributing to decrease the energy and the positive terms to increase the energy.

Substituting the local Hamiltonian [Eq. (2.63)] in the Weyl approximation [Eq. (2.60)], one gets two distinct results in terms of $\epsilon = E - E_c$ [35]: for r even (including $r = 0$), it yields

$$\overline{\nu}_{\mathbf{z}^*}(\epsilon) = f_1(\epsilon) + \frac{c_1 \hbar^{-f}}{\sqrt{\det \mathcal{H}(\mathbf{z}^*)}} (-1)^{r/2}\, \Theta(\epsilon)\, \epsilon^{f-1} \tag{2.64}$$

where f_1 is a non-singular function and c_1 is a positive constant. Note that the derivatives of $\overline{\nu}$ from order zero until $f - 2$ are continuous at $\epsilon = 0$, but the presence of the step function makes the $(f-1)$-th derivative discontinuous

$$\frac{\mathrm{d}^{f-1}\overline{\nu}_{\mathbf{z}^*}}{\mathrm{d}E^{f-1}} \propto (-1)^{r/2}\Theta(\epsilon). \tag{2.65}$$

For r odd, we have the formula

$$\overline{\nu}_{\mathbf{z}^*}(\epsilon) = f_2(\epsilon) + \frac{c_2 \hbar^{-f}}{\sqrt{\det \mathcal{H}(\mathbf{z}^*)}} (-1)^{\frac{r+1}{2}} \epsilon^{f-1} \ln|\epsilon|, \tag{2.66}$$

where again f_2 is a non-singular function and c_2 a positive constant. As in the previous case, $\overline{\nu}$ is continuous until the $(f-2)$-th derivative and the non-analyticity appears in the $(f-1)$-th derivative, now exhibiting a logarithmic divergence

$$\frac{\mathrm{d}^{f-1}\overline{\nu}_{\mathbf{z}^*}}{\mathrm{d}E^{f-1}} \propto (-1)^{\frac{r+1}{2}} \ln|\epsilon|. \tag{2.67}$$

The LMG model falls out in this last case. As shown in the appendix B, the Hessian matrix has two eigenvalues, one negative and one positive, such that the expanded Hamiltonian [Eq. (2.63)] reads

$$H(\mathbf{y}) = H(\mathbf{z}^*) - q^2 + p^2 \tag{2.68}$$

where $\mathbf{z}^* = (0,0)$ are the (q,p) coordinates of the saddle point. Then, we see that $r = 1$ in this particular case. Thus, the Weyl approximation for the LMG model is

$$\overline{\nu}(\epsilon) = \int \mathrm{d}q\, \mathrm{d}p\ \ \delta(\epsilon + q^2 - p^2). \tag{2.69}$$

By means of the identity in Eq. (2.61):

$$\delta(f(p)) = \sum_i \frac{\delta(p - p_i)}{|f'(p_i)|} \tag{2.70}$$

where $\chi(\mathbf{z}) \equiv f(p) = \epsilon + q^2 - p^2$ and whose roots are $p_\pm = \pm\sqrt{q^2+\epsilon}$, we can write

$$\delta(\epsilon + q^2 - p^2) = \frac{1}{2\sqrt{q^2+\epsilon}} \left[\delta(p - \sqrt{q^2+\epsilon}) + \delta(p + \sqrt{q^2+\epsilon})\right]. \tag{2.71}$$

Integrating over p

$$\int \mathrm{d}p\ \ \delta(\epsilon + q^2 - p^2) = \frac{1}{\sqrt{q^2+\epsilon}}. \tag{2.72}$$

Finally, it remains the integral

$$\overline{\nu}(\epsilon) = \frac{1}{2\pi\hbar} \int_{-\Lambda}^{\Lambda} \frac{\mathrm{d}q}{\sqrt{q^2+\epsilon}} = \frac{1}{\pi\hbar} \int_0^{\Lambda} \frac{\mathrm{d}q}{\sqrt{q^2+\epsilon}} \tag{2.73}$$

with Λ being the boundary of the interval on which the local quadratic expansion of H holds. The integral yields

$$\overline{\nu}(\epsilon) = \frac{1}{\pi\hbar} \left[\ln\left(\Lambda + \sqrt{\Lambda^2+\epsilon}\right) - \ln\left(\sqrt{\epsilon}\right)\right]. \tag{2.74}$$

The asymptotic behavior close to E_c corresponds to $|\epsilon| \ll \Lambda$. After expanding

$$\sqrt{\Lambda^2+\epsilon} = \Lambda + \mathcal{O}(\epsilon), \tag{2.75}$$

we finally obtain the logarithmic divergence of $\overline{\nu}$ close to E_c

$$\overline{\nu}(E) \sim \frac{1}{\pi\hbar} \left[\ln(2\Lambda) - \frac{1}{2}\ln|E - E_c| + \mathcal{O}(\epsilon)\right]. \tag{2.76}$$

As mentioned above, the physical origin of the non-analytic behavior in $\nu(E)$ lies in the change of topology of the classical energy surface. When one crosses the critical energy E_c, an abrupt connection occurs between the two previously unconnected sectors of phase space. This connection causes an abrupt change in the volume function $\Omega(E)$, which is captured by the

derivative in Eq. (2.60).

The period of the classical orbit with energy E_c shall also be a marker of the ESQPT, since these two quantities are directly linked. The classical action of a certain orbit with energy E in a 1D system is given by

$$S(E) = \oint p(q;E)dq. \tag{2.77}$$

The Bohr-Sommefeld quantization rule imposes that for a given energy level E_n

$$S(E_n) = 2\pi\hbar\left(n + \frac{1}{2}\right). \tag{2.78}$$

Differentiating the equation above, we have

$$\frac{\mathrm{d}S}{\mathrm{d}E}\frac{\mathrm{d}E_n}{\mathrm{d}n} = 2\pi\hbar. \tag{2.79}$$

But the first derivative is precisely the period of the orbit

$$\frac{\mathrm{d}S}{\mathrm{d}E} = \oint \frac{\mathrm{d}p(q,E)}{\mathrm{d}E}dq = \oint \frac{\mathrm{d}q}{\dot{q}} = T(E) \tag{2.80}$$

where it was used that the condition $H(q,p(q;E)) = E$ implies that $\frac{\partial H}{\partial p}\frac{\partial p}{\partial E} = 1$ and also the Hamilton equation $\dot{q} = \frac{\partial H}{\partial p}$. The second derivative, $\frac{\mathrm{d}E_n}{\mathrm{d}n}$, measures the spacing between quantum levels and the quantum level density, $\nu(E)$, is precisely the inverse of that

$$\nu(E) = \frac{\mathrm{d}n}{\mathrm{d}E} = \frac{T(E)}{2\pi\hbar}. \tag{2.81}$$

Therefore, if $\nu(E)$ diverges at $E = E_c$, the period $T(E)$ of the separatrix orbit must diverge as well. See [24, 38] for explicit and exact calculations of the period in the LMG model.

2.6 Generalized microcanonical ensemble

A central assumption underlying conventional statistical mechanics is that the equilibrium properties of many-body systems are determined by a small set of conserved quantities, typically restricted to the total energy. Under this assumption, generic quantum systems are expected to thermalize and be described by standard statistical ensembles, such as the microcanonical or canonical ensemble. However, this paradigm breaks down in the presence of additional constraints, most notably in integrable quantum systems, which possess an extensive number of conserved quantities that strongly restrict their accessible phase space.

The relevance of generalized ensembles extends beyond strictly integrable models and plays an important role in understanding equilibration in systems with constrained or fragmented Hilbert spaces [39–41], including collective quantum models with emergent symmetries and macroscopic degeneracies. In this direction, Corps and Relaño [32] identified the important symmetries in the LMG model and derived a generalized microcanonical ensemble (GME) which describes exactly the long-time stationary properties, thereby stabilishing a connection between two important phenomena: dynamical phase transitions (DPT) and the ESQPT. Moreover, by considering a minimal set of symmetry assumptions, which are fulfilled by a broad class of quantum many-body systems with infinite-range interactions, Corps and Relaño [9] showed that the crossing of the critical energy is a necessary condition for the emergence of DPTs. We reproduce in this section the GME for the LMG model and cover the connection between DPT and ESQPT in the next chapter.

As the authors emphasize in Ref. [32], although all numerical results in the paper concern the LMG model (the FCTFIM restricted to the Dicke subspace), their theory is applicable to a broad class of collective quantum systems fulfilling the following assumptions: Given a Hamiltonian $\hat{H}(\lambda)$ depending on some experimentally controllable parameter λ, then

1. There is a discrete $\mathbb{Z}_2$ symmetry represented by an operator $\hat{\Pi}$ with eigenvalues $\alpha = \pm 1$ satisfying $[\hat{H}(\lambda), \hat{\Pi}] = 0, \ \ \forall \lambda$, which allows to classify the eigenstates of $\hat{H}$ according to $\hat{\Pi}|E_n, \alpha\rangle = \alpha|E_n, \alpha\rangle$. Examples of this symmetry are the spin-flip symmetry $\hat{S}_z \to -\hat{S}_z$ in the LMG model and the symmetry $\hat{a} \to -\hat{a}$ in Rabi and Dicke models [42].

2. There is a critical value $\lambda = \lambda_c$, which marks a QPT and separates two ground-state phases. For $\lambda < \lambda_c$, the ground-state is two-fold degenerate in the TL (the pair of states with different parity $|E_0, +\rangle, |E_0, -\rangle$ has the same energy) and breaks the symmetry $\hat{\Pi}$. For $\lambda > \lambda_c$, the ground-state is unique and preserves the symmetry $\hat{\Pi}$. In the LMG model, the first phase is the ferromagnetic ordered phase and the second phase is the paramagnetic phase.

3. In the ordered phase, $\lambda < \lambda_c$, some properties of the ground-state are extended to some excited states with energy $E_0 < E < E_c$. For exemple, all the eigenstates of $\hat{H}$ with energy $E < E_c$ are two-fold degenerate in the TL, but the eigenstates with $E > E_c$ are unique. These two new phases are separated by a critical energy E_c which marks a singularity in the DOS. The nature of this singularity depends on the semiclassical limit of the system. For systems with only one semiclassical degree of freedom, the singularity is typically a logarithmic divergence.

If a closed quantum system reaches an equilibrium state representing an equilibrium ensemble, this state is necessarily equal to the infinite-time average of the real time-evolved wavefunction [43]. Consider the time evolution of an initial state, $|\psi_0\rangle$

$$|\psi_t\rangle = \sum_{i,\alpha} c_{i,\alpha} e^{-iE_{i,\alpha}t} |E_i, \alpha\rangle \tag{2.82}$$

where $c_{i,\alpha} = \langle E_i, \alpha|\psi_0\rangle$. The equilibrium ensemble represented by the long-time averaged density matrix is

$$\begin{aligned} \rho_{eq} &= \lim_{T\to\infty} \frac{1}{T} \int_0^T |\psi_t\rangle\langle\psi_t| \, \mathrm{d}t \\ &= \sum_{i,j} \sum_{\alpha,\beta} \lim_{T\to\infty} \frac{1}{T} \int_0^T c_{i,\alpha} c^*_{j,\beta} e^{-i(E_{i,\alpha} - E_{j,\beta})t} \, |E_i, \alpha\rangle\langle E_j, \beta| \, \mathrm{d}t. \end{aligned} \tag{2.83}$$

The integral above is usually evaluated using the diagonal approximation. It consists of eliminating all the terms for which $E_{i,\alpha} \neq E_{j,\beta}$, since they contribute to the integral with fastly oscillating terms, thus averaging to zero. However, for the class of systems we are considering, the degeneracies play special role. Below the critical energy E_c, the eigenvalues of $\hat{H}$ are degenerate in pairs ($E_{i,+} = E_{i,-}$) and therefore, the corresponding non-diagonal terms remain after the integration. On the other hand, above the critial energy $E_{i,+} \neq E_{i,-}$ and only diagonal terms contribute to the average. Thereby, the equilibrium state is qualitatively different in both regions of the spectrum

$$\hat{\rho}_{\text{eq}}(E < E_c) = \sum_{\substack{i,\ k \\ E_i < E_c}} |c_{i,k}|^2 |E_i, k\rangle\langle E_i, k| + \sum_{\substack{i \\ E_i < E_c}} c_{i,+} c^*_{i,-} |E_i, +\rangle\langle E_i, -| + \text{h.c.} \tag{2.84a}$$

$$\hat{\rho}_{\text{eq}}(E > E_c) = \sum_{i,\ k} |c_{i,\alpha}|^2 |E_i, k\rangle\langle E_i, k|. \tag{2.84b}$$

where $k = \pm 1$ are the eigenvalues of $\hat{\Pi}$.

Below E_c, the degenerate parity doublets support a nontrivial internal structure. A consistent description of the stationary state therefore requires the inclusion of the operator $\hat{\mathcal{C}}$ in the generalized ensemble describing this region of the spectrum. However, the noncommuting charges $\hat{\Pi}$ and $\hat{\mathcal{C}}$ are not sufficient to completely specify the stationary state, since there is an additional continuous degree of freedom associated to the relative phase between $\{|E_n, +\rangle, |E_n, -\rangle\}$. Note that the $\hat{\Pi}$ acts as $\hat{\sigma}_z$ [Eq. (2.47)] and $\hat{\mathcal{C}}$ acts as $\hat{\sigma}_x$ [Eq. (2.56)] in the degenerate parity subspace. The missing part is another charge which acts as $\hat{\sigma}_y$ to close the internal $\mathfrak{su}(2)$ algebra. For this

reason, Corps and Relaño [32] postulated the operator[5]

$$\hat{\mathcal{Q}} = \frac{i}{2}[\hat{\mathcal{C}}, \hat{\Pi}]. \tag{2.85}$$

Similarly to $\hat{\mathcal{C}}$, $\hat{\mathcal{Q}}$ commutes only with $\hat{H}$ projected on the region $E_n < E_c$. Given that $\hat{\Pi}|E_n, \pm\rangle = \pm|E_n, \pm\rangle$ and $\hat{\mathcal{C}}|E_n, \pm\rangle = |E_n, \mp\rangle$, one can show that $\hat{\mathcal{Q}}|E_n, \pm\rangle = \pm i|E_n, \mp\rangle$. Therefore, within each degenerate parity doublet, $\langle\hat{\Pi}\rangle$ measures the population imbalance between even and odd sectors, corresponding to the z-component of an effective Bloch vector, while $\langle\hat{\mathcal{C}}\rangle$ and $\langle\hat{\mathcal{Q}}\rangle$ give information about the relative phases, corresponding to the x and y components of an effective Bloch vector.

One can think that is necessary two different ensembles to describe the equilibrium state of the model, implying that the transition between the two regions separated by E_c is ill defined. However, we can connect the two parts by defining global operators

$$\widetilde{\mathcal{C}} = \mathbb{I}_{E<E_c}\hat{\mathcal{C}}\,\mathbb{I}_{E<E_c} \tag{2.86}$$

$$\widetilde{\mathcal{Q}} = \mathbb{I}_{E<E_c}\hat{\mathcal{Q}}\,\mathbb{I}_{E<E_c} \tag{2.87}$$

where $\mathbb{I}_{E<E_c} = \sum_n \theta_n P_n$, P_n is the projector onto the subspace with energy E_n and $\theta_n = 1$ if $E < E_c$ or $\theta_n = 0$ if $E > E_c$. In this form, $\langle\widetilde{\mathcal{C}}\rangle$ and $\langle\widetilde{\mathcal{Q}}\rangle$ are equal to $\langle\hat{\mathcal{C}}\rangle$ and $\langle\hat{\mathcal{Q}}\rangle$ respectively below the critical energy and identically equal to zero above it.

While the infinite-time averaged density matrix provides an exact description of the stationary state of a closed quantum system, it remains strongly dependent on microscopic details of the initial condition, as it retains the full set of overlaps with the energy eigenstates. As such, this object does not yet constitute a statistical ensemble in the thermodynamic sense. In order to obtain a universal description of equilibration, it is necessary to perform a coarse-graining in energy, replacing the exact diagonal ensemble by a statistical ensemble defined within a narrow microcanonical window centered at the mean post-quench energy. This step is fully analogous to the standard construction of equilibrium statistical mechanics and reflects the fact that, in the thermodynamic limit, the energy distribution of the time-evolved state becomes sharply peaked.

In generic quantum systems, such a microcanonical description is sufficient to characterize stationary properties. However, in the presence of macroscopic degeneracies associated with emergent symmetries, as occurs below the critical energy E_c in the LMG model, the microcanonical ensemble alone fails to capture the internal structure of the degenerate subspaces. In this regime, equilibration does not lead to a complete loss of coherence within each parity doublet, and additional conserved quantities are required to fully specify the stationary state. This observation motivates the introduction of a generalized microcanonical ensemble (GME), which

[5]We changed the original notation from $\hat{\mathcal{K}}$ to $\hat{\mathcal{Q}}$ in order to avoid confusion with the notation from chapter 4.

supplements the energy constraint with additional charges encoding the internal $SU(2)$ structure of the degenerate parity subspaces. As the authors in [32] argument, the simplest choice for such an ensemble is

$$\rho_{\text{GME}}(E,p,c,q) = \hat{\rho}_{\text{ME}} \cdot \left(\mathbb{I} + p\hat{\Pi} + c\,\widetilde{\mathcal{C}} + q\,\widetilde{\mathcal{Q}}\right) \tag{2.88}$$

where

$$\hat{\rho}_{\text{ME}} = \frac{1}{2(N_+ + N_-)} \sum_{n:|E-E_n|<\Delta E} |E_{n,+}\rangle\langle E_{n,+}| + |E_{n,-}\rangle\langle E_{n,-}| \tag{2.89}$$

denotes the usual microcanonical ensemble in which the parity doublets lie within a small energy window centered on E and are equally populated irrespective of whether these parity doublets are degenerate. The terms $N_\pm$ denote the number of parity doublets populated by the dynamics above (N_+) or below (N_-) E_c. The numbers (p,c,k) are real parameters fixed by requiring that $\text{Tr}\left[\rho_{\text{GME}}\hat{\Pi}\right] = \langle\hat{\Pi}\rangle$, $\text{Tr}\left[\rho_{\text{GME}}\,\widetilde{\mathcal{C}}\right] = \langle\widetilde{\mathcal{C}}\rangle$ and $\text{Tr}\left[\rho_{\text{GME}}\,\widetilde{\mathcal{Q}}\right] = \langle\widetilde{\mathcal{Q}}\rangle$. In the large-$j$ limit, these values can be deduced exactly

$$\langle\hat{\Pi}\rangle = p, \tag{2.90a}$$

$$\langle\widetilde{\mathcal{C}}\rangle = c\frac{N_-}{N_+ + N_-}, \tag{2.90b}$$

$$\langle\widetilde{\mathcal{Q}}\rangle = q\frac{N_-}{N_+ + N_-}, \tag{2.90c}$$

thus, allowing to calculate (p,c,q). We list some properties of the GME:

- For a state with $E_{n,k} < E_c$ within the energy window, the matrix form of the GME in the subspace spanned by $\{|E_{n,+}\rangle, |E_{n,-}\rangle\}$ is

$$\rho_n(E_{n,k} < E_c) = \frac{1}{2}\begin{pmatrix} 1+p & c-iq \\ c+iq & 1-p \end{pmatrix}. \tag{2.91}$$

  We see that $\text{Tr}[\rho_n^2(E_{n,k} < E_c)] = (1+p^2+c^2+q^2)/2$, so any physical state must satisfy $p^2+c^2+q^2 \leq 1$.

- For a state with $E_{n,k} > E_c$ within the energy window, the GME takes the diagonal form

$$\rho_n(E_{n,k} < E_c) = \frac{1}{2}\begin{pmatrix} 1+p & 0 \\ 0 & 1-p \end{pmatrix}. \tag{2.92}$$

- For a state with energy value lying outside the energy window, the GME is a null matrix $\rho_n = 0 \times \mathbb{I}_2$.

Symmetry	Operator	Condition of commutation with $\hat{H}$
Spin-flip symmetry	$\hat{\Pi} = e^{-i\pi\hat{S}_x}$	All values of E, J and h
Sign symmetry	$\hat{\mathcal{C}} = \text{sign}(\hat{S}_z)$	$E < E_c$
Complex symmetry	$\hat{\mathcal{Q}} = \frac{i}{2}[\hat{\mathcal{C}}, \hat{\Pi}]$	$E < E_c$

TABLE 2.1: Table of the relevant symmetries of the LMG model represented by operators which commute with the hamiltonian in the TL under the condition specified in the third column.

- For the three cases above, in the parity basis $\{|E_{0,+}\rangle, |E_{0,-}\rangle, \cdots, |E_{N-1,+}\rangle, |E_{N-1,-}\rangle\}$, the complete density matrix of the GME is the block-diagonal matrix given by $\rho_{\text{GME}} = \bigoplus_n \rho_n/Z$, where $Z = N_+ + N_-$ is a normalization constant.

We close this section summarizing the relevant symmetries of the LMG Hamiltonian in the table 2.1

2.7 Experimental realizations

Despite its origin as a theoretical many-body model, the LMG Hamiltonian has found multiple avenues for experimental implementation and simulation across contemporary quantum platforms. These experimental efforts serve both to probe fundamental aspects of collective quantum behavior — including quantum phase transitions and dynamics — and to benchmark emerging technologies such as noisy intermediate-scale quantum (NISQ) devices.

One of the most direct experimental routes to realize LMG-like dynamics uses ultracold atomic ensembles coupled to optical cavities [44, 45]. In such systems, atoms confined in a high-finesse cavity interact collectively via the cavity mode, inducing effective all-to-all spin interactions characteristic of the LMG model. By tuning the detuning and driving parameters, the interaction Hamiltonian can be engineered to interpolate between central-mode and LMG regimes, revealing ferromagnetic to paramagnetic crossovers and low-energy excitation structures reflective of the underlying collective spin model. This experimental route allowed the observation of dynamical phase transition in the LMG model [45], which will be covered in the next chapter.

More recently, the LMG model has also been investigated within the framework of quantum computing, particularly through hybrid quantum–classical algorithms such as the Variational Quantum Eigensolver (VQE) [46]. In these experiments, the dynamics or spectral properties of the LMG Hamiltonian are digitally encoded into quantum circuits acting on a finite register of qubits, rather than arising from intrinsic interactions of the physical system itself. The implementation on neutral-atom quantum processor employed VQE to approximate ground-state properties of the LMG model by mapping the collective spin Hamiltonian onto controllable atomic qubits and engineering the corresponding unitary evolution through sequences of quantum gates. In this sense, what is realized experimentally is not an analog physical system governed by an effective

LMG interaction, but rather a digital simulation of the action of the LMG Hamiltonian on the atomic degrees of freedom.

This distinction highlights the conceptual difference between analog quantum simulations, where the target Hamiltonian emerges naturally from the system's microscopic interactions, and digital quantum simulations, where its effects are reconstructed algorithmically through gate-based control. Despite current limitations imposed by finite system size and noise, such digital simulations establish the LMG model as a valuable benchmark for variational algorithms and as a testbed for exploring collective many-body physics on noisy intermediate-scale quantum (NISQ) devices.

Still quite recently, the LMG model has been implemented in the context of analog quantum simulation using superconducting circuits [47]. A particularly striking example is the use of a single transmon qudit with d up to 9 levels to simulate its dynamics directly in hardware. In this approach, effective evolution under the LMG Hamiltonian is engineered by moving to a rotated frame in which continuous analog drives realize both local fields and collective spin-twisting interactions. This allows the experimental observation of finite-size precursors of quantum criticality, such as dynamical phase transitions, energy gap closing, Kibble-Zurek-like scaling, order parameter statistics, and signatures of excited-state phase transitions, all without decomposing the evolution into discrete quantum gates.

Finally, there are other theoretical proposals for experimental implementation, for example, based on Bose-Einstein condensates by coupling dispersively a Bose-Einstein condensate (BEC) to an optical cavity and using Feshbach resonance to have complete control of the physical parameters [48] or coupling the BEC to mechanical resonators [49]. These schemes also allows the exploration of transitions between magnetic orderings and probing long-range interaction effects. Experimental setups for dissipative versions of the LMG hamiltonian are also present in the literature, which offers measurable signatures of the critical behavior, including that of the spin-spin entanglement [50].

Chapter 3

Dynamical Phase Transitions

In this chapter, we introduce the theory of the dynamical quantum phase transitions (DQPT), giving an account of the most important concepts underlying these phenomena. Two variants of this phenomenon are presented: DQPTs described in terms of Loschmidt functions (dubbed as DPT-II) and DQPTs described in terms of equilibrium order parameters (dubbed as DPT-I). Although we chose to cover firstly the DPT-II, the variant of our main interest is DPT-I. After presenting the theory, we particularize the discussion on the LMG model and cover the connection between DPT-I and ESQPT.

3.1 Dynamical quantum phase transition

3.1.1 Global Quenches and Survival Amplitude

The theory described in this chapter finds application to quantum many-body systems described by a Hamiltonian $\hat{H}(\lambda_1, \cdots, \lambda_M)$, which can depend on a set of externally controllable parameters $\{\lambda_i\}_i$, i.e., parameters that can be freely tuned in the experiment along the dynamics. However, all the examples appearing in this thesis corresponds to the case when the set of parameters $\{\lambda_i\}_i$ consists of a unique parameter λ for simplicity. In our treatment, we will consider this quantum many-body system very well isolated from its surrounding environment such that its unitary dynamics can be satisfactorily realized in the laboratory.

One very important protocol widely used in the study of non-equilibrium dynamics is the so-called global quench. It consists of preparing the system in a certain initial state $|\psi_0\rangle$ of the hamiltonian $H(\lambda_0) \equiv H_0$ for an initial value of the parameter, $\lambda = \lambda_0$. Afterwards, we make a sudden change $\lambda_0 \to \lambda_f$ in the parameter and we let the system to evolve under the new hamiltonian $\hat{H}(\lambda_f) \equiv \hat{H}_f$, such that, for $t > 0$ the future state will be ($\hbar = 1$):

$$|\psi_t\rangle = e^{-iH_f t}|\psi_0\rangle. \tag{3.1}$$

In other words, what precisely defines the quench is when the sudden change in the hamiltonian by the parameter from λ_0 to λ_f happens instantaneously fast. This protocol quickly drives the

system far from equilibrium if $|\psi_0\rangle$ is not an eigenstate of $\hat{H}_f$ [2], as it will be the cenario treated throughout this text. The adjetive global in *global quenches* here referes to the fact that the sudden change $\lambda_0 \rightarrow \lambda_f$ is extensively appreciated by the system, that is, if we take a spin system, it means that all spins in the lattice *feels* the quench at the same time. This protocol contrasts with the *local quenches*, in which a smaller part of the system suffers the quench, a protocol also widely studied [51, 52]. The hamiltonians $\hat{H}_0$ and $\hat{H}_f$ will be frequently refered as pre-quench and post-quench hamiltonian respectively throughout this thesis.

When the initial state $|\psi_0\rangle$ lies in the ground-state manifold of $\hat{H}_0$, an interesting phenomenon called Dynamical Quantum Phase Transition (DQPT) can be triggered by the quench[1] [5, 53]. The central quantity in the theory behind DQPT is the survival amplitude

$$A(t) = \langle\psi_0|\psi_t\rangle = \langle\psi_0|e^{-iH_f t}|\psi_0\rangle \tag{3.2}$$

also called return probability amplitude or Loschmidt amplitude in this context. In the expression above, $|\psi_0\rangle$ is the ground state of the prequench hamiltonian $\hat{H}_0$ and $\hat{H}_f$ is the postquench hamiltonian. The survival amplitude has a formal connection with the canonical partition function, as it shall be shown later. For this reason, if we recall that the canonical partition function, Z, is linked to the Helmholtz free-energy F according to

$$Z = e^{-\beta F} = e^{-\beta N f} \tag{3.3}$$

where β is the inverse of temperature and $f = F/N$ is the free-energy per particle [54]. Then we shall expect a scaling relation for the survival amplitude given by

$$A(t) = e^{-Nf(t)} \tag{3.4}$$

in which

$$f(t) = -\lim_{N\to\infty} \frac{1}{N} \log\left[A(t)\right] \tag{3.5}$$

is called rate function and plays the role of a dynamical free-energy, since F is proportional to the logarithm of Z in (3.3). From the equation above, we see that if $\langle\psi_0|$ and $|\psi_t\rangle$ become orthogonal at a certain instant t', then the unscaled rate function $F(t') = -\log[A(t')]$ diverges, exactly what happens for equilibrium phase transitions. We will see along this chapter that $\langle\psi_0|$ and $|\psi_t\rangle$ being orthogonal is not the only condition for occurring DQPTs.

The probability of return of $|\psi_t\rangle$ to the ground-state is given by

$$\mathcal{L}(t) = |A(t)|^2 \tag{3.6}$$

[1] Here and from now on, quench will be used to mean global quenches. Other protocols will be left out of the scope of this text.

and it is called survival probability or Loschmidt echo in this context, having the same scaling relation as the previous quantities,

$$\mathcal{L}(t) = e^{-N\lambda(t)}, \tag{3.7}$$

with $\lambda(t) = 2\,\mathrm{Re}\{f(t)\}$.

In the presence of discrete symmetries in the system, the ground-state may be degenerate. In this case, the survival probability shall be generalized to include all the states spanning the manifold to the form

$$\mathcal{L}(t) = \sum_{i=1}^{\nu} \mathcal{L}_i(t) = \sum_{i=1}^{\nu} |\langle \psi_i^0 | \psi_t \rangle|^2 \tag{3.8}$$

with ν being the degeneracy. This definition can also be generalized in terms of an integral over the ground-state manifold in the presence of continuum symmetries [55]. It suggests that the phenomenon of DQPT is linked to the return of $|\psi_t\rangle$ to the ground-state manifold and not uniquely one of the spanning states of this manifold.

Let us now give the precise definition of an DQPT. Typically, a DQPT is associated with a kink in the rate function $\lambda(t)$ at certain time instants called critical times, t_c. The typical functional behavior in the vicinity of the critical time, t_c, is given by

$$\lambda(t) \sim \left| \frac{t - t_c}{t_c} \right|. \tag{3.9}$$

This behavior appears in several 1D systems, however, the manifestation of DQPT's surprisingly showed itself dependent of the dimensionality and some characteristics of the model. In 2D systems different structures have been found, for example, in Chern insulators a sudden change in the topology of the hamiltonian can induce DQPT with power-law nonanalyticities [56] and in 2D Ising models one finds logarithmic singularities [57].

It is important to mention that nonanalytic real-time behavior of survival amplitudes has been previously recognized already by Pollmann *et. al,* [58], but the interpretation as a dynamical critical phenomenon was only first pointed out by Heyl *et. al.* in Ref.[53]. In order to explain how the survival amplitude can give rise to a phenomenon that can be described as a phase transition, we resort on the theory of Lee-Yang-Fisher zeros [59–61], which are the zeros of the complex partition function.

3.1.2 Complex partition functions and Lee-Yang-Fisher zeros

We start by noting that the survival amplitude has a formal relation with a specific class of partition functions called boundary partition function. Consider a system in equilibrium with boundary conditions imposed on two ends with a distance z apart from each other. Then the

boundary partition function is given by [62]

$$Z_B = \langle\psi_1|e^{-z\hat{H}}|\psi_2\rangle \tag{3.10}$$

where $|\psi_1\rangle$ and $|\psi_2\rangle$ are the boundary conditions and $\hat{H}$ the bulk hamiltonian. Thus, the survival amplitude is the boundary partition function in the particular case when $z = it$ and $|\psi_1\rangle = |\psi_2\rangle = |\psi_0\rangle$ and in this case the ket $|\psi_0\rangle$ plays the role of a boundary in time instead of space. Once recognized this formal relation, we can now apply the standard method in the study of phase transitions, namely, the extension to the complex plane.

Let us consider the survival amplitude now with $t \to z = t + i\tau$ being a complex number:

$$A(z) = \langle\psi_0|e^{-iHz}|\psi_0\rangle. \tag{3.11}$$

In the case of finite systems, the survival amplitude is an analytical function. For a wide range of quantum systems, such as spins systems and fermionic systems, this fact can be shown by inserting the completeness of the energy basis in the expression above, which reads

$$A(z) = \sum_n |\langle E_n|\psi_0\rangle|^2 e^{-iE_n z}. \tag{3.12}$$

If the system is finite sized, then the sum above involve a finite number of analytic functions and therefore yields an analytic function. Because $A(z)$ is analytic, then the Weierstrass factoration theorem allows us to write [63]

$$A(z) = e^{\mu(z)} \prod_j \left(1 - \frac{z}{z_j}\right) \tag{3.13}$$

where z_j are the roots of $A(z)$ in the complex plane and $\mu(z)$ is an analytic function. As the function $\mu(z)$ is analytic, then the singular part of the rate function [Eq. (3.5)] will be uniquely due to the zeros of $A(z)$ and given by

$$f_s(z) = -\frac{1}{N} \sum_j \log\left(1 - \frac{z}{z_j}\right). \tag{3.14}$$

Just as for the equilibrium phase transitions, the points z_j are isolated points in the complex plain for $N < \infty$, however as we increase the system size, these points accumulate in lines or areas depending on the system characteristics [64] (see the figure 3.1 for an illustration). We see that after the complexification in Eq.(3.10), if the complex parameter $z = t$, i.e., its imaginary part is zero, then Z_B will coincide with the survival amplitude, $A(t)$. Therefore, a DQPT occurs whenever the lines or areas of Fisher zeros cross the real time axis and this crossing point is called critical time. A further characterization of the Fisher zeros can be devised firstly taking the

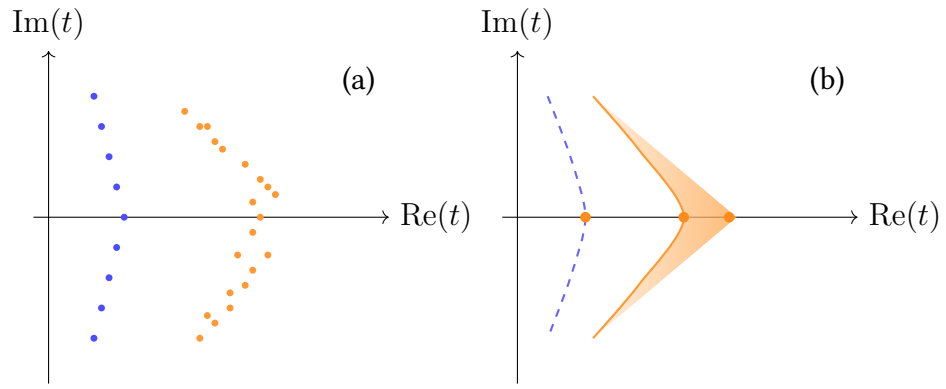

FIGURE 3.1: Schematic illustration of Fisher zeros: (a) When the system is finite sized, the zeros appear as points in the complex plain and (b) upon increasing the system size, we can observe two different situations: the Fisher zeros can accumulate in lines or areas and the DQPT occurs whenever these lines or areas cross the real time axis. Figure inspired by Ref.[5].

thermodynamic limit (TL) in the singular part of the rate function. In the TL, the sum is replace by an integral over some continuous variable $x \in X \subset \mathbb{R}^n$

$$f_s(z) = -\int_X \mathrm{d}x \log\left(1 - \frac{z}{\tilde{z}(x)}\right) \tag{3.15}$$

where the zeros z_j now become a function of x, $\tilde{z}(x)$. Performing a change of variable, we have

$$f_s(z) = -\int_{z(X)} \mathrm{d}\tilde{z}\rho(\tilde{z}) \log\left(1 - \frac{z}{\tilde{z}}\right) \tag{3.16}$$

where the Jacobian determinant $\rho(\tilde{z})$ can be interpreted as the density of zeros in the complex plain [64]. The integral can be extended to the whole complex plain setting $\rho(z) = 0$ if $z \notin z(X)$.

Interestingly, DQPT can be understood through an analogy with classical electrodynamics. Consider the real part of $f_s(z)$,

$$\lambda(z) = \mathrm{Re}\{f_s(z)\} = -\int_{\mathbb{C}} \mathrm{d}\tilde{z}\rho(\tilde{z}) \log\left|1 - \frac{z}{\tilde{z}}\right|. \tag{3.17}$$

For $z = x + iy$ with $x, y \in \mathbb{R}$, $\log|z|$ is the Green function of the Laplacian $\Delta = \frac{\partial^2}{\partial x^2} + \frac{\partial^2}{\partial y^2}$, that is,

$$\Delta\lambda(z) = -2\pi\rho(z). \tag{3.18}$$

In analogy with electrodynamics, the real part of the dynamical free-energy can be interpreted as an electrostatic potential, $\lambda(z)$, which is produced by a charge density $\rho(z)$ in two dimensions and the problem of the behavior of the dynamical free energy in the critical points becomes the problem of the behavior of the electrostatic potential in the surfaces. If the Fisher zeros coalesce

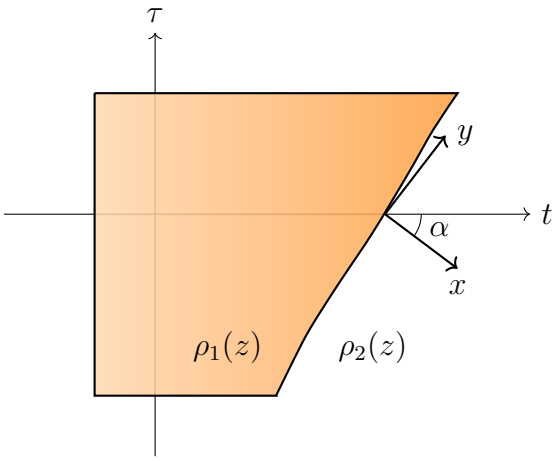

FIGURE 3.2: Schematic illustration of a surface of Fisher zeros in the complex plain separating two regions of different charge densities and the relevant coordinates frame used to determine the behavior of $\lambda(z)$ (Eq.(3.17)). Figure inspired by Ref.[66].

in lines, we can obtain the order of the phase transition directly from the density of zeros [65].

In the case of the Fisher zeros coalescing in areas, let us consider the situation depicted in Fig. 3.2, in which the density of zeros is $\rho_1(z)$ in the region I and $\rho_2(z)$ in the region II. We assume that the respective electrostatic potentials $\lambda_1(z)$ and $\lambda_2(z)$ satisfy the Laplace equation (3.18), thereby

$$\lambda(z) = \begin{cases} \lambda_1(z), \ z \in I \\ \lambda_2(z), \ z \in II \end{cases} \tag{3.19}$$

and we focus in the intersection of the boundary with the real time axis t. Choosing the frame $x - y$ coordinate frame, the continuity of $\lambda(z)$ implies that on the boundary

$$\frac{\partial^2}{\partial y^2}\lambda_1(z) = \frac{\partial^2}{\partial y^2}\lambda_2(z). \tag{3.20}$$

Making a change of variables

$$t = \frac{x}{\cos(\alpha)} + \frac{y}{\sin(\alpha)} \tag{3.21}$$

$$y' = y \tag{3.22}$$

the Laplace equation then yields

$$(\cos\alpha)^{-2}\frac{\partial^2}{\partial t^2}\lambda_i(z) + [1 + (\sin\alpha)^{-1}]^2\frac{\partial^2}{\partial y'^2}\lambda_i(z) = -2\pi\lambda_i(z) \tag{3.23}$$

and, hence

$$\frac{\partial^2}{\partial t^2}[\lambda_1(z) - \lambda_2(z)] = -2\pi(\cos\alpha)^2[\lambda_1(z) - \lambda_2(z)]. \tag{3.24}$$

This equation means that if an area of Fisher zeros touches the real time axis, the second derivative of the free energy is discontinuous.

3.1.3 DQPT in the Transverse Field Ising Chain

As we mentioned previously, nonanalytic real-time behavior of survival amplitudes had been recognized already by Pollmann *et. al*, [58], however only three years later it was interpreted as a dynamical critical phenomenon in Ref.[53], firstly in the Transverse-Field Ising model. Thus, it turns out illuminating discuss the phenomenon in this specific model as it makes possible to visualize what happens in the critical times in a microscopic level.

The authors in [53] considered the one-dimensional Transverse Field Ising model (TFIM) described by the hamiltonian

$$H(g) = -\frac{1}{2}\sum_{i=1}^{N}\sigma_i^z\sigma_{i+1}^z + \frac{g}{2}\sum_{i=1}^{N}\sigma_i^x \tag{3.25}$$

in the case with periodic boundary condition (PBC). It is well known that this model features ferromagnetic order for $|g| < 1$ and paramagnetic order for $|g| > 1$ with a quantum phase transition at the quantum critical point $g = g_c = 1$ at zero temperature [4]. Using Jordan-Wigner transformation, followed with Fourier transformation and Bogolyubov transformation [4], this model can be mapped into a spinless free fermions model in the momentum space assuming a diagonal form. This sequence of transformations yields the dispersion relation [4]

$$\epsilon_k(g) = \sqrt{(g - \cos(k))^2 + \sin^2(k)}. \tag{3.26}$$

For a quench in the magnetic field from g_0 to g_1, the rate function can be analytically calculated and it is given by [53]

$$f_{g_0,g_1}(z) = -\int_0^\pi \frac{dk}{2\pi}\ln\left[\cos^2(\phi_k) + \sin^2(\phi_k)e^{-2z\epsilon_k(g_1)}\right] \tag{3.27}$$

where the Bogolyubov angles $\phi_k = \theta_k(g_0) - \theta_k(g_1)$ with the terms $\theta_k(g)$ defined by the equation $\tan[2\theta_k(g)] = \sin(k)/(g - \cos(k))$, given that $\theta_k(g) \in [0, \pi/2]$. The equation above ignores an additive term $zE_{GS}(g_1)/N$ that involves the ground state of $H(g_1)$, but vanishes in the TL.

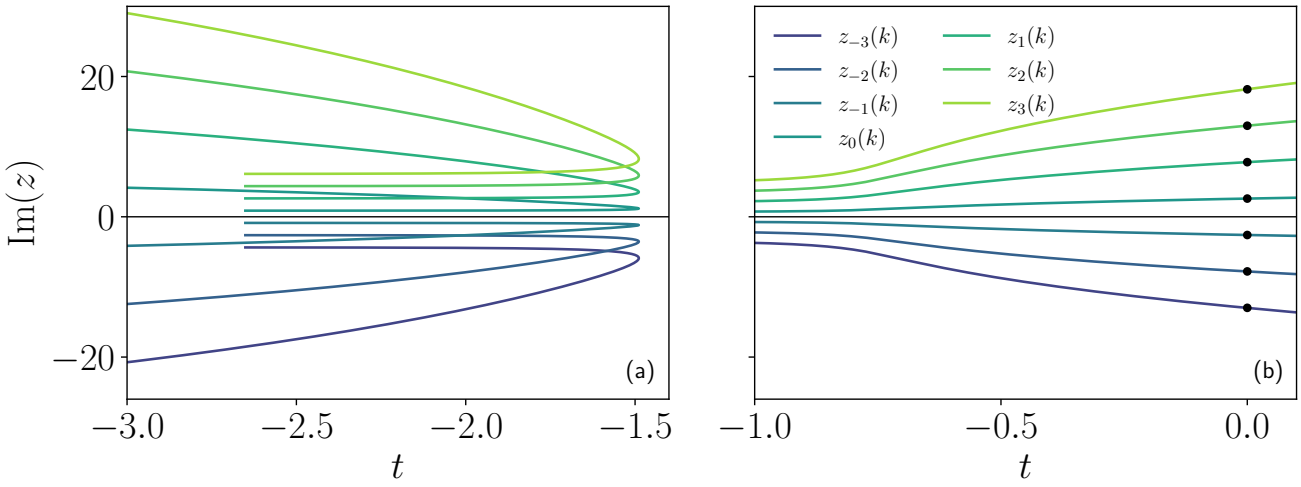

FIGURE 3.3: Line Fisher zeros for a quench within the same phase $g_0 = 0.4 \to g_1 = 0.8$ (left) and across the quantum critical point $g_0 = 0.4 \to g_1 = 1.3$ (right). Notice that the Fisher zeros cut the time axis for the quench across the quantum critical point, giving rise to nonanalytic behavior at t_n^* (the times t^* are marked with black dots in the plot). Figure inspired by Ref.[53].

In the TL, the Fisher zeros accumulate in families of lines labeled by an integer $n \in \mathbb{Z}$ and they are given by [53]

$$z_n(k) = \frac{1}{2\epsilon_k(g_1)} \left[\ln\left(\tan^2 \phi_k\right) + i\pi(2n+1)\right], \quad n \in \mathbb{Z}. \tag{3.28}$$

A thorough analysis of the equations (3.27) and (3.28) call the attention for the infrared ($k = 0$) and ultraviolet ($k = \pi$) behaviour of the Bogolyubov angles

$$\phi_{k=0} = \begin{cases} 0, & \text{quench in the same phase} \\ \pi/4, & \text{quench to/from the quantum critical point} \\ \pi/2, & \text{quench crossing the quantum critical point} \end{cases} \tag{3.29}$$

$$\phi_{k=\pi} = 0 \tag{3.30}$$

and allow us to conclude that only for a quench crossing the quantum critical point, the Fisher zeros cross the time axis, see Fig. 3.3, since[2]

$$\lim_{k\to 0} \mathrm{Re}[z_n(k)] = -\lim_{k\to\pi} \mathrm{Re}[z_n(k)] = \infty \tag{3.31}$$

Therefore, the condition for the DQPT occurring in the TFIM, i.e., in order to have non-analytic

[2]Note that in Ref.[53], the authors define the boundary partition function as in (3.11), but with the imaginary unit i absorbed in the complex number z.

behaviour in the rate function, the quench must cross the quantum critical point. In this cenario, the short time expansion for the rate function of the return amplitude or probability breaks down in the TL, which is analogous to the impossibility of the analytic extension for high temperature expansions close to thermodynamic transition. The crossing points in the time axis of the Fisher zeros, that is, the critical times are given by the expression [53]

$$t_n^* = t^* \left(n + \frac{1}{2} \right), \quad n \in \mathbb{Z} \tag{3.32}$$

where $t^* = \pi/\epsilon_{k^*}(g_1)$ and k^* determined by $\cos(k^*) = \frac{1+g_0 g_1}{g_0+g_1}$. The interpretation of the mode k^* follows from the fact that $n(k^*) = 1/2$ where $n(k)$ is the occupation of the excited state with k-mode in the eigenbasis of the postquench hamiltonian. Modes with $k > k^*$ have thermal occupation ($n(k) < 1/2$) and modes with $k < k^*$ have inverted population ($n(k) > 1/2$) and the mode k^* corresponds to infinite temperature [67].

We now turn to analyze the behaviour of the system at the critical times in terms of spins. The ground state of the hamiltonian (3.25) in the broken-symmetry phase ($|g| < 1$) is doubly degenerate, which makes more appropriate to use the definition (3.8) instead of (3.6) for the return amplitude. The return probability to the ground-state manifold will be given by

$$\mathcal{L}(t) = \mathcal{L}_+(t) + \mathcal{L}_-(t) \tag{3.33}$$

where $\mathcal{L}_\eta(t) = |\langle \eta | \psi(t) \rangle|^2$ is the probability associated to the ground-state $|\eta\rangle$ with positive magnetization ($\eta = +$) or negative magnetization ($\eta = -$). More specifically, these ground-states correspond to the states $|\uparrow\rangle^{\otimes N}$ and $|\downarrow\rangle^{\otimes N}$ respectively. Each of these probabilities feature large-deviation scaling and can be written as $\mathcal{L}_\eta(t) = \exp[-N\lambda_\eta(t)]$ with the rate functions $\lambda_\eta(t)$ being intensive functions, independent of the number of degrees of freedom N in the TL[3]. Due to this exponential dependence on N, we have that $\mathcal{L}(t)$ is either dominated by $\mathcal{L}_+(t)$ or $\mathcal{L}_-(t)$, such that

$$\lambda(t) = -\frac{1}{N} \log[\mathcal{L}(t)] = \min_\eta \lambda_\eta(t) \tag{3.34}$$

when $N \to \infty$ [4]. Thereby, before the critical time, $t < t_n^*$, we have the dominance of one of the rate functions over the other, until the moment when this dominance changes. This crossing point marks the DQPT in the form of a kink [68]. This is the reason behind the population inversion in the spin configuration at the critical time in the TFIM and guarantees the existence of an infinite temperature mode k.

[3] This fact is important, since it allows to use the finite-size experimental data to predict the behaviour of λ in the TL. See [68] for an experimental realization with $L = 10$.

[4] Remember that $\mathcal{L}(t) \in [0, 1]$ and therefore $-\log[\mathcal{L}(t)]$ is a decreasing function in this interval. Hence, $\lambda(t)$ will be dominated by the $\min\{\lambda_+, \lambda_-\}$, not the maximum.

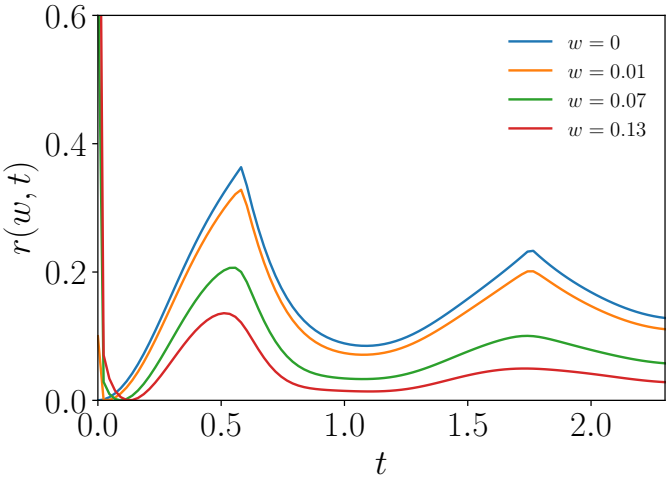

FIGURE 3.4: Work distribution function $r(w,t)$ for several values of density of work w. Notably, when $w = 0$, $r(w,t)$ corresponds to the rate function $\lambda(t)$ and dominates over higher values of w. Its behaviour for $w > 0$ becomes smooth, playing a similar role to the temperature in generic equilibrium phase diagrams. Figure inspired by Ref.[53].

Another quantity sensitive to the Fisher zeros is the work probability distribution following a double quench protocol, which we now introduce. Suppose we prepare the system in the ground state of $H(g_0)$, then we quench to $H(g_1)$ at $t = 0$ and afterwards we quench back to $H(g_0)$ at some time $t > 0$. The amount of work performed on the system is given by the distribution function

$$P(W,t) = \sum_j |\langle E_j|\psi(t)\rangle|^2 \delta\left[W - (E_j - E_{GS}(g_0))\right] \tag{3.35}$$

where the sum runs over the eigenstates $|E_j\rangle$ of $H(g_0)$ and $|E_{GS}(g_0)\rangle$ is the ground state of $H(g_0)$. Such as the return probability, the work distribution function obeys large deviation scaling and can written in the form $P(W,t) \sim e^{-Nr(w,t)}$ with a rate function $r(w,t) \geq 0$ depending on the work density $w = W/N$. In the TL, the rate function $r(w,t)$ can be analytically derived noting that according to the Gärtner-Ellis theorem [69], it is the Legendre-Fenchel transform

$$r(w,t) = \inf_{R\in\mathbb{R}}[c(R,t) - wR] \tag{3.36}$$

where for the TFIM [53]

$$c(R,t) = -\int_0^\pi \frac{dk}{2\pi} \ln\left[1 + \sin^2(2\phi_k)\sin^2(\epsilon_k(g_1)t)(e^{-2\epsilon_k(g_0)R} - 1)\right] \tag{3.37}$$

is the rate function $c(R,t)$ of the cumulant generating function, i.e., $c(R,t) = -\frac{1}{N}\ln\left[\int \mathrm{d}W P(W,t)e^{-RW}\right]$.

The figure 3.4 shows $r(w,t)$ for a quench across the quantum critical point. Interestingly, since the DQPT is related to the probability of return of the system state to the initial state, then it means a work performed on the system equal to zero, which implies $P(0,t) = |A(t)|^2$. Thus, we can think of the work distribution function as some kind of thermodynamic generalization of $\mathcal{L}(t)$ and hence $r(w,t)$ as a thermodynamic generalization of $\lambda(t)$ with the identity $r(0,t) = \lambda(t)$. In the figure 3.4 we see $r(w,t)$ exhibiting the same kink structures at the critical times as expected for $\lambda(t)$. Since the work w plays a role similar to the temperature for the phase diagram of equilibrium phase transitions, this is main reason for the authors in [53] call this phenomenon DQPT.

As a final remark, we discuss the possibility of observing DQPT when the quench starts at the paramagnetic phase ($h_0 > 1$) and ends in the ferromagnetic phase ($h_1 < 1$) of the TFIM, since in this situation, the initial ground-state is not degenerate. It turns out that all results above carry over for this situation. Specifically, one finds the nonanalytic behavior in the Loschmidt echo and the work distribution function for quenches from the paramagnetic to the ferromagnetic phase. For quenches originating in the ferromagnetic phase, the Loschmidt echo calculated above corresponds to working in the Neveu-Schwarz sector [70]. Experimentally, one derives the same result in the thermodynamic limit as above when starting from either of the two degenerate ferromagnetic ground states [71].

3.2 Order Parameters

A natural question is asking if there would exist some quantity that plays the role of an order parameter displaying a clear relation with DQPTs, given some resemblance of this phenomenon with equilibrium phase transitions. It has been found that a DQPT is typically accompanied by a zero of the equilibrium order parameter, in this case being time dependent, and therefore a periodic sequence of DQPTs with an oscillatory decay of the order parameter. Examples of this coincidence of critical times with zeros of the order parameter are particular quenches in the XXZ chain [72, 73], the $O(N)$ model [55] and broken-symmetry Ising models [68]. In other cases, the critical times are shifted from zeros or minima of order parameter by a constant factor as in TFIM [53], the TFIM with power-law decaying interactions [74], the Bose-Hubbard model [75] and the Fermi-Hubbard model [76]. However, in many others the relation between DQPT and order parameters still remains elusive such as for some nonintegrable models [77].

Let us overview some of these examples, starting by the TFIM in continuity to the previous section. The authors in [53] considered the total longitudinal magnetization

$$s_z(t) = \left\langle \psi_t \middle| \frac{1}{N} \sum_i \hat{\sigma}_i^z \middle| \psi_t \right\rangle, \tag{3.38}$$

which is the expected order parameter in this case for the same hamiltonian (3.25). It is well-known that for quenches lying in the ferromagnetic phase, the order parameter decays exponentially [78, 79], while for a quench across the quantum critical point, an oscillatory behavior is overlaid on the exponential decay (see figure 3 from Ref.[53]). Ones notes that the behavior of the magnetization remains analytical for all times and that the period of the oscillations exactly agrees with the time scale t^* of the critical times. A conjecture consistent with this observation had been formulated already in Ref.[70].

One may want to study the behavior of the order parameter as a function of the quench parameter instead of time. In this case, it is wise integrating the order parameter over time in order to eliminate this variable. This process typically yields a Landau order parameter [80], i.e., a quantity which is finite in a certain interval of the quench parameter and zero in the rest of the relevant values [38, 74, 81–87]. For instance, in the case of spin chains, the dynamical order parameter is typically the long-time averaged magnetization

$$\overline{S_\alpha} = \lim_{T\to\infty} \frac{1}{T} \int_0^T \langle\psi(t)|\hat{S}_\alpha|\psi(t)\rangle \mathrm{d}t \tag{3.39}$$

where $\hat{S}_\alpha \propto \sum_i \hat{\sigma}_i^\alpha$ ($\alpha = x, y, z$) is the total magnetization in α direction. The limit $T \to \infty$ above is usually employed based on the expectation that the system relaxes into a quasi-steady state and remain in this state for a long time, a typical phenomenon in quenched quantum many-body systems called prethermalization [88–90]. In fact, this approach for the study of the nonequilibrium dynamics after quenches in quantum many-body systems is at least as rich as the phenomenon of DQPTs described in terms of the survival probability and along the years has received the name DPT-I in order to differentiate it from the DPQTs, which has been dubbed DPT-II, since it was discovered latter[5].

The approach in terms of dynamical order parameters also brings at least three new understandings about the nonequilibrium dynamics after quenches [5–7]: (i) we can understand the different quantitative regions of the dynamical order parameter as dynamical phases induced by the quench analogously to equilibrium phases separated by equilibrium phase transitions [80], (ii) the point separating the two dynamical phases has a clear physical meaning, namely, the analogous to the equilibrium critical point which marks the minimum quench necessary to induce a transition and (iii) we can ask about the existence of a symmetry which is dynamically broken or restored when the dynamical critical point (DCP) is crossed.

For the case of the TFIM, the DCP, that is, the crossing point responsible for triggering the DQPT, coincides with the equilibrium critical point [53]. In the past, one used to believe that this connection between the DQPT and equilibrium QPT was a general aspect, however exceptions started to appear [66, 74, 91–93] and nowadays DQPTs are understood as a unique phenomenon

[5] As far as we know, this nomenclature was firstly adopted in Ref.[82].

apart from QPTs [5, 6]. It means that for many models, the DCP does not coincide with quantum critical point.

3.2.1 DPT-I in the LMG model

To investigate the DPT-I in the LMG model, we consider the parametrized Hamiltonian

$$\hat{H}_h = -\frac{1-h}{N}\hat{S}_x^2 - h\hat{S}_z. \tag{3.40}$$

which is slightly different of $\hat{H}_h$ from Eq. (2.57). For mathematical convenience, and since the DPT is governed by the same separatrix mechanism and symmetry restoration, we adopt the parametrization where the quadratic interaction acts along the $\hat{x}$-direction, which allows for an explicit analytical treatment without loss of physical generality inspired by Ref. [24]. We perform quenches in the parameter h. In the classical limit, we introduce spherical coordinates,

$$X = \sin\theta\cos\phi, \qquad Y = \sin\theta\sin\phi, \qquad Z = \cos\theta, \tag{3.41}$$

where the components (X, Y, Z) are defined in Eq. (2.21). In terms of these angular variables, the resulting classical Hamiltonian per spin reads

$$H_{\mathrm{cl}}(\theta,\phi) = -(1-h)\sin^2\theta\cos^2\phi + \frac{h}{2}\left(\cos\theta + 1\right). \tag{3.42}$$

As a dynamical order parameter, we consider the long-time average of the longitudinal magnetization,

$$\overline{X} = \lim_{T\to\infty}\frac{1}{T}\int_0^T \sin\theta(t)\cos\phi(t)\mathrm{d}t, \tag{3.43}$$

which will be the central quantity of interest in what follows. A substantial simplification arises by restricting the analysis to initial conditions with $\phi = 0$, a choice that will be adopted throughout this thesis. In this case, the initial Bloch vector $\mathbf{M}(0) = (X(0), Y(0), Z(0))$ lies entirely in the x–z plane, since $Y(0) = 0$. In the TL, the Heisenberg equation of motion

$$\frac{\mathrm{d}\hat{O}}{\mathrm{d}t} = i[\hat{H}, \hat{O}] \tag{3.44}$$

leads to a Landau–Lifshitz–like equation for the Bloch vector [82],

$$\dot{\mathbf{M}} = \mathbf{M} \times \frac{\partial H}{\partial \mathbf{M}}. \tag{3.45}$$

For $\phi = 0$, both $\mathbf{M}$ and $\partial H/\partial\mathbf{M}$ lie in the x–z plane, implying that their cross product is always

parallel to the $\hat{y}$ direction. As a consequence, the plane $Y = 0$ constitutes an invariant submanifold of the classical dynamics. Coherent states initialized with $\phi = 0$ therefore evolve entirely within this plane. Upon this choice, the dynamics becomes a problem described by

$$H_{\text{cl}}(\theta) = -(1-h)\sin^2\theta + \frac{h}{2}(\cos\theta + 1), \qquad \text{for } \phi = 0. \tag{3.46}$$

As we are taking the TL, it is reasonable to invoke the double-well potential picture for the analysis of the dynamics. Suppose the initial state is a ferromagnetic state and we quench the system. As discussed in the previous chapter, if the post-quench energy of the system is smaller than the critical energy E_c, the average longitudinal magnetization $S_x(t) = \langle\psi_t|\hat{S}_x|\psi_t\rangle$ as a function of time will display oscillations around its initial value $S_x(0)$ and its long-time integration yields a finite value. On the other hand, if the post-quench energy of the system is greater than E_c, we shall observe oscillations of $S_x(t)$ around zero, since in this case the classical particle can overcome the potential barrier. Thus, if the symmetry $\mathcal{C} = \text{sign}(\hat{S}_x)$ is responsible for identifying in which well the particle is localized, then from the first case ($E_f < E_c$) to the second one ($E_f > E_c$), the quantity $\langle\mathcal{C}\rangle$ must change abruptly from ± 1, depending on the initial conditions, to zero [6]. Therefore, it is clear that what is behind DPT-I in the LMG model is the breaking/restoration of the symmetry $\mathcal{C}$. There shall exist a critical dynamical point h_c^d for which $h < h_c^d$ defines a $\mathcal{C}$-breaking phase and $h > h_c^d$ defines a $\mathcal{C}$-symmetric phase. A numerical exploration of $S_\alpha(t)$ as a function of t is done in the end of this section.

Insight into the dynamics can be gained by noting that the time integral defining $\overline{X}$ can be rewritten as

$$\overline{X} = \frac{1}{T}\int_0^T \sin\theta(t)\cos\phi(t)\mathrm{d}t = \frac{\int_{\theta_-}^{\theta_+} \frac{\mathrm{d}\theta \sin\theta\cos\phi}{\dot{\theta}}}{\int_{\theta_-}^{\theta_+} \frac{\mathrm{d}\theta}{\dot{\theta}}}, \tag{3.47}$$

where we used $\mathrm{d}t = \mathrm{d}\theta/\dot{\theta}$. The new integration limits θ_- and θ_+ are called return points and correspond to the values of θ for which $H_{\text{cl}}(\theta) = E \equiv E_f$, i.e., the turning points at which $\dot{\theta} = 0$. Although a closed analytical expression for the return points is impracticable, the expression for the DCP is simple. Once fixed the initial state as the ground-state of the pre-quench hamiltonian, the DCP occurs when the energy of the initial state evaluated at the post-quench hamiltonian, $E_f = H_{\text{cl}}(h_f, \theta_0)$, coincides with the energy of the classical separatrix ($E_c = 0$), thus making the trajectory touch the fixed unstable point responsible for the restoration of the symmetry $\mathcal{C}$. Proceeding with the algebraic calculations, we get for the DCP the expression

$$h_c^d = \frac{1}{1 + \cos^2\frac{\theta_0}{2}}. \tag{3.48}$$

[6] Corps and Relaño demonstrate exactly this behavior for the LMG model in the Ref. [32]

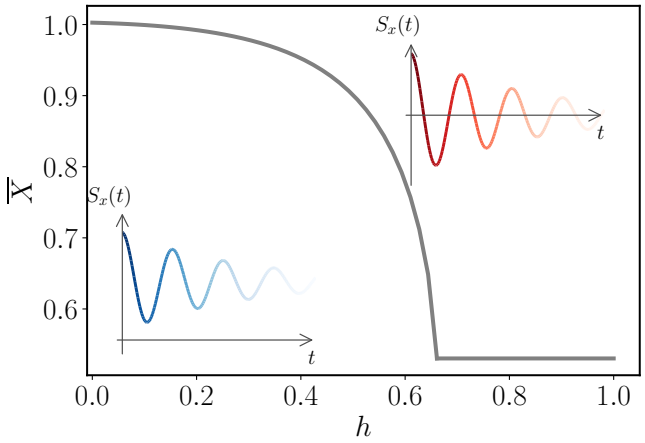

FIGURE 3.5: Dynamical order parameter $\overline{X}$ given by Eq. (3.49) for $h_0 = 0.2$. The DCP divides the parameter space in two dynamical regions: one phase at which the long-time system state exhibits finite longitudinal magnetization (the lower left inset displays the corresponding qualitative behavior of $S_x(t)$ as a function of time) and another phase at which long-time system state exhibits zero longitudinal magnetization (the upper right inset displays the corresponding qualitative behavior of $S_x(t)$). At $h = h_c^d$, the $\overline{X}$ is non-analytic.

After a sequence of cumbersome algebraic manipulations, we obtain the final expression for the order parameter [24]

$$\overline{X} = \begin{cases} \frac{\pi}{2\sin\theta_0}\frac{1}{K(\kappa(h,\theta_0))}, & h < h_c^d \\ 0 & h > h_c^d \end{cases} \tag{3.49}$$

where $K(x)$ is the complete elliptic integral of the first kind and

$$\kappa(h,\theta_0) = \frac{4(1-h)\sin^2\theta_0}{h(2+\sin^2\theta_0)}. \tag{3.50}$$

See the appendix C for the detailed derivation. The graph of $\overline{X}$ as a function of h is shown in the figure (3.5) for $h_0 = 0.2$. The possibility of obtaining an analytical expression for $\overline{X}$ is striking, as results such as this one are quite rare in the literature. The expression for $\overline{X}$ allows us, for instance, to have access to the scaling close to $h = h_c^d$. For the sake of completeness, we mention that the DCP for the non-parametrized version of the LMG Hamiltonian [Eq. (2.2)] is given by [83]

$$h_c^d = \frac{h_0 + J}{2}. \tag{3.51}$$

The non-parametrized version will be used to explore the relation between DPT-I and Krylov complexity in the chapter 5, while the parametrized version will be used to explore the relation

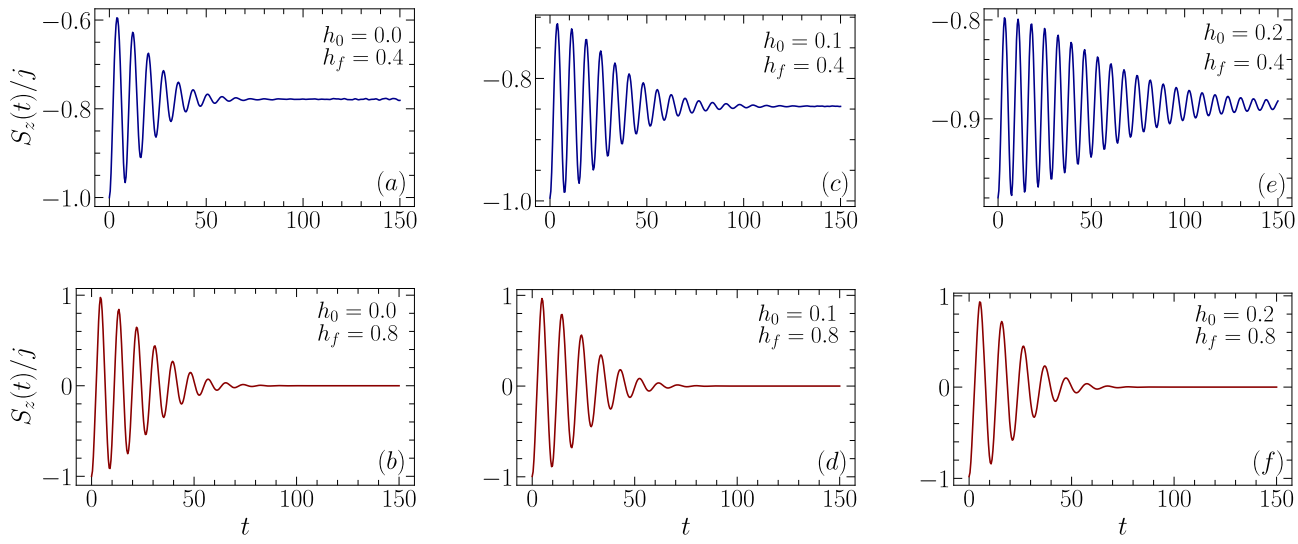

FIGURE 3.6: Normalized longitudinal magnetization $S_z(t) = \frac{1}{j}\sum_i \hat{\sigma}_i^z(t)$ of the LMG model as a function of time for several values of h_0 and h_f and $N = 200$ sites. The initial state considered is $|\psi_0\rangle = |\uparrow\rangle$. The magnetization $S_z(t)$ always oscillates and then stagnates around some finite value close to $S_z(0)$ (the closer h_f is to h_0, the closer $S_z(t \gg 1)$ is to $S_z(0)$) for quenches such that $h_f < h_c^d$. On the other hand, the magnetization $S_z(t)$ always oscillates and then stagnates around zero for quenches fulfilling $h_f > h_c^d$.

between ESQPT and Krylov complexity.

Magnetization of a finite size system

Once obtained the analytical results above, we return to the hamiltonian in Eq. (2.2) for a more detailed analysis of the longitudinal magnetization $S_z(t) = \sum_i \hat{\sigma}_i^z(t)$ as a function of time, which will be useful for comparisons with results presented in chapter 5. The figure 3.6 displays instances of the normalized magnetization $S_z(t)/j$ for the LMG model with $N = 2j = 200$ sites. The quench dynamics was initialized in one of the ground-states of $\hat{H}(h_0)$, which was evolved with the final hamiltonian $\hat{H}(h_f)$ for the indicated values of h_0 and h_f in the figure.

For quenches lying in the same phase as the initial hamiltonian [see panels (a), (c) and (e)], we see the magnetization oscillating and then stagnating around a finite value which is as close to $S_z(0)$ as smaller is the quench intensity $h_f - h_0$, thus making its time-average $\overline{S_z} \neq 0$. On the other hand, quenches crossing the dynamical critical point h_c^d [see panels (b), (d) and (f)] make the magnetization oscillate and later stagnate always around zero, yielding a time-average $\overline{S_z} = 0$.

3.3 Connecting DPT-I and ESQPT

As our last discussion in this chapter, we address the relation between DPT-I and ESQPT in the LMG model based on the results from Ref. [9, 32], which put this relation on solid grounds. From the whole analysis conducted in the last section, it is clear that these two phenomena are directly linked. The DCP expression was obtained following the fact that h_c^d is the value of h for which the final energy of the system after the quench is equal to the critical energy of the ESQPT. Also, if $\mathcal{C}$ is restored by any eigenstate of $\hat{H}$ with energy $E > E_c$, then $\mathcal{C}$ must be the symmetry underlying the DPT-I in the LMG model.

We can probe the relation between these two phenomena taking as control parameter not the magnetic field strength itself, but rather the final energy given by $E_f = \langle\psi_0|\hat{H}_f|\psi_0\rangle$. In this way, the dynamical order parameter $\overline{S_z}$ shall exhibit non-analytic behavior at $E = E_c$. For this, we employ the following protocol [33]:

1. Start from the ground-state manifold of the pre-quench hamiltonian $\hat{H}(h_0)$ in the degenerate phase ($E < E_c$) at a certain initial value of the control parameter, h_0. In this phase, we have two ground-states $\{|E_0, +\rangle, |E_0, -\rangle\}$ and any linear combination of these states is also a ground-state. Thus, we choose

$$|\psi_0\rangle = \cos(\chi)|E_0, +\rangle + \sin(\chi)|E_0, -\rangle \tag{3.52}$$

   where χ defines how much the eigenstates of $\hat{\Pi}$ [see Eq. (2.35)] are mixed.

2. Perform the quench $h_0 \to h_f$. This implies an energy cost $\Delta E = E(h_f) - E(h_0)$ where $E(h_f) = \langle\psi_0|\hat{H}(h_f)|\psi_0\rangle$ and $E(h_0) = \langle\psi_0|\hat{H}(h_0)|\psi_0\rangle$. This change of energy (or simply $E(h_f)$) is the actual control parameter of the ESQPT, since it can lead the system above or below E_c properly choosing h_0 and h_f.

3. Let the system evolve under the final hamiltonian $\hat{H}(h_f)$ until it reaches the final equilibrium state ρ_{eq}.

4. Study the results for $\text{Tr}\left[\rho_{\text{eq}}\mathcal{O}\right]$ in terms of the energy E and the angle χ.

The choice of the operator $\mathcal{O}$ is not arbitrary. Suppose we quench the system such that $E_f < E_c$. Then the long-time evolution will be described by Eq. (2.84a). Thus, a relevant piece of information about the initial state is stored in the coherences $c_{k,+}c^*_{k,-}$, which can be inferred by measuring an adequate observable $\mathcal{O}$ for which $\text{Tr}\left[\rho_{\text{eq}}\mathcal{O}\right] = f(c_{k,+}c^*_{k,-}) \neq 0$ in this region of the spectrum. On the other hand, if we quench the system above the critical energy, $E_f > E_c$, the equilibrium state will lie above E_c and it will be described by Eq. (2.84b). In this situation, the equilibrium state no longer depends on the coherences $c_{k,+}c^*_{k,-}$, the information about the initial state was completely washed out and therefore $\text{Tr}\left[\rho_{\text{eq}}\mathcal{O}\right] = 0$. In the end, the operator $\mathcal{O}$

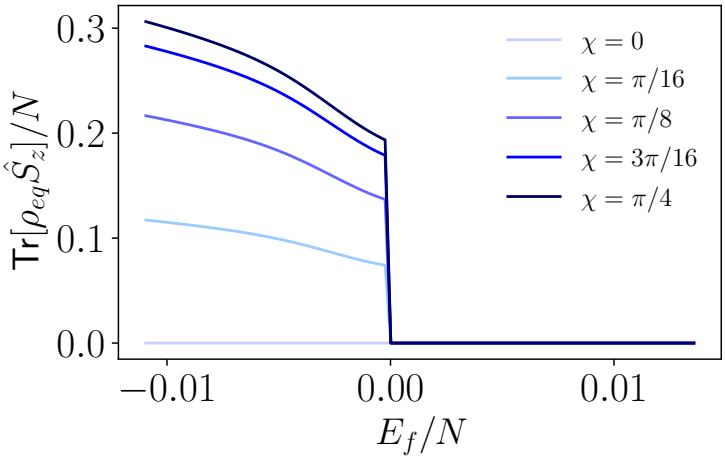

FIGURE 3.7: N-normalized average longitudinal magnetization as a function of the normalized post-quench energy E_f/N for different values of χ. An abrupt change takes place at the ESQPT critical energy $E_c = 0$ as expected from the link between DPT and ESQPT in the LMG model. The initial state with $\chi = \pi/4$ displays the sharpest change, since it is the initial with most undefined (defined) $\hat{\Pi}$ ($\mathcal{C}$) symmetry.

will work as an order parameter that can also be used to characterize the ESQPT. For the LMG model, the appropriate choice for the operator $\mathcal{O}$ is the longitudinal magnetization. Although the correct equilibrium ensemble is the GME in Eq. (2.88), we emphasize that the density matrix in Eqs.(2.84a) and (2.84b) is sufficient to detect the ESQPT as shown in Ref. [33].

Figure 3.7 illustrates the numerical evaluation of $\mathrm{Tr}\left[\rho_{\mathrm{eq}}\hat{S}_z\right]$ as a function of the final energy E_f, obtained from the parametrized Hamiltonian $\hat{H}_h$ [Eq. (2.57)] for $N = 2000$ and $h_f = 0.7$. Different values of the pre-quench parameter h_0 are considered, leading to different initial states and, consequently, to different final energies $E_f = \langle\psi_0|\hat{H}_f|\psi_0\rangle$. From the step 2 in the protocol above, note that when $\chi = \pi/4$, the initial state mixes both energy eigenstates $\{|E_0, +\rangle, |E_0, -\rangle\}$ with equal weight, thus corresponding to the maximum $\hat{\Pi}$-symmetry breaking state, since $\langle\psi_0|\hat{\Pi}|\psi_0\rangle = 0$. In contrast, the state with $\chi = \pi/4$ preserves $\mathcal{C}$ for $E < E_c$ and has this symmetry broken for $E > E_c$. If the initial state has definite $\hat{\Pi}$ symmetry (see the curve for $\chi = 0$ in the graph) and hence definite $\mathcal{C}$ symmetry, the overlaps $c_{i,k} = \langle E_i, k|\psi_0\rangle$ appearing in ρ_{eq} would be zero and ρ_{eq} would become the usual microcanonical ensemble at both regions of the spectrum. Other values of χ produce less abrupt changes of the order parameter when one crosses E_c.

The analysis presented here shows that the nonanalytic behavior characterizing DPT-I is deeply rooted in the presence of ESQPTs in the energy spectrum. This insight motivates the detailed exploration of nonequilibrium dynamics carried out in the remainder of the thesis. We finish this chapter putting together the phase transitions of the LMG model in the table 3.1

Phase transition	Critical point	Order Parameter
[Equilibrium] QPT	$h = J$	$\langle E_0 \vert \hat{S}_\alpha \vert E_0 \rangle$
DPT-I	$h = \frac{h_0+J}{2}$	$\overline{S_\alpha} \propto \int \langle \psi_t \vert \hat{S}_\alpha \vert \psi_t \rangle \mathrm{d}t$
ESQPT	$E = -h$ or $E = 0$	DOS

TABLE 3.1: Table of the quantum phase transitions in the LMG model with the corresponding critical points and order parameters .

Chapter 4

Krylov Complexity

4.1 Krylov Complexity of Quantum States

Let us suppose that the state of an isolated quantum many-body system is $|\psi_0\rangle$ at $t = 0$. The evolved state can be written as ($\hbar = 1$)

$$|\psi_t\rangle = e^{-i\hat{H}t}|\psi_0\rangle = \sum_{n=0}^{\infty} \frac{(-it)^n}{n!}\hat{H}^n|\psi_0\rangle. \tag{4.1}$$

We will also suppose that the evolution is always not trivial, i.e., $|\psi_0\rangle$ is not an eigenstate of $\hat{H}$. As the sum is iterated, the action of powers of $\hat{H}$ on the initial state can be thought in terms of the trajectory of $|\psi_0\rangle$ in the Hilbert space. Also this process lead $|\psi_0\rangle$ into the combination of an increasing number of eigenstates of $\hat{H}$. It can be intuitively visualized by the following abstract image: the initial state starts to spread through the Hilbert space. This image must be appreciated carefully: we are not just talking about spreading in the real space, but also spreading in the Hilbert space in the sense that more and more bases are being occupied as time passes and the sum is iterated.

It is reasonable to think that for some hamiltonian and for some initial state, the evolution remains restricted to a certain subspace of the Hilbert space $\mathcal{H}$. This idea can be used to formulate a notion of complexity based on the spread of the initial state: the more it spreads through the Hilbert space, the more complex is the dynamics. Let us formalize this notion. The set $\{\hat{H}^n|\psi_0\rangle\}_n$ contains all the information only about the portion of the Hilbert space visited by $|\psi_0\rangle$ evolving under $\hat{H}$, therefore this set can be used to span the subspace mentioned above. However, this set cannot be used as a basis, since its elements are not orthogonal. Moreover, as it is infinitely large, it might contain some kind of *redundancy* between its elements[1]. To solve this problem, we can perform Gram-Schmidt orthogonalization, giving as output a set called *Krylov basis*. Along this text, we'll interchangeably use $\mathcal{K}_{|\psi_0\rangle}$ or just $\mathcal{K}$ when there is no chance of confusion to refer to the Krylov basis or the Krylov subspace of the initial state $|\psi_0\rangle$, its elements by the kets $\{|K_n\rangle\}$ and its dimension by K.

[1] What we mean by redundancy will be clear along this chapter.

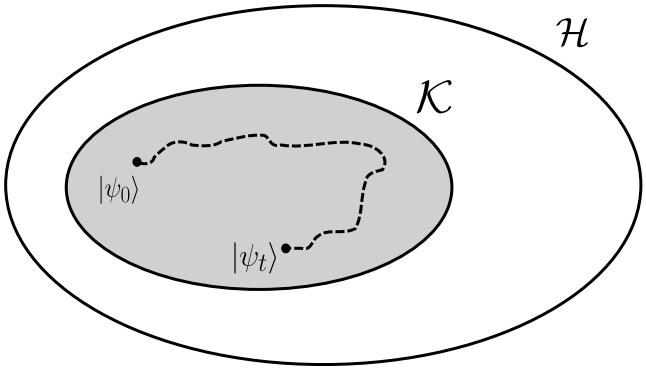

FIGURE 4.1: Illustrative representation of the Krylov subspace. If $K < \dim(\mathcal{H})$, then the dynamics of an initial state $|\psi_0\rangle$, which is represented by the dashed line, belonging to this subspace (grey region) remains restricted to it. If we find a basis for the grey region, then a quantum state lying outside of it cannot be properly represented in terms of this basis.

Thus, the subspace in which the dynamics of $|\psi_0\rangle$ remain restricted is called Krylov subspace, see figure (4.1) for an illustration. As a consequence of this construction, a quantum state belonging to $\mathcal{H}\backslash\mathcal{K}$, i.e., a state lying outside the Krylov subspace cannot be properly expanded in the Krylov basis. In other words, the Krylov basis is not complete for the whole $\mathcal{H}$.

In the sum (4.1), the index n ranges from zero to infinity, however it is clear that the number of terms in the Krylov basis is finite and it may even be smaller than the dimension of the whole Hilbert space by construction. It only means that the number of orthogonal states necessary to represent $|\psi_t\rangle$ is smaller than the number of orthogonal states necessary to represent another arbitrary state lying outside $\mathcal{K}_{|\psi_0\rangle}$, but each state $\{|K_n\rangle\}_{n=0}^{K-1}$ is a column vector with a number of entries equal to the Hilbert space dimension.

Another way to find the Krylov basis is using the so-called Lanczos algorithm [94]. Starting with the initial state as the first Krylov state $|K_0\rangle = |\psi_0\rangle$, the next state is obtained as $|K_1\rangle = \frac{1}{b_1}\hat{H}|K_0\rangle$, where $b_1 = \sqrt{\langle K_1|K_1\rangle}$ is a normalization factor. The subsequent states $\{|K_n\rangle\}_{n\geq 2}$ are calculated using the following recursion method

$$|A_n\rangle = H|K_{n-1}\rangle - a_n|K_{n-1}\rangle - b_{n-1}|K_{n-2}\rangle \tag{4.2}$$

$$|K_n\rangle = b_n^{-1}|A_n\rangle \tag{4.3}$$

with $b_0 = 0$. The constants a_n and b_n are called Lanczos coefficients and they are defined as

$$a_n = \langle K_n|\hat{H}|K_n\rangle, \qquad b_n = \langle K_n|K_n\rangle^{1/2}. \tag{4.4}$$

Substituting (4.3) in (4.2) and isolating the first term in the r.h.s. of (4.2), we see that the hamiltonian is tridiagonal in the Krylov basis

$$H|K_{n-1}\rangle = b_n|K_n\rangle + a_n|K_{n-1}\rangle + b_{n-1}|K_{n-2}\rangle \tag{4.5}$$

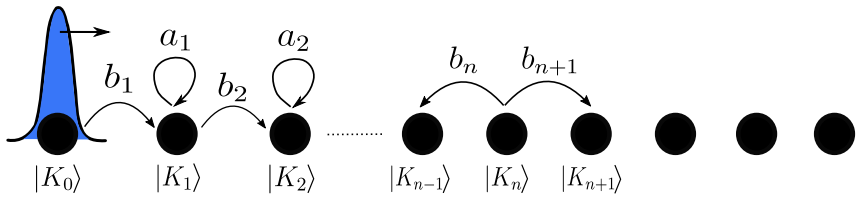

FIGURE 4.2: Analogy of the spreading of $|\psi_0\rangle$ with a hopping particle in a tight-binding chain. At $t = 0$, the initial state is fully localized on the first site of the Krylov chain, which represents the first Krylov state $|K_0\rangle$. As time passes, the particle explores deeper sites of the chain, representing the delocalization process in the Krylov basis. The hopping terms between nearest neighbors sites are the Lanczos coefficients b_n and the on-site energies are a_n.

that is, it has the following matrix representation in the Krylov basis

$$\hat{H} = \begin{pmatrix} a_0 & b_1 & 0 & 0 & 0 & \cdots \\ b_1 & a_1 & b_2 & 0 & 0 & \cdots \\ 0 & b_2 & a_2 & b_3 & 0 & \cdots \\ 0 & 0 & b_3 & a_3 & b_4 & \cdots \\ \vdots & \vdots & \vdots & \vdots & \vdots & \ddots \end{pmatrix}. \tag{4.6}$$

The physical meaning of the matrix elements of the hamiltonian $\hat{H}$ in the Krylov basis is inspired by the fact that it has the same structure as a tight-binding hamiltonian [95]. The tight-binding model is used in condensed matter physics to describe the behaviour of electrons in solids and uses a set of wavefunctions based in the superposition of wavefunctions of isolated atoms located in each site of the lattice. Therefore, it suggests that the electron is tightly bound to the atom to which it belongs. In the tight-binding model, the terms in its hamiltonian corresponding to b_n from (4.6) are called hopping parameters and are related to the probability of the electron to hop between neighboring sites in the lattice, while the terms corresponding to a_n are related to self-energies on each site. Thus, this analogy inspire us to think of the dynamics in the Krylov basis as a particle hopping between the sites of an semi-infinite 1D chain, each site representing one Krylov state, with hopping probability between nearest neighbor sites related to b_n and self-energy on site a_n[2] (see the figure 4.2 for an illustration). We will refer to this semi-infinite chain analogy by Krylov chain throughout the text.

Now we have all we need to discuss the definition of complexity. For an arbitrary basis $\mathcal{B}$ for $\mathcal{H}$, whose elements we denote generically by $\{|B_n\rangle\}$ and its dimension by B, the complexity of the evolution of an initial state $|\psi_0\rangle$ according to (4.1) is defined as [13, 14]

$$C_{\mathcal{B}}(t) = \sum_{n=0}^{B-1} c_n |\langle B_n|\psi_t\rangle|^2. \tag{4.7}$$

[2]See the figure 1 in the reference [14] for a perspective in terms of *Markov chain*.

Some constraints must be imposed on the coefficients c_n. For a real and positive-definite measure of complexity, regardless of the state of the system, $c_n \in \mathbb{R}^+$ is required. The coefficients should vary with n and grow monotonically with n to assign higher complexity to components $|\langle\psi_t|B_n\rangle|^2$ with higher index n. Note that the choice of constants coefficients $c_n = c$ is excluded as the complexity would reduce to the sum over all probabilities $p_n(t) = |\langle\psi_t|B_n\rangle|^2$ times c, yielding c at all t.

The measure of complexity (4.7) is dependent of a basis choice, which represents a problem since different basis would yield a different amount of complexity for the same initial state and the same hamiltonian. So we would like to perform some kind of minimization over all basis in $\mathcal{H}$,

$$C(t) = \min_{\mathcal{B}} C_{\mathcal{B}}(t) \tag{4.8}$$

in order to have a measure of complexity which is basis independent.

The authors of reference [14] were able to prove that the basis which minimizes (4.7) for $c_n = n$ is the Krylov basis,

$$C(t) = C_{\mathcal{K}}(t) = \sum_{n=0}^{K} n|\langle K_n|\psi_t\rangle|^2 \tag{4.9}$$

Thus, the measure above is called *Krylov complexity*. We will consider the definition above throughout the text. The choice $c_n = n$ is not just a coincidence, but intentional. For this definition, the Krylov complexity is the average position of the wave function (or the hopping particle) in the Krylov chain and for a complex dynamics, the initial state which starts at $t = 0$ sharply localized in the first site $|K_0\rangle$, quickly delocalizes along the time evolution, reflecting on the average position.

The Krylov complexity was firstly introduced in Ref. [13] in the context of evolution of operators, i.e., in the Heisenberg picture (see the next section for an overview). Based on this concept, an universal hypothesis for the maximum growth of local operators in quantum many-body systems was presented. Later, Balasubramanian and collaborators [14] extended the idea to the evolution of quantum states, in the Schrödinger picture as described above. Although the literature about the version for operators is vaster, Krylov complexity for quantum states has been employed for different purposes, ranging from the study on the transition from integrability to chaos [96, 97], distinguishing different topological phases of matter [98, 99], evolutions governed by dynamical symmetry groups associated with specific Lie algebras [100] and random matrix models [14, 101]. For a comprehensive overview of the current state of the art in Krylov complexity, we refer the reader to two recent reviews [10, 11]. In the next section, we revise the theory of Krylov complexity of operators.

4.2 Krylov Complexity of Operators

In the Heisenberg picture, the time evolution of an operator $O(0) \equiv O_0$ at time $t = 0$ of an isolated quantum many-body system is given by

$$O(t) = e^{i\hat{H}t} O_0 e^{-i\hat{H}t} = \sum_{n=0}^{\infty} \frac{(it)^n}{n!} \mathcal{L}^n(O_0) \tag{4.10}$$

where $\mathcal{L}(\bullet) = [\hat{H}, \bullet]$ is called Liouvillian. In order to speak about Krylov basis for operators, first we need to construct a new Hilbert space whose elements are now operators. An essential element to construct this new vector space is setting an inner product between operators satisfying two desired properties:

1. $\left(\hat{A}|\mathcal{L}\hat{B}\right) = \left(\mathcal{L}\hat{A}|\hat{B}\right), \ \forall \hat{A}, \hat{B}.$
2. $\left(\hat{A}|\mathcal{L}\hat{A}\right) = 0, \quad \forall \ \hat{A}$ hermitian.

where $(\hat{A}|\hat{B})$ will be the notation used for the inner product between two operators $\hat{A}$ and $\hat{B}$. One possible choice is

$$\left(\hat{A}|\hat{B}\right) = \left\langle e^{\beta\hat{H}/2} \hat{A}^\dagger e^{-\beta\hat{H}/2} \hat{B} \right\rangle_\beta, \tag{4.11}$$

with $\langle O \rangle_\beta = \frac{1}{Z} \mathrm{Tr}\left(e^{-\beta\hat{H}} O\right)$ representing the thermal average and $\beta = 1/T$ is the inverse of temperature T. In the limit $T \to \infty$, this inner product reduces to the Hilbert-Schmidt product

$$\left(\hat{A}|\hat{B}\right) = \mathrm{Tr}\left(\hat{A}^\dagger \hat{B}\right) \tag{4.12}$$

up to a normalizing constant. Equipped with inner product, we can now map operators O into vectors of this new operator linear space which we denote by $|O)$ to differentiate from kets.

The idea behind the Krylov complexity for operators is essentially the same: quantifying the complexity looking at the spread of an operator beyond real space, i.e., also the spread in the Hilbert space. Analogously, the set $\{\mathcal{L}^n \ |O_0)\}_n$ contains all the information only concerning the portion of the operators Hilbert space explored by $|O_0\rangle$. Orthogonalization is again necessary in order to have a basis for the Krylov subspace of operators. The Lanczos algorithm in this case reads [13]

$$|A_n) = \mathcal{L} \ |K_{n-1}) - b_{n-1} \ |K_{n-2}) \tag{4.13}$$

$$|K_n) = b_n^{-1} \ |A_n) \tag{4.14}$$

with $b_n = \sqrt{(K_n|K_n)}$ calculated via Eq. (4.11) or (4.12) and $b_0 = 0$. In the case of operators, note that the Lanczos algorithm involves only one Lanczos coefficient, b_n, while in the case of

quantum states evolution we have two Lanczos coefficients, a_n and b_n. Hence, in the Krylov basis $\{|K_n)\}_n$ for the operator vector space, the Liouvillian has the following matrix representation

$$\mathcal{L} \doteq \begin{pmatrix} 0 & b_1 & 0 & 0 & 0 & \cdots \\ b_1 & 0 & b_2 & 0 & 0 & \cdots \\ 0 & b_2 & 0 & b_3 & 0 & \cdots \\ 0 & 0 & b_3 & 0 & b_4 & \cdots \\ \vdots & \vdots & \vdots & \vdots & \vdots & \ddots \end{pmatrix}. \tag{4.15}$$

now with the terms corresponding to the coefficients a_n from the quantum state version equal to zero. Similarly, the matrix form of the Liouvillian in the Krylov basis inspires us to think of the dynamics in this basis as a particle hopping between neighbouring sites from a semi-infinite chain whose hopping terms are the Lanczos coefficients b_n, but now without on-site energy terms.

In the Heisenberg picture, we consider the definition of Krylov complexity given by the same expression as in the Schrödinger picture

$$C_{\mathcal{K}}(t) = \sum_{n=0}^{K} n \Big| \Big(K_n | O(t) \Big) \Big|^2. \tag{4.16}$$

As far as we know, there is not a rigorous proof that the Krylov basis minimizes the definition above for the case of operators. The fact that in the Schrödinger picture there is no need for the choice of a inner product between states can be seen as an advantage over the Heisenberg picture, since in this latter one there are many definitions satisfying the two properties mentioned above.

4.2.1 Dimension of Krylov Subpace

Since the set $\{\mathcal{L}^n \, |O_0)\}_n$ contains all the information about the evolution of $|O_0)$, then it is correct to say that the Krylov subspace

$$\mathcal{K}_{\hat{O}_0} = \text{span}\{\mathcal{L}^n \hat{O}_0\}_{n=0}^{\infty} = \text{span}\Big\{ \hat{O}_0, [\hat{H}, \hat{O}_0], [\hat{H}, [\hat{H}, \hat{O}_0]], \cdots \Big\}, \tag{4.17}$$

that is, the Krylov subspace of the operator $\hat{O}_0$ is given by all the linear combinations of nested commutators between $\hat{H}$ and $\hat{O}_0$. However, as mentioned previously for the evolution of quantum states, the set above also extends to infinity while the Krylov basis has finite dimension, which means that the orthogonalization process might get rid of the *redundancies* between the infinite number of nested commutators. In other words, after the orthogonalization, it is guaranteed that the output set, namely the Krylov basis for operator Hilbert space, is the minimal set of elements needed to span the Krylov subspace. This reasoning gives rise to the question: when does the Lanczos algorithm must stop? or equivalently, how big is $\dim(\mathcal{K}_{\hat{O}_0}) = K$? Now we proceed to answer this question.

The quantity K obviously depends on $\hat{O}_0$ and $\mathcal{L}$, ultimately the system in consideration, so the best we can do is finding an upper bound for K for now. Another obvious fact is that K must be less than the dimension of the whole space of operators. If the Hilbert space has dimension D, then the space of bounded linear operators $\mathcal{B}(\mathcal{H})$, in which $\hat{O}_0$ lies, has dimension D^2. Therefore, we conclude that $K < D^2$. A tighter upper bound can be found noticing that $\ker(\mathcal{L}) \nsubseteq \mathcal{K}_{O_0}$ and to prove this fact we reproduce the analysis from Ref. [102].

The dimension K can be calculated studying the cardinality of the maximal set of linearly independent elements of the form $\mathcal{L}^n(O_0)$. This is equivalent to compute the rank of the matrix

$$(O_0, \mathcal{L}(O_0), \mathcal{L}^2(O_0), \cdots, \mathcal{L}^n(O_0), \cdots)^T \tag{4.18}$$

in a given representation. On the one hand, by choosing the energy basis $|\omega_{ab}) = |E_a\rangle\langle E_b|$, it is true that

$$\mathcal{L}^n \, |O_0) = \delta_{n0} \sum_{a=1}^{D} O_{aa} \, |\omega_{aa}) + \sum_{\substack{a,b=1 \\ a \neq b}}^{D} O_{ab} \omega_{ab}^n \, |\omega_{ab}) \tag{4.19}$$

where the terms $\omega_{ab} = E_a - E_b$ are the "eigenvalues" of $\mathcal{L}$ corresponding to the eigenoperators $|\omega_{ab})$. We notice that the eigenvalues of the eigenvectors $|\omega_{aa})$, $\forall a \in \{1, \cdots, D\}$ and $n \geq 1$, are zero. Now, let us arrange the matrix elements from (4.19) as the rows in the matrix (4.18). When we do this, we obtain a matrix that is a Vandermonde matrix

$$\begin{pmatrix} O_{11} & O_{22} & \cdots & O_{DD} & O_{12} & O_{13} & \cdots & O_{D-1,D} \\ 0 & 0 & \cdots & 0 & O_{12}\omega_{12} & O_{13}\omega_{13} & \cdots & O_{D-1,D}\omega_{D-1,D} \\ 0 & 0 & \cdots & 0 & O_{12}\omega_{12}^2 & O_{13}\omega_{13}^2 & \cdots & O_{D-1,D}\omega_{D-1,D}^2 \\ \vdots & \vdots & \ddots & \vdots & \vdots & \vdots & \ddots & \vdots \\ 0 & 0 & \cdots & 0 & O_{12}\omega_{12}^{D^2-1} & O_{13}\omega_{13}^{D^2-1} & \cdots & O_{D-1,D}\omega_{D-1,D}^{D^2-1} \end{pmatrix}. \tag{4.20}$$

Note that the first row contains the coordinates from (4.19) for $n = 0$, the second line contains the coordinates for $n = 1$ and so on. Note also that the first D terms in the second row and the next ones ($n \geq 1$) are zero due to the Kronecker delta δ_{n0} appearing in (4.19). In order to calculate the rank of this matrix, we can compute its determinant, which is given by

$$\Delta\left(\{\omega_{ab}\}\right) \prod_{i,j=1}^{D} O_{ij} \tag{4.21}$$

where $\Delta(\{\omega_{ab}\})$ is the Vandermonde determinant of the phases $\{\omega_{ab}\}_{a,b}$. The determinant will be zero if any of the phases $\{\omega_{ab}\}$ are degenerate and if any of the terms $\{O_{ij}\}$ are zero. In these circumstances, the columns (or rows) must be removed from the matrix to be left with a matrix with maximal rank. Therefore we can formulate the problem in the following way: K is equal

to the number of distinct phases corresponding to the indices of non zero matrix elements of the operator O_0 in the energy basis, O_{ij}. Since the phase $\omega_{aa} = 0$ is at least D-fold degenerate and therefore it can only be counted once in order to the determinant do not vanish, then we conclude

$$1 \leq K \leq D^2 - D + 1. \tag{4.22}$$

Another way to get to the same bound was used in Ref. [103]. Since the Liouvillian $\mathcal{L}$ is a linear superoperator and we are looking at its rank, we recall from Linear Algebra that

$$\text{rank}(\mathcal{L}) = \dim(\text{img}(\mathcal{L})) \tag{4.23}$$

and from the rank-nullity theorem that

$$\dim(\text{img}(\mathcal{L})) + \dim(\ker(\mathcal{L})) = \dim(\text{Dom}(\mathcal{L})). \tag{4.24}$$

Once the Liouvillian can act on any element of the whole space of operators, then $\dim(\text{Dom}(\mathcal{L})) = D^2$. By definition, the kernel of the Liouvillian is the subset from its domain whose elements are mapped to the null vector by it. As $\mathcal{L}(\bullet) = [\hat{H}, \bullet]$, it is clear that $\mathcal{L}$ acting on vector like $|H^n)$ results in the null vector, because the hamiltonian commutes with any power of itself. Since we have at least $D - 1$ distinct elements of this form, then $\dim(\ker(\mathcal{L})) \leq D - 1$ and therefore

$$\text{rank}(\mathcal{L}) = K \leq D^2 - D + 1 \tag{4.25}$$

from (4.24).

Still following the analysis from Ref. [102], the degenerate eigenoperators $|\omega_{ab})$ of $\mathcal{L}$ with the same eigenvalue ω_{ab} also contribute to vanish the determinant (4.21) and must be accounted for. If the operator $\hat{O}_0$ has a non-vanishing overlap with these degenerate eigenoperators, then they contribute only once to the Krylov subpace. Now we refer to this set of eigenoperators corresponding to the same eigenvalue $\omega_{ab} = \omega$ as the ω-eigenspace of $\mathcal{L}$.

Then, we can ask: what particular linear combination of the elements belonging to each ω-eigenspace is actually contained in the Krylov subspace? Suppose that, for some set I of pairs of indices, the eigenoperator is degenerate

$$\mathcal{L}\,|\omega_{ab}) = \omega\,|\omega_{ab})\,, \quad \forall (a,b) \in I. \tag{4.26}$$

Assuming also that $\omega_{ab} \neq \omega$ for any $(a,b) \notin I$, then inserting (4.26) in (4.19), we find

$$\mathcal{L}^n(O_0) = \omega^n \sum_{(a,b)\in I} O_{ab}\,|\omega_{ab}) + \sum_{(a,b)\notin I} O_{ab}\omega_{ab}^n\,|\omega_{ab})\,. \tag{4.27}$$

Therefore, the direction of the ω-eigenspace that contributes to the Krylov space is precisely the projection of the operator O over such an eigenspace:

$$|\mathcal{K}_\omega) = \sum_{(a,b)\in I} O_{ab}\,|\omega_{ab})\,. \tag{4.28}$$

The authors in [102] call $|\mathcal{K}_\omega)$ the eigenspace representative for the phase ω. Thus, the structure of the Krylov subspace is now fully understood: *each eigenspace of the Liouvillian over which the operator O_0 has a non-vanishing projection contributes one Krylov dimension, through a linear combination of the basis of the eigenspace of the form* (4.28). We can thus redefine the Krylov subspace as

$$\mathcal{K}_{\hat{O}_0} = \text{span}\Big\{\,|\mathcal{K}_\omega)\,, \omega \in \text{Spec}(\mathcal{L})\Big\} \tag{4.29}$$

with $\text{Spec}(\mathcal{L})$ denoting the spectrum of $\mathcal{L}$. Hence, *the Krylov dimension K is equal to the number of non-zero eigenspaces representatives $|\mathcal{K}_\omega)$*.

For instance, if we have a system whose Liouvillian has a spectrum with no degeneracies (other than the unavoidable null phases $\omega_{aa} = 0, \forall a.$) and an operator that is dense in the energy basis, the Krylov dimension will be maximal, $K = D^2 - D + 1$. Thus, in general, the more degeneracies there are in the spectrum of the Liouvillian, the lower will be the Krylov dimension. From these observations, the authors in [102] conjecture the following: as the spectrum of chaotic systems is well described by Wigner-Dyson statistics and therefore do not feature degeneracies, thus typical operators in chaotic systems saturate the upper bound in (4.22); while for integrable systems, whose spectrum is well described by Poisson statistics, it is expected K to be significantly smaller than the upper bound. This conjecture has met support in different systems, as in the SYK_2 and SYK_4 [102] and the integrable XXZ spin chain [104, 105]. For the case of Krylov complexity in the Schrödinger picture, the conjecture also finds support in Ref. [97] for the Ising model with a tilted magnetic field.

Finally, we can properly interpret the Lanczos algorithm: each Lanczos step produces a new element $|A_n)$ orthogonal to all previous $|K_m)$, with $m < n$. This new element is either zero or a new direction in Krylov space. For $n < K$, $|A_n) \neq 0$, since the set that is being orthogonalized with this procedure has rank K. However, $|A_K)$ is orthogonal to $\{|K_n)\}_{n=0}^{K-1}$, which is already a complete orthogonal basis of $\mathcal{K}_{O_0}$, then it must therefore vanish, just as $b_K = \sqrt{(A_K|A_K)}$. We conclude that the Lanczos algorithm must terminate by hitting a zero once all directions in Krylov space have been exhausted. This is also valid in the Schrödinger picture.

Chapter 5

Krylov Complexity as a Probe of Dynamical and Spectral Transitions

Having introduced dynamical phase transitions of type I (DPT-I), excited-state quantum phase transitions (ESQPTs), and the notion of Krylov complexity in the previous chapters, we are now in a position to explore whether these concepts are intrinsically connected in the LMG model.

On the one hand, DPT-I is associated with symmetry restoration and is traditionally characterized through the long-time behavior of an order parameter. This naturally raises the question of whether Krylov complexity can capture the corresponding dynamical critical behavior and effectively act as a dynamical order parameter.

On the other hand, since DPT-I has been shown to be directly related to the presence of an ESQPT in the energy spectrum, it is equally compelling to ask whether Krylov complexity is sensitive to spectral criticality and can therefore serve as a probe of ESQPTs.

This chapter addresses these questions by presenting new results concerning the relation between DPT, ESQPT and the Krylov complexity of quantum state evolution following sudden quenches in the LMG model. All results reported here were obtained combining numerical simulations based on exact diagonalization with analytical insights. The connection between DPT-I and Krylov complexity has been published in Ref. [106] and the connection between ESQPT and Krylov complexity is still object of our investigation. Throughout this chapter, we set the coupling constant to $J = 1$. We recommend the use of the List of Symbols of this thesis to recall the notation.

5.1 Krylov complexity and DPT-I

We begin by analyzing the time evolution of the Krylov complexity $C_{\mathcal{K}}(t)$, defined in Eq. (4.9), following a quench in the LMG model described by the Hamiltonian in Eq. (2.2). The system is initially prepared in one of the ground states of the pre-quench Hamiltonian $H(h_0)$, and the quench is performed by suddenly changing the transverse field from h_0 to h_f.

By employing exact diagonalization, we compute $C_{\mathcal{K}}(t)/j$, where $j = N/2$ is the total spin angular momentum, for several values of h_0 and h_f. Representative results are shown in Fig. 5.1

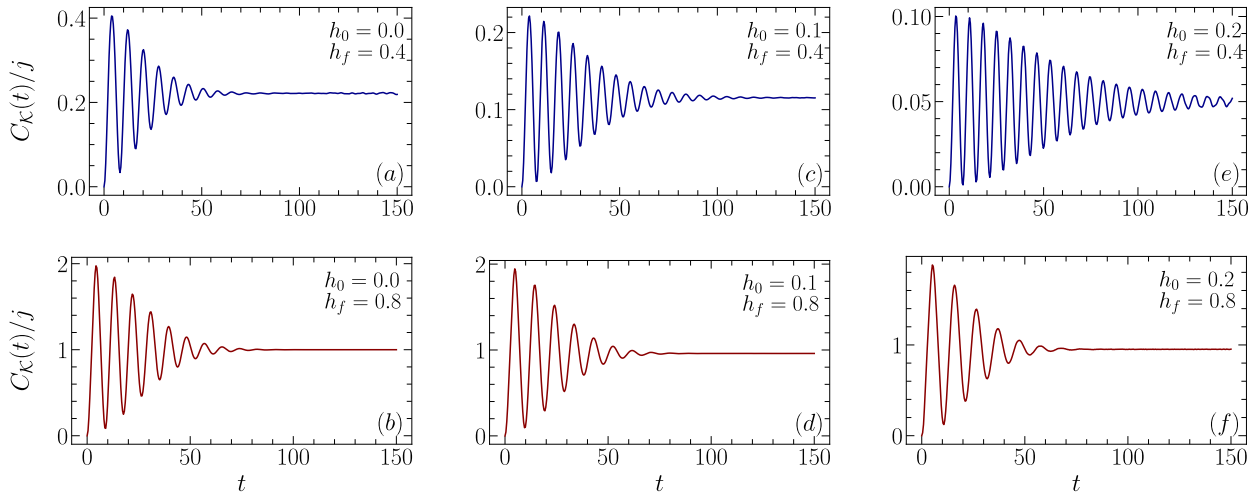

FIGURE 5.1: Krylov complexity as a function of time for several values of h_0 and h_f and $N = 200$. (a) For $h_0 = 0$, the calculations suggest that in the TL, the complexity oscillates and later stagnates around a finite value for quenches within the dynamical ferromagnetic phase ($h_f < h_c^d$). (b) Conversely it oscillates and later stagnates on the unit value for a quench into the paramagnetic phase. (c)-(f) As we increase h_0, we observe the same pattern for quenches within the same phase, however it stagnates on progressively smaller values than unity for $h_f > h_c^d$.

for a system size $N = 200$. These calculations reveal distinct dynamical behaviors depending on whether the quench remains within the same dynamical phase or crosses the dynamical critical point $h_c^d = (h_0 + J)/2$ [Eq. (3.51)].

For quenches starting at $h_0 = 0$, we observe that, in the TL, the Krylov complexity oscillates around a finite value when the post-quench parameter satisfies $h_f < h_c^d$, *i.e.*, when the quench remains within the dynamical ferromagnetic phase. Moreover, the amplitude of these oscillations progressively decays in time, causing the complexity to remain consistently below unity, as illustrated in Fig. 5.1(a). In contrast, when the quench crosses the dynamical critical point into the paramagnetic phase, $C_{\mathcal{K}}(t)$ exhibits oscillations that eventually stagnate at the unit value, as shown in Fig. 5.1(b). The choice behind normalizing $C_{\mathcal{K}}(t)$ by j is precisely to set the stagnation value $C(t \gg 1)$ to unit.

When the initial field is increased to $h_0 > 0$, the qualitative behavior of the Krylov complexity remains the same. For quenches within the dynamical ferromagnetic phase, $C_{\mathcal{K}}(t)$ continues to oscillate around a finite value, while for quenches across the dynamical critical point it exhibits a long-time saturation. However, in this case the saturation value is progressively smaller than unity as h_0 increases, as shown in Figs. 5.1(c)–(f). This behavior closely mirrors that of the dynamical magnetization discussed in Sec. 3.2 and illustrated in Fig. 3.6, indicating a clear correspondence between the Krylov complexity and the conventional dynamical order parameter of the LMG model.

These numerical observations were extensively tested and found to persist for larger system

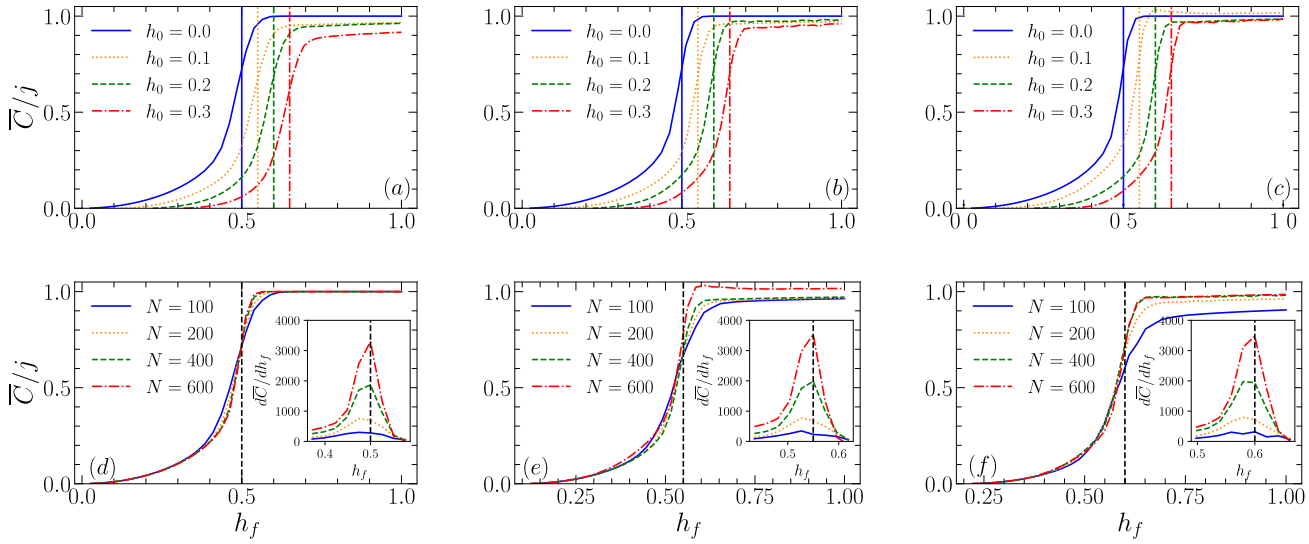

FIGURE 5.2: Normalized time averaged Krylov complexity $\overline{C}/j$ as a function of the post-quench parameter h_f. Panels (a)-(c) correspond to $N = 200$, $N = 400$ and $N = 600$ respectively for several values of h_0. $\overline{C}$ exhibits exactly the same transition as $\overline{S_z}$ at the dynamical critical point $h_c^d = (h_0 + J)/2$ indicated by the vertical lines. Panels (d)-(f) show $\overline{C}/j$ for several values of N corresponding to $h_0 = 0$, $h_0 = 0.1$ and $h_0 = 0.2$ respectively. As N increases, the nonanalytical point approaches the exact value indicated by the black vertical line at $h_c^d = (h_0 + J)/2$. The insets show the derivative of $\overline{C}$ w.r.t. h_f diverging at h_c^d as N increases. In all panels, we used $T = 150$.

sizes. As in the case of the magnetization, the Krylov complexity also displays revivals during the time evolution. The amplitude of these revivals decreases and they appear at later times as the system size N increases. Furthermore, when the ground state of $H(h_0)$ is twofold degenerate, we verified that choosing either of the degenerate ground states as the initial state leads to exactly the same behavior of $C(t)$.

5.1.1 Long-time average

Given this behaviour of $C_{\mathcal{K}}(t)$ in time, thus it is expected that its long-time average feature a nonanalytic transition in the dynamical critical point. By employing the time average

$$\overline{C} = \lim_{T\to\infty} \frac{1}{T} \int_0^T C_{\mathcal{K}}(t)\mathrm{d}t, \tag{5.1}$$

we observe the same qualitative behaviour as the dynamical order parameter $\overline{S_z}$. The figures 5.2(a)-(c) illustrate this result by showing the normalized time-averaged complexity as a function of the quenching intensity $h_0 < h_f \leq 1$ for several values of h_0, whose the only difference in comparison to $\overline{S_z}$ being the numerical values assumed in both dynamical phases. Note that as

discussed above, since $C_{\mathcal{K}}(t)$ stagnates on progressively smaller values than unity for $h_0 > 0$, thus its time-average features smaller plateaus as h_0 increases.

Moreover, the calculations reveal that $\overline{C}/j$ exhibits the same dynamical critical point as $\overline{S_z}$, h_c^d. The corresponding dynamical critical point for each value of h_0 is indicated by the vertical dashed lines in figure 5.2. This coincidence of the dynamical critical point is guaranteed by the fact that as N increases, the nonanalytical point approaches the exact value h_c^d as illustrated in the panels (d)-(f) in figure 5.2. This fact implies that the derivative of $\overline{C}$ with respect to h_f increasingly reaches higher values as N increases and shall diverge at h_c^d in the TL as observed in the insets from panels (d)-(f).

Despite a smaller plateau, $\overline{C}$ seems to reach a constant and maximum value for $h_f > h_c^d$, which suggests that DPT-I causes the maximum spreading regime of the dynamics. Based on these findings, we can argue that the time-averaged Krylov complexity reliably characterizes a DPT-I, being this fact our main result. In the calculations involving $\overline{C}$, both the degenerate ground-states were tested, yielding exactly the same results just as for $C_{\mathcal{K}}(t)$, which is another similarity with $\overline{S_z}$.

Once the DPT-I is related to the breaking/restoration of symmetry, we can infer that the Krylov basis is also sensitive to the symmetry of the model and, therefore, a deeper relation between the energy basis and Krylov basis should exist. The following discussions delve on this relation.

5.2 Inverse participation ratio

In order to understand the relation between the energy basis, which is the natural basis to probe symmetry breaking/restoration, and the Krylov basis, we employ the inverse participation ratio (IPR). The IPR is given by

$$\mathrm{IPR}(t) = \sum_n |\langle n|\psi(t)\rangle|^4 = \sum_n p_n^2(t) \tag{5.2}$$

for some basis whose elements we generically denote by $\{|n\rangle\}$. The IPR defined above measures how many states of the chosen basis effectively participate along the time evolution of the system. This quantity was proposed as a measure of localization on a certain basis in the context of quantum chaos [107, 108], thus originally, the IPR is time independent. However here we employ a dynamical version, probing how the system's state $|\psi_t\rangle$ explores a certain basis along time. Using the analogy with the Krylov chain, it means that the IPR should measure the level of localization of $|\psi_t\rangle$ in this chain for a nontrivial time evolution, since at $t = 0$, $|\psi_t\rangle$ is sharply localized in the first site of the Krylov chain as demands the first step of the Lanczos algorithm [see Eq. (4.2)].

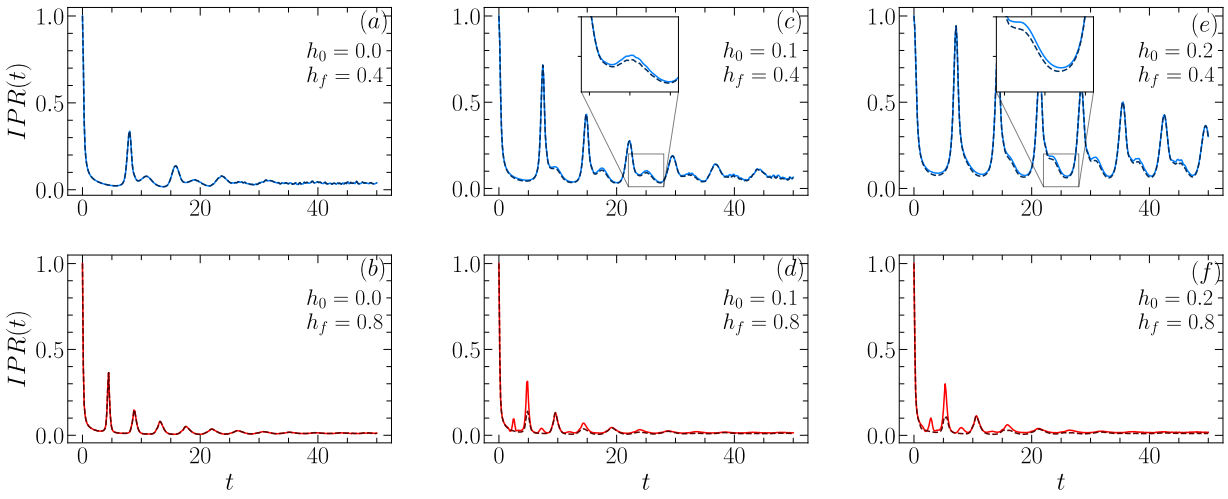

FIGURE 5.3: Inverse participation ratio calculated in the Krylov basis (dashed lines) and the prequench energy basis (solid lines) ($N = 200$). (a)-(b) Interestingly, for quenches starting at $h_0 = 0$, the IPR in both bases coincide. (c)-(d) In other hand, for quenches starting at $h_0 \neq 0$, the IPR shows itself different in both bases. Note that quenches crossing the dynamical critical point yield more delocalization of the system state in both bases in comparison to quenches within the same phase of h_0. The insets in (c) and (e) only helps to visualize the discrepancy between the curves.

From the definition above, we see that the maximum value the IPR(t) can assume is one. Since we choose $|\psi_0\rangle$ as being the ground-state of $\hat{H}(h_0)$ and the basis $\{|n\rangle\}_n$ being the pre-quench energy or the Krylov basis (with $|K_0\rangle = |\psi_0\rangle$), then IPR$(0) = 1$ and therefore IPR(t) must always decrease along the dynamics. The smaller IPR becomes, the more delocalized is $|\psi_t\rangle$ on the chosen bases.

Considering the same protocol as before, we compute the IPR for two distinct bases: the pre-quench energy eigenbasis (the eigenvectors of H_0) and the Krylov basis. Instances of the results are shown in Fig. 5.3. Interestingly, the IPR computed in both bases are identical only for quenches starting at $h_0 = 0$ [see the panels (a) and (b)]. On the other hand, when $h_0 \neq 0$, the IPR in the pre-quench energy basis do not coincide with that in the Krylov basis [see the panels (c)-(f)]. The reason behind these observations will be analytically shown in the last part of this chapter. Interestingly, the IPR in the Krylov basis for $h_0 > 0$ is slighly smaller than IPR in the pre-quench energy basis, which means along the dynamics the system state $|\psi_t\rangle$ is slightly more delocalized in the Krylov basis than the pre-quench energy, as expected since the Krylov basis minimizes the spreading in the Hilbert space.

We call the attention for two other aspects of the IPR. The first one is the appearance of periodic peaks that decay in amplitude along the dynamics. These peaks are due to partial revivals in the dynamics, that is, the state of the system periodically returns almost completely to the initial state, a feature expected for systems that exhibit DQPT including the LMG model [82, 109, 110]. This fact can also be seen by noticing that the first term of the sum in the IPR is the squared

survival probability

$$\mathrm{IPR}(t) = \mathcal{L}^2(t) + \sum_{k>0} p_k^2(t), \tag{5.3}$$

which characterizes DQPT (see the Eq. (3.6)), and the relation above holds for both the pre-quench energy basis and the Krylov basis in our protocol. Therefore, the IPR is also controlled by the survival probability. The second aspect of the IPR that we highlight is the decay rate. We observe that the larger is the difference between h_0 and h_f, more states participate in the dynamics, and hence, the faster the IPR decreases.

5.3 $\mathcal{K}$-Entropy - Shannon entropy in the Krylov basis

To further compare the Krylov basis with the pre-quench energy basis, we now consider the Shannon entropy, defined as

$$\mathcal{E}(t) = -\sum_n p_n(t) \ln[p_n(t)], \tag{5.4}$$

where $p_n(t)$ denotes the probability distribution associated with a given basis. The Shannon entropy quantifies the uncertainty of the quantum state over the chosen basis and therefore provides complementary information to the inverse participation ratio discussed in the previous section.

As before, we consider two distinct choices of basis. In the pre-quench energy basis, the probabilities are given by $p_n(t) = |\langle E_n^0|\psi_t\rangle|^2$, where $|E_n^0\rangle$ are the eigenstates of $H(h_0)$. In the Krylov basis, the probabilities read $p_n(t) = |\langle K_n|\psi_t\rangle|^2$.

The motivation for employing the Shannon entropy in this context is well established. In quantum information theory, the von Neumann entanglement entropy provides an estimate of the effective Hilbert space dimension explored by a quantum state, since the exponential of the entropy bounds the number of significantly occupied states. Extending this idea beyond entanglement measures, the exponential of the Shannon entropy may be interpreted as a measure of spread complexity [14]. This concept was originally introduced by Izrailev to characterize localization properties of chaotic quantum states [107] and was later employed in the context of Krylov complexity in Ref. [111].

Using the same quench protocol as in the previous sections, Fig. 5.4 shows the time evolution of the Shannon entropy computed in both the pre-quench energy basis (solid lines) and the Krylov basis (dashed lines). Panels (a) and (b) correspond to quenches starting at $h_0 = 0$, while panels (c)–(f) show representative results for quenches starting at $h_0 > 0$.

Similarly to the behavior observed for the IPR, we find a perfect agreement between the Shannon entropy computed in the two bases when $h_0 = 0$. In contrast, for $h_0 > 0$, the entropy exhibits a clear mismatch between the bases, irrespective of whether the quench remains within the same

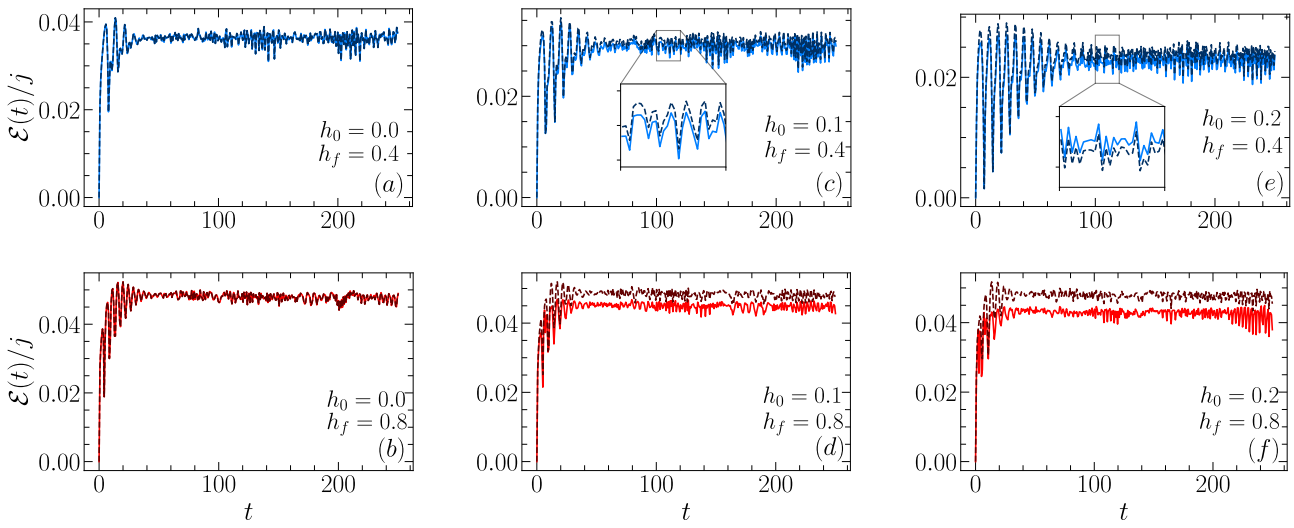

FIGURE 5.4: Shannon entropy calculated in the Krylov basis (dashed lines) and pre-quench energy basis (solid lines) ($N = 200$). (a) and (b) show its behaviour for a quench within the dynamical ferromagnetic phase and a quench across h_c^d respectively, in both cases one can see a perfect match between the curves. (c)-(f) show its behaviour for $h_0 > 0$, exhibiting a mismatch between the curves. In all the instances shown from (c)-(f), the Shannon entropy is bigger in the Krylov basis than the prequench energy basis, which is in accordance with the IPR's behaviour for the sames quenches. The insets help to visualize the mismatch.

dynamical phase or crosses the dynamical critical point. In all cases with $h_0 > 0$, the Shannon entropy in the Krylov basis is systematically larger than that in the pre-quench energy basis.

This behavior is fully consistent with the IPR results discussed previously. A smaller IPR in the Krylov basis indicates a stronger delocalization of the state $|\psi_t\rangle$, which naturally translates into a larger uncertainty and hence a larger Shannon entropy. Finally, as in the case of the IPR, we verified that choosing either of the twofold degenerate ground states as the initial state yields identical results for the Shannon entropy.

The systematic agreement observed at $h_0 = 0$, in contrast with the behavior for $h_0 > 0$, suggests that the coincidence between the two bases in this particular case is rooted in a specific structural property of the model, which will be addressed in the following section.

5.4 Krylov basis for $h_0 = 0$

We provide an analytical explanation for the coincidence observed between the IPR and the Shannon entropy computed in the Krylov basis and in the pre-quench energy basis for quenches starting at $h_0 = 0$. As shown in the previous sections, this agreement is a non-generic feature that breaks down as soon as the initial field is taken to be $h_0 > 0$. We show that, in the special case $h_0 = 0$, the Krylov basis can be constructed explicitly and, in fact, coincides with the angular

momentum basis associated with the eigenstates of the pre-quench Hamiltonian. This allows us to establish a direct analytical connection between the Krylov complexity and the dynamical magnetization, thereby explaining the numerical results reported above.

Let us consider quenches starting from $h_0 = 0$. The eigenstates of the pre-quench Hamiltonian

$$\hat{H}_0 = -\frac{1}{2j}\hat{S}_z^2, \tag{5.5}$$

are simple, they are the usual angular momentum basis $|j, m_z\rangle$, with the index $m_z \in \{-j, -j+1, \cdots, j-1, j\}$ specifying the $2j+1$ spin projections. The two degenerate ground-states are $|j, -j\rangle$ and $|j, j\rangle$. Then, the quench is performed in the magnetic field h such that the post-quench Hamiltonian can be written in terms of collective ladder operators

$$\hat{H}_f = -\frac{1}{2j}\hat{S}_z^2 - \frac{h_f}{2}\left(\hat{S}_+ + \hat{S}_-\right). \tag{5.6}$$

Now we observe that the set of operators $\{S_z, S_+, S_-\}$ are the operators defining the well-known $\mathfrak{su}(2)$ algebra, thus the following commutation relations hold

$$[S_z, S_\pm] = \pm S_\pm, \quad [S_+, S_-] = 2S_z. \tag{5.7}$$

The action of the Hamiltonian given in Eq. (5.6) on one of the basis states $|j, m_z\rangle$ is

$$H_f|j, m_z\rangle = c_0|j, m_z\rangle + c_+|j, m_z+1\rangle + c_-|j, m_z-1\rangle, \tag{5.8}$$

where $c_0 = -m_z^2/2j$, $c_+ = -\frac{h}{2}\sqrt{j(j+1) - m_z(m_z+1)}$ and $c_- = -\frac{h}{2}\sqrt{j(j+1) - m_z(m_z-1)}$. Comparing Eq. (5.8) with the tridiagonal form of the Hamiltonian in the Krylov basis, Eq. (4.5), we immediately see that the states satisfying the Lanczos algorithm for $|\psi_0\rangle = |j, m_z\rangle$ are precisely the set $\{|j, m_z\rangle\}$ up to a factor ± 1, that is

$$|K_i\rangle = \pm|j, m_z\rangle. \tag{5.9}$$

with the relation between the indices i and m_z being clarified below. Therefore, we conclude that the Krylov states are proportional to the pre-quench energy eigenstates. This explains why both the IPR and the Shannon entropy are the same in the Krylov and prequench energy bases.

The action of $\hat{H}_f$ on the state $|j, m_z\rangle$, Eq. (5.8), provides us an analytical expression for the Lanczos coefficients, which correspond to the constant c_-. For convenience, we relabel the index m_z as $m_z \to -j + m_z$ such that now m_z runs through the set $\{0, 1, \cdots, 2j\}$. With this change,

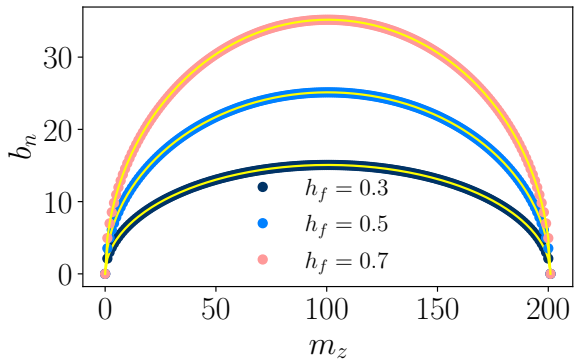

FIGURE 5.5: Comparison between the numerical (dots) and analytical (yellow lines) Lanczos coefficients for $N = 200$. They feature perfect agreement showing that $b_{m_z} = c_-(m_z)$ and attesting that the Krylov states are the usual angular momentum states $|j, m_z\rangle$ if the initial state is equal to any one of the ground-states.

the constant c_- becomes

$$c_-(m_z) = \frac{h_f}{2}\sqrt{m_z(2j - m_z + 1)}, \tag{5.10}$$

where we absorbed the minus sign in the state $|j, m_z\rangle$. The Figure 5.5 shows the perfect agreement between the Lanczos coefficients calculated numerically through the Lanczos algorithm [Eq. (4.3)] and the analytical expression for c_- above. Thus, we prove that $c_-(m_z)$ is the exact expression for the Lanczos coefficients b_{m_z} for quenches starting at $h_0 = 0$.

Since $|K_{m_z}\rangle = \pm|j, m_z\rangle$, the Krylov basis must share the same symmetries as the pre-quench energy basis. This fact turns the Krylov basis sensitive to the break or restoration of the spin-flip symmetry if a quench is performed in the LMG model, which explains the ability of the Krylov complexity to characterize DPT-I. Moreover, note that we can write the expression of the Krylov complexity in the form

$$C_{\mathcal{K}}(t) = \sum_{m_z=0}^{2j} m_z |\langle\psi_t|K_{m_z}\rangle|^2. \tag{5.11}$$

Considering now the expression of $S_z(t)$,

$$S_z(t) = \langle\psi_t|\hat{S}_z|\psi_t\rangle. \tag{5.12}$$

and employing the completeness of the angular momentum basis, $\sum_{m_z=0}^{2j} |j, -j + m_z\rangle\langle j, -j + m_z| = \mathbb{I}$, we can readily show that

$$C_{\mathcal{K}}(t) = S_z(t) + j, \tag{5.13}$$

thus, by taking the long-time average, confirming that

$$\overline{C} = \overline{S_z} + j. \tag{5.14}$$

The above construction shows that, for quenches starting at $h_0 = 0$, the Krylov basis generated by the post-quench Hamiltonian coincides exactly with the angular momentum basis associated with the eigenstates of the pre-quench Hamiltonian. As a consequence, the Krylov subspace spans the entire Hilbert space in the maximal-spin sector (Dicke subspace) for arbitrary finite system size N, highlighting that this result holds exactly and does not rely on the thermodynamic limit.

This exact correspondence provides a direct analytical explanation for the numerical results reported in the previous sections. Since the Krylov basis and the pre-quench energy basis are identical in this case, quantities that probe the spreading of the quantum state, such as the inverse participation ratio and the Shannon entropy, necessarily coincide when computed in either basis. Moreover, the explicit relation between the Krylov complexity and the magnetization establishes the time-averaged Krylov complexity as a genuine dynamical order parameter for the LMG model.

Finally, it is important to emphasize that this analytical construction relies crucially on the special structure of the initial state at $h_0 = 0$. As soon as the initial field is taken to be $h_0 > 0$, the Krylov basis no longer admits a closed-form construction and ceases to coincide with the pre-quench energy basis, in agreement with the numerical observations presented above. Obtaining an explicit analytical construction of the Krylov basis for $h_0 > 0$ and any system size N is a nontrivial problem, as the simple algebraic structure underlying the $h_0 = 0$ case is no longer present.

5.5 Krylov complexity and ESQPT

Once established the connection between DPT-I and ESQPT [section 3.3], if the long-time averaged Krylov complexity, $\overline{C}$, is sensitive to the DCP, then it is reasonable to think that $\overline{C}$ is sensitive to the ESQPT critical energy as well. This investigation can be carried out by employing the same quench protocol described in the section 3.3, in which the final energy $E_f = \langle\psi_0|\hat{H}_f|\psi_0\rangle$ becomes the control parameter by varying the pre-quench parameter h_0.

The quantity of interest in this case will be $\mathrm{Tr}\left[\rho_{\mathrm{eq}}\hat{K}\right]$, where

$$\hat{K} = \sum_{n=0}^{K-1} n|K_n\rangle\langle K_n| \tag{5.15}$$

is the Krylov operator. The figure 5.6 illustrates the behavior of $\mathrm{Tr}\left[\rho_{\mathrm{eq}}\hat{K}\right]/N$ with respect to E_f/N for several values of χ [See Eq. (3.52)] with $\hat{\rho}_{\mathrm{eq}}$ given by Eqs. (2.84a) and (2.84b). A sharp

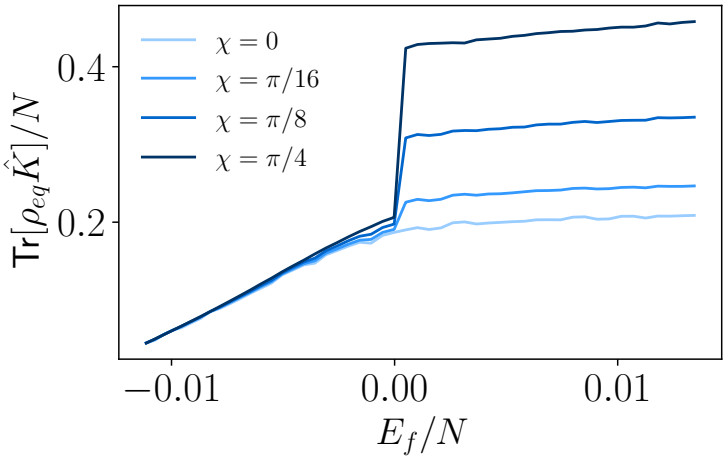

FIGURE 5.6: Average Krylov complexity as a function of the post-quench energy for different values of χ and $N = 600$. A sharp change of the average takes place at the ESQPT critical energy $E_c = 0$ when the initial state has undefined $\hat{\Pi}$ symmetry ($\chi \neq 0$). The closer is χ to $\pi/4$, the sharper is the change of the average Krylov complexity.

change in the averaged complexity is seen at the critical energy $E_c = 0$ when the initial state has undefined $\hat{\Pi}$ symmetry corresponding to $\chi \neq 0$. The closer χ is to $\pi/4$, the sharper is the change at $E_c = 0$.

Note that the average Krylov complexity $\mathrm{Tr}\left[\hat{\rho}_{\mathrm{eq}}\hat{K}\right]$ is sensitive to the degree of symmetry breaking in the initial state. In Fig. 5.6, the sharpest change at $E = 0$ occurs for $\chi = \pi/4$, corresponding to an initial state in which the $\hat{\Pi}$ symmetry is maximally broken, while the $\mathcal{C}$ symmetry remains well defined, the latter being responsible for the ESQPT in the LMG model. These results indicate that Krylov complexity provides a faithful probe of the ESQPT in this system. These findings open the way for further investigations currently in progress.

Chapter 6

Conclusions and future perspectives

Understanding nonequilibrium quantum dynamics remains one of the central challenges in the physics of many-body systems, particularly in the presence of critical phenomena that cannot be described in terms of conventional order parameters. Dynamical quantum phase transitions and excited-state quantum phase transitions exemplify this scenario, in which spectral and dynamical properties become inseparably linked in a highly nontrivial manner. The aim of this thesis was to investigate these transitions from the perspective of quantum complexity, exploring its ability to unveil critical structures underlying nonequilibrium dynamics. By employing a combination of analytical and numerical tools, we demonstrate that Krylov complexity provides a coherent and sensitive framework to characterize such phenomena, establishing a connection between nonequilibrium dynamics, spectral structure and information spreading.

By choosing the Lipkin–Meshkov–Glick model as a testbed, we showed that Krylov complexity in the Schrödinger picture under quench dynamics captures the same physical information as the collective magnetization as a function of time. In particular, Krylov complexity reveals distinct dynamical phases induced by quenches, mirroring the qualitative behavior observed in the magnetization dynamics. This initial result naturally motivated us to investigate the relation between the energy basis and the Krylov basis. To this end, we employed two quantities from information theory—the Shannon entropy and the inverse participation ratio—which quantify how the initial state spreads over a given basis. Our analysis shows that, in the specific case of quenches starting from a vanishing magnetic field, $h_0 = 0$, the energy and Krylov bases yield identical results for both measures, indicating a perfect correspondence between them. By contrast, for $h_0 \neq 0$, no such match is observed. Nevertheless, for any value of h_0, both quantities consistently capture the expected physics, clearly signaling the delocalization process induced by the quench.

We now turn to the main results of this thesis. We analytically proved that, for $h_0 = 0$, the Krylov basis coincides with the energy basis, up to an overall factor of ± 1. This equivalence establishes the long-time averaged Krylov complexity as an order parameter for the dynamical phase transition in the LMG model. For $h_0 \neq 0$, an exact analytical construction of the Krylov basis is no longer accessible; nevertheless, numerical analysis indicates that the long-time averaged Krylov complexity exhibits the same critical scaling behavior, supporting its role as a robust

diagnostic of dynamical phase transitions. All of these results mentioned above are published in Ref. [106].

These results naturally raise two fundamental issues. First, since the DPT-I in the LMG model is rooted in an excited-state quantum phase transition in its spectrum, an immediate question is whether Krylov complexity is also capable of detecting the ESQPT itself. Second, one may ask whether Krylov complexity can serve as an order parameter for ESQPTs and dynamical phase transitions in more general models. For the first issue, we have obtained an affirmative answer. Our analysis shows that the long-time averaged Krylov complexity faithfully signals the ESQPT in the LMG model, with its behavior depending on whether the initial state possesses indefinite or definite $\hat{\Pi}$ ($\mathcal{C}$) symmetry. This result indicates that Krylov complexity also acts as a sensitive probe of spectral phase transitions and constitutes part of an ongoing investigation into its ability to characterize ESQPTs.

We conjecture that Krylov complexity provides a universal framework for detecting excited-state and dynamical quantum phase transitions in a broad class of infinite-range interacting many-body systems. This conjecture is consistent with recent results by Corps and Relaño [9, 32], who established a causal connection between DPT-I and ESQPTs in systems satisfying a set of symmetry conditions. Representative examples include the LMG model, the Dicke model, the Rabi model, and spinor Bose–Einstein condensates. In this class of infinite-range interacting systems, ESQPTs share a common physical origin: an abrupt restructuring of the classical phase space at a critical energy, associated with a sudden change in the volume of accessible phase space. We argue that such a sharp spectral and semiclassical reorganization is naturally captured by the long-time averaged Krylov complexity. Establishing this conjecture in full generality remains an open problem and a natural direction for future work.

Taken together, the results presented in this thesis highlight the central role of Krylov complexity as a physically meaningful measure of information spreading in nonequilibrium quantum many-body systems. By establishing direct connections between nonequilibrium dynamics, spectral structure, and underlying semiclassical features, this work shows that Krylov complexity goes beyond a mere diagnostic tool, providing a unifying framework to characterize critical phenomena such as dynamical and excited-state quantum phase transitions. We expect that the perspective developed here will contribute to a deeper understanding of nonequilibrium quantum dynamics in interacting systems and motivate further studies of quantum complexity in a broad range of models.

Appendix A

The Symmetric Group

The purpose of this appendix is not to provide a comprehensive introduction to the symmetric group, but rather to fix notation and introduce a few group-theoretical notions that will be repeatedly used in the discussion of permutation-invariant Hamiltonians in the chapter 2.

In a system of N identical particles, there are $N!$ permutations of the particles and we can represent each permutation by a linear operator P. The set of all these permutations forms the permutation group or the symmetric group, which we denote by $\mathcal{S}_N$. It means that

1. It shall exists a permutation that represents the identity of $\mathcal{S}_N$, which we will denote by $\mathbb{I}$, that satisfies $P\mathbb{I} = \mathbb{I}P = P, \forall P \in \mathcal{S}_N$.

2. Every permutation P has its inverse P^{-1} such that $PP^{-1} = P^{-1}P = \mathbb{I}$.

3. The product of two permutations is also a permutation, which implies that any function of permutations is reducible to a linear function of them.

Suppose you have a system consisting of five spins-$1/2$ and whose quantum state is $|\uparrow\uparrow\downarrow\uparrow\downarrow\rangle$, where $\{\uparrow, \downarrow\}$ represent the two possible projections along $\hat{z}$-direction. This state can be written as the product of unique particle states

$$|\uparrow\uparrow\downarrow\uparrow\downarrow\rangle = |\uparrow\rangle_1 \otimes |\uparrow\rangle_2 \otimes |\downarrow\rangle_3 \otimes |\uparrow\rangle_4 \otimes |\uparrow\rangle_5 \tag{A.1}$$

where the integer subscript in each state denotes for example the corresponding site on a one-dimensional chain. In this case, applying a permutation operator on this state means simply change the integer subscript of each unique particle state. For this reason, instead of writing the explicitly quantum state, we can apply the permutation operators on lists of integer numbers, in this particular case the list $[12345]$.

A certain permutation can be written as the product of permutations of two particles that are called transpositions. For example, to transform the list $[123]$ into $[312]$ we can interchange 1 and 3, the operation which is denoted by (13) and then we interchange 1 and 2, which is denoted by (12). The composition of these two transpositions will be simply the product $P = (12)(13)$, which is read from right to left.

The representation of permutations is not unique, for instance another possible representation is written in terms of cycles. A permutation is in the cycles representation if its cycles have no number in common. For instance the composition $P = (12)(13)$ in cycles representation is written as $P = (132)$. In a permutation, the unchanged numbers of the list on which it acts are usually suppressed and they are called fixed points of the permutation. It means that the transposition $(12) \equiv (12)(3)$, where (3) is the fixed point. Therefore, the identity of $\mathcal{S}_N$ must the permutation $\mathbb{I} = (1)(2)\cdots(N)$, in which all the numbers are fixed points and acts in the list $[12\cdots N]$ keeping all the numbers unchanged. The number of transpositions necessary to represent a permutation is called the rank, $R(P)$. If $P \in \mathcal{S}_N$ and $\ell(P)$ is the number of cycles in P, then $R(P) = N - \ell(P)$.

Instead of studying the action of permutations on lists, we can define actions of the group $\mathcal{S}_N$ on itself. One of these actions is called *adjunct*, defined through the multiplication by left, that is, P "acts" on the permutation Q producing PQ. Given a permutation R, it is always possible to find Q such that $PQ = R$. Hence, the image of $\mathcal{S}_N$ under the action of P is always itself, $P\mathcal{S}_N = \mathcal{S}_N$. Another possible action of $\mathcal{S}_N$ on itself is the *conjugation*. In this case, P acts on Q through the operation $PQP^{-1} = R$, also called similarity transformation. If $PQP^{-1} = R$, then R and Q are said conjugate permutations. Differently from the action adjunct, the conjugation is not transitive, since the conjugation forms invariant subspaces, which means that there are sets of permutations that are conjugate only between themselves. The set of permutations which are conjugate between themselves constitutes a *conjugacy class*.

What the similarity transformation does is only to rearrange the numbers in a permutation, leaving its cycles with the same length, for example, $(134)(12345)(143) = (13542)$ and $(12)(13)(24)(12) = (14)(23)$. Here one stabilishes the connection between permutations and integer partitions. The partitions of an integer n are defined as all the monotonically decreasing sequences of positive integers $(\lambda_1, \lambda_2, \cdots)$ such that $\sum_{i=1}^{\ell(\lambda)} \lambda_i = n$. For instance, the partitions of 4 are $\{(4), (3,1), (2,2), (2,1,1), (1,1,1,1)\}$[1]. If a certain permutation P has $\hat{\lambda}_j$ cycles of length j, the partition $1^{\hat{\lambda}_1}2^{\hat{\lambda}_2}\cdots$ is called the cycle-type of P, for example the cycle-type of $P = (123)(45)(67)$ is $1^0 2^2 3^1 \equiv (3,2,2)$. As we shall see in the chapter 2, the cycle-type provides a natural label for invariant subspaces induced by permutation symmetry of the Hilbert space of a quantum system.

It turns out that all the possibilities of cycle-types of the permutations from $\mathcal{S}_N$ are exactly the partitions of the integer N. This fact makes it easy to identify the conjugacy classes of $\mathcal{S}_N$, for instance the conjugacy classes of $\mathcal{S}_4$ are $\mathcal{C}_{(1,1,1,1)} = \{(1)(2)(3)(4)\}$, $\mathcal{C}_{(2,1,1)} = \{(12), (13), (14), (23), (24), (34)\}$, $\mathcal{C}_{(2,2)} = \{(12)(34), (13)(24), (14)(23)\}$, $\mathcal{C}_{(3,1)} = \{(123), (132), (124), (142), (134), (143), (234), (243)\}$ and $\mathcal{C}_{(4)} = \{(1234), (1243), (1324), (1342)\ (1423), (1432)\}$. We denote the number of partitions of an integer n by $p(n)$.

[1] If we take into account all the distinct rearrengements of these partitions, then we are talking about compositions. The number 4 has eight compositions, which include besides the aforementioned ones, the following $\{(3,1), (1,2,1), (1,1,2)\}$

These notions allow us to classify permutations in $\mathcal{S}_N$ in a way that is particularly suited to the analysis of symmetric Hamiltonians. In the chapter 2, this structure will be exploited to characterize invariant subspaces and degeneracies induced by permutation symmetry

Appendix B

Stability of the saddle point

In order to know how the orbits in the phase space behave near the stationary points, we conduct an analysis of their stability. If the orbits move away from a certain stationary point, this point is considered unstable and otherwise stable.

Consider an orbit close to the stationary point (q_0, p_0)

$$q(t) = q_0 + \delta q(t), \qquad p(t) = p_0 + \delta p(t). \tag{B.1}$$

By writing the Hamilton equations in these two points and expanding until first order in the deviations δq e δp, we have

$$\frac{\partial H}{\partial p}(q_0 + \delta q, p_0 + \delta p) = \left.\frac{\partial H}{\partial p}\right|_{(q_0,p_0)} + \left.\frac{\partial^2 H}{\partial q \partial p}\right|_{(q_0,p_0)} \delta q + \left.\frac{\partial^2 H}{\partial p^2}\right|_{(q_0,p_0)} \delta p + \mathcal{O}(||\delta||^2) \tag{B.2}$$

$$\frac{\partial H}{\partial q}(q_0 + \delta q, p_0 + \delta p) = \left.\frac{\partial H}{\partial q}\right|_{(q_0,p_0)} + \left.\frac{\partial^2 H}{\partial q^2}\right|_{(q_0,p_0)} \delta q + \left.\frac{\partial^2 H}{\partial p \partial q}\right|_{(q_0,p_0)} \delta p + \mathcal{O}(||\delta||^2). \tag{B.3}$$

and thus we get

$$\delta\dot{q} = \quad H_{qp}\delta q + H_{pp}\delta p \tag{B.4}$$

$$\delta\dot{p} = -H_{qq}\delta q - H_{pq}\delta p \tag{B.5}$$

where the first term in each equation is zero, since (q_0, p_0) are stationary points and we used a compact notation for the second derivatives. In matrix notation, we have

$$\begin{pmatrix} \delta\dot{q} \\ \delta\dot{p} \end{pmatrix} = \begin{pmatrix} H_{qp} & H_{pp} \\ -H_{qq} & -H_{pq} \end{pmatrix} \begin{pmatrix} \delta q \\ \delta p \end{pmatrix} \tag{B.6}$$

and in sympletic notation, we have

$$\delta\dot{\eta} = JH''\delta\eta \tag{B.7}$$

where J is the sympletic matrix given by

$$J = \begin{pmatrix} 0 & 1 \\ -1 & 0 \end{pmatrix} \tag{B.8}$$

and $H''_{ij} = \partial^2 H / \partial\eta_i \partial\eta_j$ is the usual matrix of the second derivatives of H evaluated in the stationary point (q_0, p_0), with $\eta_1 = q$ and $\eta_2 = p$.

The eigenvalues of $A = JH''$ are important to determine the stability of the stationary points and they are given by

$$\lambda = \pm\sqrt{-\det H''}. \tag{B.9}$$

Since A is a real matrix, there are only two possible cases:

1. λ is a real eigenvalue and $-\lambda$ is the second one. In this case $\det H'' < 0$.
2. λ is pure imaginary and $\lambda^* = -\lambda$ is the second one. In this case $\det H'' > 0$.

In the ferromagnetic phase of the LMG model, we know from our previous discussion in the section 2.4 that the point $(q, p) = (0, 0)$ becomes unstable. We solve the equation (B.7) around this point in what follows.

We can always choose the eigenvectors of A to expand the vector $\delta\eta$ [ref]. Let v_1 and v_2 be these eigenvectors, then we have the equations

$$\dot{v}_1 = Av_1 = \lambda v_1 \quad \rightarrow \quad v_1(t) = v_1^0 e^{\lambda t} \tag{B.10a}$$

$$\dot{v}_2 = Av_2 = -\lambda v_2 \quad \rightarrow \quad v_2(t) = v_2^0 e^{-\lambda t}. \tag{B.10b}$$

For the unstable point, the matrix A takes the form

$$A = \begin{pmatrix} 0 & \frac{J}{4} + h \\ J - h & 0 \end{pmatrix} \tag{B.11}$$

whose eigenvectors and eigenvalues are

$$v_1 = \begin{pmatrix} -\frac{1}{2}\sqrt{\frac{J+4h}{J-h}} \\ 1 \end{pmatrix}, \qquad v_2 = \begin{pmatrix} \frac{1}{2}\sqrt{\frac{J+4h}{J-h}} \\ 1 \end{pmatrix} \tag{B.12a}$$

$$\lambda_1 = \frac{1}{2}\sqrt{(J-h)(J+4h)}, \qquad \lambda_2 = -\frac{1}{2}\sqrt{(J-h)(J+4h)}. \tag{B.12b}$$

Thus, we can write the expansion

$$\delta\eta(t) = \alpha_1 v_1(t) + \alpha_2 v_2(t) = \alpha_1 v_1^0 e^{\lambda t} + \alpha_2 v_2^0 e^{-\lambda t} \tag{B.13}$$

and explicitly in terms of q and p

$$\begin{pmatrix} \delta q(t) \\ \delta p(t) \end{pmatrix} = \begin{pmatrix} v^0_{1,q} & v^0_{2,q} \\ v^0_{1,p} & v^0_{2,p} \end{pmatrix} \begin{pmatrix} e^{\lambda t} & 0 \\ 0 & e^{-\lambda t} \end{pmatrix} \begin{pmatrix} \alpha_1 \\ \alpha_2 \end{pmatrix} \tag{B.14}$$

$$= \begin{pmatrix} \frac{1}{2}\sqrt{\frac{J+4h}{J-h}} & -\frac{1}{2}\sqrt{\frac{J+4h}{J-h}} \\ 1 & 1 \end{pmatrix} \begin{pmatrix} e^{\lambda t} & 0 \\ 0 & e^{-\lambda t} \end{pmatrix} \begin{pmatrix} \alpha_1 \\ \alpha_2 \end{pmatrix}. \tag{B.15}$$

After algebraic manipulations, we finally get the final form

$$\begin{pmatrix} \delta q(t) \\ \delta p(t) \end{pmatrix} = \begin{pmatrix} \cosh(\lambda t) & \frac{1}{2}\sqrt{\frac{J+4h}{J-h}}\sinh(\lambda t) \\ \frac{2}{\sqrt{\frac{J+4h}{J-h}}}\sinh(\lambda t) & \cosh(\lambda t) \end{pmatrix} \begin{pmatrix} \delta q(0) \\ \delta p(0) \end{pmatrix} \tag{B.16}$$

which shows that there is a direction in which the orbits approach exponentially fast (q_0, p_0) and another direction in which the orbits move away exponentially fast from (q_0, p_0). This unstable point is also called hyperbolic.

Appendix C

Dynamical order parameter of the LMG model

In this Appendix we derive an analytic expression for the long-time averaged magnetization

$$\overline{X} \equiv \lim_{T\to\infty} \frac{1}{T} \int_0^T X(t)\, dt, \tag{C.1}$$

in the semiclassical (thermodynamic) limit of the LMG model, for initial conditions of the form $(\theta_0, \phi_0 = 0)$. In the TL $N \to \infty$, the LMG Hamiltonian reduces to the classical energy function

$$H_{\rm cl}(X, Y, Z) = -sZ - \frac{1-s}{2} X^2, \tag{C.2}$$

with the constraint $X^2 + Y^2 + Z^2 = 1$. Using spherical coordinates,

$$X = \sin\theta\cos\phi, \qquad Y = \sin\theta\sin\phi, \qquad Z = \cos\theta, \tag{C.3}$$

the classical energy becomes

$$E(\theta, \phi) = -(1-s)\cos\theta - \frac{s}{2}\sin^2\theta\cos^2\phi. \tag{C.4}$$

For the class of initial conditions considered here, $\phi_0 = 0$, the motion remains confined to the plane $\phi(t) = 0$, and the dynamics reduces to a one-dimensional problem in the variable $\theta(t)$. The conserved energy is therefore

$$E_0 = -(1-s)\cos\theta_0 - \frac{s}{2}\sin^2\theta_0. \tag{C.5}$$

From the classical equations of motion, we have

$$\dot\theta = -s\sin\theta\sin\phi, \qquad \dot\phi = (1-s) - s\cos\theta\cos\phi, \tag{C.6}$$

and imposing $\phi = 0$, one finds

$$\dot{\theta}^2 = s^2 \sin^2\theta \,(\cos\theta - \cos\theta_-)\,(\cos\theta_+ - \cos\theta)\,, \tag{C.7}$$

where $\theta_\pm$ are the turning points of the motion, determined by $E(\theta_\pm, 0) = E_0$.

The dynamics is therefore periodic whenever the motion is bounded between θ_- and θ_+, with period

$$T = 2\int_{\theta_-}^{\theta_+} \frac{d\theta}{|\dot{\theta}|}. \tag{C.8}$$

C.1 Determination of the turning points

The turning points of the motion correspond to the solutions of the equation $\dot{\theta} = 0$, which occurs when $\phi = 0$ and the energy condition $E(\theta, 0) = E_0$ is satisfied. Using Eq. (C.5), this condition reads

$$-(1-s)\cos\theta - \frac{s}{2}\sin^2\theta = -(1-s)\cos\theta_0 - \frac{s}{2}\sin^2\theta_0. \tag{C.9}$$

Introducing the variable

$$u \equiv \cos\theta, \tag{C.10}$$

and using $\sin^2\theta = 1 - u^2$, the above equation becomes

$$\frac{s}{2}u^2 - (1-s)u - \left[\frac{s}{2}\cos^2\theta_0 - (1-s)\cos\theta_0\right] = 0. \tag{C.11}$$

Solving Eq. (C.11) yields the two real roots

$$u_\pm = \frac{1-s}{s} \pm \sqrt{\left(\frac{1-s}{s} - \cos\theta_0\right)^2 + \sin^2\theta_0}, \tag{C.12}$$

which define the classical turning points of the motion. The trajectory is therefore confined to the interval $u_- \le u \le u_+$.

C.2 Time-averaged magnetization

The long-time average of $X = \sin\theta$ can be written as

$$\overline{X} = \frac{\displaystyle\int_{\theta_-}^{\theta_+} \frac{\sin\theta\, d\theta}{\dot{\theta}}}{\displaystyle\int_{\theta_-}^{\theta_+} \frac{d\theta}{\dot{\theta}}}. \tag{C.13}$$

Substituting Eq. (C.7) into Eq. (C.13), we obtain

$$\overline{X} = \frac{\displaystyle\int_{\theta_-}^{\theta_+} \frac{\sin\theta\, d\theta}{\sqrt{(\cos\theta_+ - \cos\theta)(\cos\theta - \cos\theta_-)}}}{\displaystyle\int_{\theta_-}^{\theta_+} \frac{d\theta}{\sqrt{(\cos\theta_+ - \cos\theta)(\cos\theta - \cos\theta_-)}}}. \tag{C.14}$$

Performing the change of variables $u = \cos\theta$, $du = -\sin\theta\, d\theta$, the numerator becomes

$$\int_{u_-}^{u_+} \frac{du}{\sqrt{(u_+ - u)(u - u_-)}} = \pi, \tag{C.15}$$

while the denominator reads

$$\int_{u_-}^{u_+} \frac{du}{\sqrt{(1-u^2)(u_+ - u)(u - u_-)}}, \tag{C.16}$$

which is a complete elliptic integral of the first kind.

The final result can therefore be written as

$$\overline{X} = \frac{\pi}{\displaystyle\int_{u_-}^{u_+} \frac{du}{\sqrt{(1-u^2)(u_+ - u)(u - u_-)}}}. \tag{C.17}$$

C.2.1 Reduction to elliptic integrals and phase-dependent behavior

We now show how the integral

$$\overline{X} = \frac{\pi}{\displaystyle\int_{u_-}^{u_+} \frac{du}{\sqrt{(1-u^2)(u_+ - u)(u - u_-)}}}, \tag{C.18}$$

leads to the piecewise result given in Eq. (C.29).

$\mathbf{E} > \mathbf{E_c}$: For $s \geq s_c^d(\theta_0)$, the initial energy exceeds the separatrix energy and the classical orbit spans symmetrically both hemispheres of the Bloch sphere. In this case, $u(t) = \cos\theta(t)$ changes sign during the evolution, and the time average of $X = \sin\theta$ vanishes by symmetry,

$$\overline{X} = 0, \qquad s > s_c^d(\theta_0). \tag{C.19}$$

$\mathbf{E} < \mathbf{E_c}$: For energies below the separatrix, corresponding to $s < s_c^d(\theta_0)$, the classical trajectory becomes self-trapped in a single hemisphere. In this regime, $u(t)$ remains of fixed sign and $\overline{X}$ acquires a finite value.

The integral in the denominator of Eq. (C.18),

$$I = \int_{u_-}^{u_+} \frac{du}{\sqrt{(1-u^2)(u_+-u)(u-u_-)}}, \tag{C.20}$$

is a complete elliptic integral of the first kind. To make this explicit, we introduce the standard substitution

$$u = u_- + (u_+ - u_-)\sin^2\psi, \qquad du = 2(u_+ - u_-)\sin\psi\cos\psi\, d\psi. \tag{C.21}$$

With this change of variables, the factors in the square root become

$$u - u_- = (u_+ - u_-)\sin^2\psi, \tag{C.22}$$

$$u_+ - u = (u_+ - u_-)\cos^2\psi, \tag{C.23}$$

$$1 - u^2 = (1-u_-^2)\left(1 - \kappa\sin^2\psi\right), \tag{C.24}$$

where the elliptic modulus is defined as

$$\kappa = \frac{u_+^2 - u_-^2}{1-u_-^2}. \tag{C.25}$$

Substituting into Eq. (C.20), the integral reduces to

$$I = \frac{2}{\sqrt{1-u_-^2}} \int_0^{\pi/2} \frac{d\psi}{\sqrt{1-\kappa\sin^2\psi}} = \frac{2}{\sqrt{1-u_-^2}}\, K(\kappa), \tag{C.26}$$

where $K(\kappa)$ denotes the complete elliptic integral of the first kind.

Final expression. Inserting Eq. (C.26) into Eq. (C.18), we obtain

$$\overline{X} = \frac{\pi}{2}\sqrt{1-u_-^2}\,\frac{1}{K(\kappa)}. \tag{C.27}$$

Using the explicit expression of the turning point u_- in terms of the initial condition θ_0, one finds in the regime $E < E_c$

$$\sqrt{1-u_-^2} = \frac{2\sin\theta_0}{1+\cos^2(\theta_0/2)}. \tag{C.28}$$

Substituting Eq. (C.28) into Eq. (C.27), we finally arrive at

$$\overline{X} = \begin{cases} 0, & s \geq s_c(\theta_0), \\ \dfrac{2}{\pi}\dfrac{\sin\theta_0}{1+\cos^2(\theta_0/2)} K(\kappa(\theta_0, s)), & s < s_c(\theta_0), \end{cases} \tag{C.29}$$

which explicitly shows the emergence of a finite time-averaged magnetization upon crossing the classical separatrix.

Bibliography

[1] A. Polkovnikov, K. Sengupta, A. Silva, and M. Vengalattore, Colloquium: nonequilibrium dynamics of closed interacting quantum systems, Rev. Mod. Phys. **83**, 863–883 (2011).

[2] J. Eisert, M. Friesdorf, and C. Gogolin, Quantum many-body systems out of equilibrium, Nature Physics **11**, 124–130 (2015).

[3] S. L. Sondhi, S. M. Girvin, J. P. Carini, and D. Shahar, Continuous quantum phase transitions, Rev. Mod. Phys. **69**, 315–333 (1997).

[4] S. Sachdev, *Quantum phase transitions* (Cambridge University Press, 2011).

[5] M. Heyl, Dynamical quantum phase transitions: a review, Reports on Progress in Physics **81**, 054001 (2018).

[6] J. Marino, M. Eckstein, M. S. Foster, and A. M. Rey, Dynamical phase transitions in the collisionless pre-thermal states of isolated quantum systems: theory and experiments, Reports on Progress in Physics **85**, 116001 (2022).

[7] N. Defenu, A. Lerose, and S. Pappalardi, Out-of-equilibrium dynamics of quantum many-body systems with long-range interactions, Physics Reports **1074**, Out-of-equilibrium dynamics of quantum many-body systems with long-range interactions, 1–92 (2024).

[8] P. Cejnar, P. Stránskỳ, M. Macek, and M. Kloc, Excited-state quantum phase transitions, Journal of Physics A: Mathematical and Theoretical **54**, 133001 (2021).

[9] Á. L. Corps and A. Relaño, Theory of dynamical phase transitions in quantum systems with symmetry-breaking eigenstates, Physical review letters **130**, 100402 (2023).

[10] E. Rabinovici, A. Sánchez-Garrido, R. Shir, and J. Sonner, *Krylov complexity*, 2025.

[11] P. Nandy, A. S. Matsoukas-Roubeas, P. Martínez-Azcona, A. Dymarsky, and A. del Campo, Quantum dynamics in krylov space: methods and applications, Physics Reports **1125-1128**, Quantum dynamics in Krylov space: Methods and applications, 1–82 (2025).

[12] J. Maldacena, S. H. Shenker, and D. Stanford, A bound on chaos, Journal of High Energy Physics **2016**, 1–17 (2016).

[13] D. E. Parker, X. Cao, A. Avdoshkin, T. Scaffidi, and E. Altman, A Universal Operator Growth Hypothesis, Phys. Rev. X **9**, 041017 (2019).

[14] V. Balasubramanian, P. Caputa, J. M. Magan, and Q. Wu, Quantum chaos and the complexity of spread of states, Phys. Rev. D **106**, 046007 (2022).

[15] H. J. Lipkin, N. Meshkov, and A. J. Glick, Validity of many-body approximation methods for a solvable model:(I). Exact solutions and perturbation theory, Nuclear Physics **62**, 188–198 (1965).

[16] N. Meshkov, A. Glick, and H. Lipkin, Validity of many-body approximation methods for a solvable model: (ii). linearization procedures, Nuclear Physics **62**, 199–210 (1965).

[17] A. Glick, H. Lipkin, and N. Meshkov, Validity of many-body approximation methods for a solvable model: (iii). diagram summations, Nuclear Physics **62**, 211–224 (1965).

[18] P. Dirac, *The Principles of Quantum Mechanics*, 4th edition, International Series of Monographs on Physics (Oxford at Clarendon Press, 1982).

[19] J. J. Sakurai and J. Napolitano, *Modern quantum mechanics*, 3rd ed. (Cambridge University Press, 2020).

[20] I. Homrighausen, "Quantum quench dynamics in the transverse field Ising model of fully connected spins: an entanglement based study beyond mean field", PhD thesis (Dissertation, Göttingen, Georg-August Universität, 2021).

[21] I. Homrighausen and S. Kehrein, Out of equilibrium mean field dynamics in the transverse field Ising model, arXiv:1908.02596 [cond-mat.stat-mech] (2019).

[22] L. G. Yaffe, Large N limits as classical mechanics, Rev. Mod. Phys. **54**, 407–435 (1982).

[23] T. Opatrnỳ, L. Richterek, and M. Opatrnỳ, Analogies of the classical euler top with a rotor to spin squeezing and quantum phase transitions in a generalized lipkin-meshkov-glick model, Scientific Reports **8**, 1984 (2018).

[24] K. Chinni, P. M. Poggi, and I. H. Deutsch, Effect of chaos on the simulation of quantum critical phenomena in analog quantum simulators, Phys. Rev. Res. **3**, 033145 (2021).

[25] L. F. Santos, M. Távora, and F. Pérez-Bernal, Excited-state quantum phase transitions in many-body systems with infinite-range interaction: localization, dynamics, and bifurcation, Physical Review A **94**, 012113 (2016).

[26] W.-M. Zhang, D. H. Feng, and R. Gilmore, Coherent states: theory and some applications, Rev. Mod. Phys. **62**, 867–927 (1990).

[27] P. Ribeiro, J. Vidal, and R. Mosseri, Exact spectrum of the lipkin-meshkov-glick model in the thermodynamic limit and finite-size corrections, Phys. Rev. E **78**, 021106 (2008).

[28] P. Ribeiro and T. Paul, Semiclassical analysis of spin systems near critical energies, Phys. Rev. A **79**, 032107 (2009).

[29] R. Botet and R. Jullien, Large-size critical behavior of infinitely coordinated systems, Phys. Rev. B **28**, 3955–3967 (1983).

[30] F. Leyvraz and W. Heiss, Large-n scaling behavior of the lipkin-meshkov-glick model, Physical review letters **95**, 050402 (2005).

[31] C. M. Newman and L. S. Schulman, Metastability and the analytic continuation of eigenvalues, Journal of Mathematical Physics **18**, 23–30 (1977).

[32] Á. L. Corps and A. Relaño, Dynamical and excited-state quantum phase transitions in collective systems, Physical Review B **106**, 024311 (2022).

[33] R. Puebla and A. Relano, Non-thermal excited-state quantum phase transitions, Europhysics Letters **104**, 50007 (2014).

[34] Q. Wang and F. Pérez-Bernal, Characterizing the lipkin-meshkov-glick model excited-state quantum phase transition using dynamical and statistical properties of the diagonal entropy, Physical Review E **103**, 032109 (2021).

[35] P. Stránský and P. Cejnar, Classification of excited-state quantum phase transitions for arbitrary number of degrees of freedom, Physics Letters A **380**, 2637–2643 (2016).

[36] M. C. Gutzwiller, *Chaos in classical and quantum mechanics*, Vol. 1 (Springer Science & Business Media, 2013).

[37] Y. Matsumoto, *An introduction to morse theory*, Vol. 208 (American Mathematical Soc., 2002).

[38] I. Homrighausen, N. O. Abeling, V. Zauner-Stauber, and J. C. Halimeh, Anomalous dynamical phase in quantum spin chains with long-range interactions, Phys. Rev. B **96**, 104436 (2017).

[39] M. Rigol, V. Dunjko, V. Yurovsky, and M. Olshanii, Relaxation in a completely integrable many-body quantum system: an ab initio study of the dynamics of the highly excited states of 1d lattice hard-core bosons, Phys. Rev. Lett. **98**, 050405 (2007).

[40] P. Sala, T. Rakovszky, R. Verresen, M. Knap, and F. Pollmann, Ergodicity breaking arising from hilbert space fragmentation in dipole-conserving hamiltonians, Phys. Rev. X **10**, 011047 (2020).

[41] V. Khemani, M. Hermele, and R. Nandkishore, Localization from hilbert space shattering: from theory to physical realizations, Phys. Rev. B **101**, 174204 (2020).

[42] D. Villaseñor, S. Pilatowsky-Cameo, J. Chávez-Carlos, M. A. Bastarrachea-Magnani, S. Lerma-Hernández, L. F. Santos, and J. G. Hirsch, *Classical and quantum properties of the spin-boson dicke model: chaos, localization, and scarring*, 2024.

[43] P. Reimann, Foundation of statistical mechanics under experimentally realistic conditions, Phys. Rev. Lett. **101**, 190403 (2008).

[44] N. Sauerwein, F. Orsi, P. Uhrich, S. Bandyopadhyay, F. Mattiotti, T. Cantat-Moltrecht, G. Pupillo, P. Hauke, and J.-P. Brantut, Engineering random spin models with atoms in a high-finesse cavity, Nature Physics **19**, 1128–1134 (2023).

[45] J. A. Muniz, D. Barberena, R. J. Lewis-Swan, D. J. Young, J. R. Cline, A. M. Rey, and J. K. Thompson, Exploring dynamical phase transitions with cold atoms in an optical cavity, Nature **580**, 602–607 (2020).

[46] R. Chinnarasu, C. Poole, L. Phuttitarn, A. Noori, T. M. Graham, S. N. Coppersmith, A. B. Balantekin, and M. Saffman, Variational simulation of the lipkin-meshkov-glick model on a neutral atom quantum computer, PRX Quantum **6**, 020350 (2025).

[47] E. Champion, A. Schwartz, M. A. Ijaz, X. Xu, S. Campbell, G. T. Landi, and M. S. Blok, *Analog quantum simulation of the lipkin-meshkov-glick model in a transmon qudit*, 2025.

[48] G. Chen, J. .-. Liang, and S. Jia, Interaction-induced lipkin-meshkov-glick model in a bose-einstein condensate inside an optical cavity, Opt. Express **17**, 19682–19690 (2009).

[49] D.-Y. Lü, G.-H. Wang, Y. Zhou, L. Xu, Y.-J. Hu, W.-Y. Zeng, and Q.-L. Wang, Collective decay induce quantum phase transition in a well-controlled hybrid quantum system, Results in Physics **21**, 103832 (2021).

[50] S. Morrison and A. S. Parkins, Dynamical quantum phase transitions in the dissipative lipkin-meshkov-glick model with proposed realization in optical cavity qed, Phys. Rev. Lett. **100**, 040403 (2008).

[51] J.-M. Stéphan and J. Dubail, Local quantum quenches in critical one-dimensional systems: entanglement, the Loschmidt echo, and light-cone effects, J. Stat. Mech. **2011**, P08019 (2011).

[52] E. J. Torres-Herrera and L. F. Santos, Local quenches with global effects in interacting quantum systems, Phys. Rev. E **89**, 062110 (2014).

[53] M. Heyl, A. Polkovnikov, and S. Kehrein, Dynamical Quantum Phase Transitions in the Transverse-Field Ising Model, Phys. Rev. Lett. **110**, 135704 (2013).

[54] R. P. RK, *Statistical mechanics* (Butterworth-Heinemann, London, 1996).

[55] S. A. Weidinger, M. Heyl, A. Silva, and M. Knap, Dynamical quantum phase transitions in systems with continuous symmetry breaking, Phys. Rev. B **96**, 134313 (2017).

[56] S. Vajna and B. Dóra, Topological classification of dynamical phase transitions, Phys. Rev. B **91**, 155127 (2015).

[57] M. Heyl, Scaling and Universality at Dynamical Quantum Phase Transitions, Phys. Rev. Lett. **115**, 140602 (2015).

[58] F. Pollmann, S. Mukerjee, A. G. Green, and J. E. Moore, Dynamics after a sweep through a quantum critical point, Physical Review E **81**, 020101 (2010).

[59] M. E. Fisher, *The nature of critical points (lectures in theoretical physics vol viic)* (University of Colorado Press, 1965).

[60] C. N. Yang and T. D. Lee, Statistical Theory of Equations of State and Phase Transitions. I. Theory of Condensation, Phys. Rev. **87**, 404–409 (1952).

[61] T. D. Lee and C. N. Yang, Statistical Theory of Equations of State and Phase Transitions. II. Lattice Gas and Ising Model, Phys. Rev. **87**, 410–419 (1952).

[62] A. LeClair, G. Mussardo, H. Saleur, and S. Skorik, Boundary energy and boundary states in integrable quantum field theories, Nuclear Physics B **453**, 581–618 (1995).

[63] J. B. Conway, *Functions of one complex variable II*, Vol. 159 (Springer Science & Business Media, 2012).

[64] W. van Saarloos and D. A. Kurtze, Location of zeros in the complex temperature plane: absence of Lee-Yang theorem, Journal of Physics A: Mathematical and General **17**, 1301 (1984).

[65] I. Bena, M. Droz, and A. Lipowski, Statistical mechanics of equilibrium and nonequilibrium phase transitions: the Yang–Lee formalism, International Journal of Modern Physics B **19**, 4269–4329 (2005).

[66] M. Schmitt and S. Kehrein, Dynamical quantum phase transitions in the Kitaev honeycomb model, Phys. Rev. B **92**, 075114 (2015).

[67] M. Kolodrubetz, B. K. Clark, and D. A. Huse, Nonequilibrium Dynamic Critical Scaling of the Quantum Ising Chain, Phys. Rev. Lett. **109**, 015701 (2012).

[68] P. Jurcevic, H. Shen, P. Hauke, C. Maier, T. Brydges, C. Hempel, B. P. Lanyon, M. Heyl, R. Blatt, and C. F. Roos, Direct Observation of Dynamical Quantum Phase Transitions in an Interacting Many-Body System, Phys. Rev. Lett. **119**, 080501 (2017).

[69] H. Touchette, The large deviation approach to statistical mechanics, Physics Reports **478**, 1–69 (2009).

[70] P. Calabrese, F. H. L. Essler, and M. Fagotti, Quantum quench in the transverse field Ising chain: I. Time evolution of order parameter correlators, Journal of Statistical Mechanics: Theory and Experiment **2012**, P07016 (2012).

[71] See the supplemental material at https://journals.aps.org/prl/abstract/10.1103/PhysRevLett.110.135

[72] M. Heyl, Dynamical Quantum Phase Transitions in Systems with Broken-Symmetry Phases, Phys. Rev. Lett. **113**, 205701 (2014).

[73] I. Hagymási, C. Hubig, Ö. Legeza, and U. Schollwöck, Dynamical Topological Quantum Phase Transitions in Nonintegrable Models, Phys. Rev. Lett. **122**, 250601 (2019).

[74] B. Žunkovi č, M. Heyl, M. Knap, and A. Silva, Dynamical Quantum Phase Transitions in Spin chains with Long-Range Interactions: Merging Different Concepts of Nonequilibrium Criticality, Phys. Rev. Lett. **120**, 130601 (2018).

[75] M. Lacki and M. Heyl, Dynamical quantum phase transitions in collapse and revival oscillations of a quenched superfluid, Phys. Rev. B **99**, 121107 (2019).

[76] J. J. Mendoza-Arenas, Dynamical quantum phase transitions in the one-dimensional extended Fermi–Hubbard model, Journal of Statistical Mechanics: Theory and Experiment **2022**, 043101 (2022).

[77] C. Karrasch and D. Schuricht, Dynamical phase transitions after quenches in nonintegrable models, Phys. Rev. B **87**, 195104 (2013).

[78] P. Calabrese, F. H. L. Essler, and M. Fagotti, Quantum Quench in the Transverse-Field Ising Chain, Phys. Rev. Lett. **106**, 227203 (2011).

[79] D. Schuricht and F. H. L. Essler, Dynamics in the Ising field theory after a quantum quench, Journal of Statistical Mechanics: Theory and Experiment **2012**, P04017 (2012).

[80] L. D. Landau and E. M. Lifshitz, *Statistical physics: volume 5*, Vol. 5 (Elsevier, 2013).

[81] A. Lerose, B. Žunkovi č, J. Marino, A. Gambassi, and A. Silva, Impact of nonequilibrium fluctuations on prethermal dynamical phase transitions in long-range interacting spin chains, Phys. Rev. B **99**, 045128 (2019).

[82] B. Žunkovič, A. Silva, and M. Fabrizio, Dynamical phase transitions and Loschmidt echo in the infinite-range XY model, Philosophical Transactions of the Royal Society A: Mathematical, Physical and Engineering Sciences **374**, 20150160 (2016).

[83] B. Sciolla and G. Biroli, Dynamical transitions and quantum quenches in mean-field models, Journal of Statistical Mechanics: Theory and Experiment **2011**, P11003 (2011).

[84] M. Schiró and M. Fabrizio, Time-Dependent Mean Field Theory for Quench Dynamics in Correlated Electron Systems, Phys. Rev. Lett. **105**, 076401 (2010).

[85] M. Schiró and M. Fabrizio, Quantum quenches in the Hubbard model: Time-dependent mean-field theory and the role of quantum fluctuations, Phys. Rev. B **83**, 165105 (2011).

[86] M. S. Foster, M. Dzero, V. Gurarie, and E. A. Yuzbashyan, Quantum quench in a $p + ip$ superfluid: Winding numbers and topological states far from equilibrium, Phys. Rev. B **88**, 104511 (2013).

[87] E. A. Yuzbashyan, M. Dzero, V. Gurarie, and M. S. Foster, Quantum quench phase diagrams of an s-wave BCS-BEC condensate, Phys. Rev. A **91**, 033628 (2015).

[88] J. Berges, S. Borsányi, and C. Wetterich, Prethermalization, Phys. Rev. Lett. **93**, 142002 (2004).

[89] M. Gring, M. Kuhnert, T. Langen, T. Kitagawa, B. Rauer, M. Schreitl, I. Mazets, D. A. Smith, E. Demler, and J. Schmiedmayer, Relaxation and Prethermalization in an Isolated Quantum System, Science **337**, 1318–1322 (2012).

[90] T. Mori, T. N. Ikeda, E. Kaminishi, and M. Ueda, Thermalization and prethermalization in isolated quantum systems: a theoretical overview, Journal of Physics B: Atomic, Molecular and Optical Physics **51**, 112001 (2018).

[91] J. C. Halimeh and V. Zauner-Stauber, Dynamical phase diagram of quantum spin chains with long-range interactions, Phys. Rev. B **96**, 134427 (2017).

[92] S. Vajna and B. Dóra, Disentangling dynamical phase transitions from equilibrium phase transitions, Phys. Rev. B **89**, 161105 (2014).

[93] F. Andraschko and J. Sirker, Dynamical quantum phase transitions and the Loschmidt echo: A transfer matrix approach, Phys. Rev. B **89**, 125120 (2014).

[94] C. Lanczos, An iteration method for the solution of the eigenvalue problem of linear differential and integral operators, Journal of research of the National Bureau of Standards **45**, 255–282 (1950).

[95] N. W. Ashcroft and N. D. Mermin, Solid state physics, college edn, Thomson Learning Inc (1976).

[96] K. Hashimoto, K. Murata, N. Tanahashi, and R. Watanabe, Krylov complexity and chaos in quantum mechanics, Journal of High Energy Physics **2023**, 1–41 (2023).

[97] G. F. Scialchi, A. J. Roncaglia, and D. A. Wisniacki, Integrability-to-chaos transition through the Krylov approach for state evolution, Phys. Rev. E **109**, 054209 (2024).

[98] P. Caputa and S. Liu, Quantum complexity and topological phases of matter, Phys. Rev. B **106**, 195125 (2022).

[99] M. Afrasiar, J. K. Basak, B. Dey, K. Pal, and K. Pal, Time evolution of spread complexity in quenched Lipkin–Meshkov–Glick model, Journal of Statistical Mechanics: Theory and Experiment **2023**, 103101 (2023).

[100] P. Caputa, J. M. Magan, and D. Patramanis, Geometry of Krylov complexity, Phys. Rev. Res. **4**, 013041 (2022).

[101] V. Balasubramanian, J. M. Magan, and Q. Wu, Quantum chaos, integrability, and late times in the Krylov basis, arXiv 2312.03848 (2023) (hep–th).

[102] E. Rabinovici, A. Sánchez-Garrido, R. Shir, and J. Sonner, Operator complexity: a journey to the edge of Krylov space, Journal of High Energy Physics **2021**, 1–24 (2021).

[103] H. Tang, Operator Krylov complexity in random matrix theory, arXiv 2312.17416 (hep–th) 2023.

[104] E. Rabinovici, A. Sánchez-Garrido, R. Shir, and J. Sonner, Krylov complexity from integrability to chaos, Journal of High Energy Physics **2022**, 1–29 (2022).

[105] E. Rabinovici, A. Sánchez-Garrido, R. Shir, and J. Sonner, Krylov localization and suppression of complexity, Journal of High Energy Physics **2022**, 1–42 (2022).

[106] P. H. S. Bento, A. del Campo, and L. C. Céleri, Krylov complexity and dynamical phase transition in the quenched Lipkin-Meshkov-Glick model, Phys. Rev. B **109**, 224304 (2024).

[107] F. M. Izrailev, Simple models of quantum chaos: Spectrum and eigenfunctions, Physics Reports **196**, 299–392 (1990).

[108] V. Zelevinsky, B. Brown, N. Frazier, and M. Horoi, The nuclear shell model as a testing ground for many-body quantum chaos, Physics Reports **276**, 85–176 (1996).

[109] S. Campbell, Criticality revealed through quench dynamics in the Lipkin-Meshkov-Glick model, Phys. Rev. B **94**, 184403 (2016).

[110] S. Lerma-Hernández, J. Chávez-Carlos, M. A. Bastarrachea-Magnani, L. F. Santos, and J. G. Hirsch, Analytical description of the survival probability of coherent states in regular regimes, Journal of Physics A: Mathematical and Theoretical **51**, 475302 (2018).

[111] J. L. F. Barbón, E. Rabinovici, R. Shir, and R. Sinha, On the evolution of operator complexity beyond scrambling, Journal of High Energy Physics **2019**, 264 (2019).